

Predictive Haptic Driver Support Near Vehicle's Handling Limits

Master Thesis

Kazimierz Dokurno

Predictive Haptic Driver Support Near Vehicle's Handling Limits

Master Thesis

by

Kazimierz Dokurno

to obtain the degree of Master of Science in Systems & Control at the University of Twente,
graduation project carried out externally at the Delft University of Technology,
to be defended publicly on Thursday July 20, 2023 at 1:00 PM.

Graduation Committee:

Prof. dr. ir. D. Gavrilu,	Delft University of Technology, Chair
dr. ir. B. Shyrokau,	Delft University of Technology, Supervisor
dr. ir. D. Dresscher,	University of Twente, Committee Member

This thesis is confidential and cannot be made public until July 14, 2025.

Acknowledgements

I would like to express my gratitude to all of those who have provided support and helped me throughout this graduation project.

First and foremost, I would like to thank my daily supervisor, Barys Shyrokau, for his invaluable guidance, continuous support, and exhaustive expertise during this research. His insightful feedback and encouragement allowed me to accomplish more during this project than I could have imagined.

My sincere thanks go to all the incredible people I had the pleasure to meet at Toyota Motor Europe. I would like to thank my mentor, Andrea Lazcano, for her continuous guidance, constructive feedback and assistance whenever needed. I would also like to thank my manager, Xabier Akutain, for his stimulating discussions and very technical brainstorming sessions that played a crucial role in shaping this project. My thanks also go to all the expert drivers and engineers whose insights and suggestions allowed me to learn from the best in the field.

I would like to thank professor Ronald Aarts, without whom this project would not have been possible. His valuable assistance in navigating the administrative process, necessary for the approval of this external graduation assignment, is deeply appreciated.

Last but not least, I would like to express my gratitude to my family, friends, and close ones whose constant encouragement throughout this endeavor has been an exceptional source of strength and motivation.

*Kazimierz Dokurno
Delft, July 2023*

Abstract

This research presents a novel advanced driver assistance system (ADAS) designed to enhance safety when the vehicle undergoes critical handling maneuvers. By increasing the driver's situational awareness and providing guidance for a safe steering input, the proposed system aims to reduce the risk of an unwanted road departure caused by vehicle understeer. The support system is able to anticipate the saturation of the front tires in advance, and can guide the driver towards a safer steering input through haptic torque directly on the steering wheel.

The proposed driver support system relies on a control framework combining Model Predictive Control (MPC) and Haptic Shared Control (HSC). MPC is used to predict the future vehicle states over an imminent time horizon, while HSC provides haptic guidance on the steering wheel in case of an unsafe driver's steering input. By means of prediction, the system can notify the driver of incoming handling limits before they are reached, and provide haptic support to mitigate understeer proactively.

The effectiveness of the driver haptic support was evaluated in a driving simulator study, in which a total of 32 participants took part. The studied scenario involved an obstacle avoidance maneuver in the middle of a turn at high velocity. Two steering support modes were investigated: 1) haptic support where additional haptic torque is provided by the designed system on the steering wheel, and 2) no support which is equivalent to manual steering. Results demonstrate that the provided haptic support helps novice and regular drivers avoid excessive front tires slip compared to driving without support. In case of regular drivers, a significant reduction in peak lane deviation is observed for the haptic support mode. Following a subjective evaluation, a significant reduction in mental workload and frustration is reported by novice drivers when the haptic support is active. Regular drivers also scored significantly higher on the self-assessed performance scale when aided by the support. No significant difference between the two driving modes was noted for expert drivers, in terms of both objective and subjective evaluations.

The findings of this research offer new perspectives for the design of human-centered vehicle safety systems. The developed haptic support has shown to positively influence drivers to promote safety. Furthermore, this work proposes a control framework that can be used by future ADAS that wish to leverage the predictive capabilities of the MPC while including the driver in the control loop.

Keywords: Haptic Shared Control, Model Predictive Control, Human-Machine Interaction, Handling Limits, Safety Envelope.

Contents

Acknowledgements	i
Abstract	ii
Contents	ii
List of Figures	v
List of Tables	viii
Nomenclature	xi
1 Introduction	1
1.1 Motivation	1
1.2 Understeer Definition	1
1.3 Understeer Mitigation	2
1.3.1 Direct Yaw Control	2
1.3.2 Integrated Understeer Mitigation Systems	2
1.3.3 Collaborative Understeer Mitigation Systems	3
1.4 Research Goal	3
1.5 Organization	4
2 Research Paper	5
A Human-Machine Interaction	15
A.1 Background	15
A.2 Human Modes of Operation	16
A.3 Human Error	17
A.4 Shared Control	18
A.5 Summary	19
B Pilot Study	21
B.1 Understeer Detection	21
B.1.1 Principle of Operation	21
B.1.2 Tire Model	22
B.1.3 Validation	24
B.2 Controller	25
B.2.1 Objective	25
B.2.2 Design	26
B.3 Experiment	26
B.4 Preliminary Results	28
B.4.1 Objective Evaluation	28
B.4.2 Subjective Evaluation	30
B.5 Discussions	30
B.6 Summary	31
C Haptic Support System Design	32
C.1 MPC Background	32

C.2	Vehicle Model	33
C.2.1	Bicycle Model	33
C.2.2	Tire Model	34
C.2.3	Safe Steering Envelope	34
C.3	Predictive Haptic Driver Support System	35
C.3.1	MPC Formulation	35
C.3.2	HSC Design	36
C.4	Implementation	37
C.4.1	MPC Settings	37
C.4.2	HSC Settings	38
C.5	Operation	39
D	Results and Discussions	40
D.1	Participants	40
D.2	Results	40
D.2.1	Objective Evaluation	41
D.2.2	Subjective Evaluation	45
D.3	Discussions	47
E	Individual Results	49
F	NASA-TLX Evaluation Form	82
G	Conference Paper	83
	References	92

List of Figures

1.1	Schematic diagram of understeer and oversteer mitigation through DYC [52]	2
A.1	Skill-based, rule-based and knowledge-based levels of performance of human operators according to Rasmussen [41]	16
A.2	Driver error model: the expected pattern of behaviour when encountering understeer	18
B.1	Forces and moments acting on the tire [44]	21
B.2	Fiala tire brush model [35]	23
B.3	Lateral force F_y , self-aligning moment M_z and the pneumatic trail t_p as a function of the slip angle α [35]	24
B.4	IPG CarMaker simulation scenario	24
B.5	Comparison between the tire brush model and the IPG CarMaker tire model in steady-state cornering for different values of μ	25
B.6	Lateral tire force as a function of distance in steady-state cornering for different values of μ	25
B.7	Haptic controller block diagram	27
B.8	Driving simulator at Toyota Motor Europe, Belgium	27
B.9	Average steering wheel torque for each variation of haptic support	28
B.10	Average steering wheel angle for each variation of haptic support	29
B.11	Average lateral force for each variation of haptic support	29
C.1	A general discrete MPC scheme	33
C.2	Bicycle model	34
C.3	Control framework: The MPC predicts the future vehicle states, which are then used to compute the safe steering envelope (in green) for each timestep of the prediction horizon. An error e (in red) is produced if the predicted steering angle leaves the envelope. The generated haptic torque τ_{hap} is equal to the weighted sum of the errors where the weighting function w is linearly decreasing. The total support torque τ_s is equal to the sum of τ_{hap} and τ_{vib} .	35
C.4	State prediction at $t = 38.17s$ during a driver-in-the-loop experimental trial	39
D.1	Average maximum lateral deviation during scenario 1 when driving without support, plotted as a function of the driving license possession years	40
D.2	Experimental results from scenario 1: mean values (solid lines), and standard deviations (shaded areas) for the 2 support cases, plotted for each driver category	41
D.3	Experimental results from scenario 2: mean values (solid lines), and standard deviations (shaded areas) for the 2 support cases, plotted for each driver category	43
E.1	Experimental results of driver 1: mean values (solid lines), and standard deviations (shaded areas) for the 2 support cases, plotted for both scenarios.	50
E.2	Experimental results of driver 2: mean values (solid lines), and standard deviations (shaded areas) for the 2 support cases, plotted for both scenarios.	51

E.27	Experimental results of driver 27: mean values (solid lines), and standard deviations (shaded areas) for the 2 support cases, plotted for both scenarios. . . .	76
E.28	Experimental results of driver 28: mean values (solid lines), and standard deviations (shaded areas) for the 2 support cases, plotted for both scenarios. . . .	77
E.29	Experimental results of driver 29: mean values (solid lines), and standard deviations (shaded areas) for the 2 support cases, plotted for both scenarios. . . .	78
E.30	Experimental results of driver 30: mean values (solid lines), and standard deviations (shaded areas) for the 2 support cases, plotted for both scenarios. . . .	79
E.31	Experimental results of driver 31: mean values (solid lines), and standard deviations (shaded areas) for the 2 support cases, plotted for both scenarios. . . .	80
E.32	Experimental results of driver 32: mean values (solid lines), and standard deviations (shaded areas) for the 2 support cases, plotted for both scenarios. . . .	81

List of Tables

B.1	NASA-TLX evaluation results for each driving mode (best results in bold)	30
C.1	MPC parameters	38
C.2	FORCES PRO NLP solver settings	38
C.3	HSC parameters	38
D.1	Averaged maximum lateral deviation during scenario 1 for each driving mode, for each driver category (standard deviations in parentheses)	42
D.2	Averaged maximum slip angle at the front axle during scenario 1 for each driving mode, for each driver category (standard deviations in parentheses)	42
D.3	Averaged maximum lateral force at the front axle during scenario 1 for each driving mode, for each driver category (standard deviations in parentheses)	42
D.4	Averaged maximum steering wheel angle during scenario 1 for each driving mode, for each driver category (standard deviations in parentheses)	42
D.5	Averaged maximum steering wheel torque during scenario 1 for each driving mode, for each driver category (standard deviations in parentheses)	43
D.6	Averaged maximum lateral deviation during scenario 2 for each driving mode, for each driver category (standard deviations in parentheses)	44
D.7	Averaged RMS slip angle at the front axle from X=400m to X=550m (around the obstacle) for each driving mode, for each driver category (standard deviations in parentheses)	44
D.8	Averaged RMS values of lateral force at the front axle from X=400m to X=550m (around the obstacle) for each driving mode, for each driver category (standard deviations in parentheses)	44
D.9	Averaged RMS values of steering wheel angle from X=400m to X=550m (around the obstacle) for each driving mode, for each driver category (standard deviations in parentheses)	45
D.10	Averaged RMS values of steering wheel torque from X=400m to X=550m (around the obstacle) for each driving mode, for each driver category (standard deviations in parentheses)	45
D.11	NASA-TLX evaluation results for expert drivers during scenario 1, for each driving mode (standard deviations in parentheses)	45
D.12	NASA-TLX evaluation results for regular drivers during scenario 1, for each driving mode (standard deviations in parentheses)	46
D.13	NASA-TLX evaluation results for novice drivers during scenario 1, for each driving mode (standard deviations in parentheses)	46
D.14	NASA-TLX evaluation results for expert drivers during scenario 2, for each driving mode (standard deviations in parentheses)	46
D.15	NASA-TLX evaluation results for regular drivers during scenario 2, for each driving mode (standard deviations in parentheses)	46
D.16	NASA-TLX evaluation results for novice drivers during scenario 2, for each driving mode (standard deviations in parentheses)	47

E.1 NASA-TLX evaluation results for driver 1, for each driving mode, for both scenarios.	50
E.2 NASA-TLX evaluation results for driver 2, for each driving mode, for both scenarios.	51
E.3 NASA-TLX evaluation results for driver 3, for each driving mode, for both scenarios.	52
E.4 NASA-TLX evaluation results for driver 4, for each driving mode, for both scenarios.	53
E.5 NASA-TLX evaluation results for driver 5, for each driving mode, for both scenarios.	54
E.6 NASA-TLX evaluation results for driver 6, for each driving mode, for both scenarios.	55
E.7 NASA-TLX evaluation results for driver 7, for each driving mode, for both scenarios.	56
E.8 NASA-TLX evaluation results for driver 8, for each driving mode, for both scenarios.	57
E.9 NASA-TLX evaluation results for driver 9, for each driving mode, for both scenarios.	58
E.10 NASA-TLX evaluation results for driver 10, for each driving mode, for both scenarios.	59
E.11 NASA-TLX evaluation results for driver 11, for each driving mode, for both scenarios.	60
E.12 NASA-TLX evaluation results for driver 12, for each driving mode, for both scenarios.	61
E.13 NASA-TLX evaluation results for driver 13, for each driving mode, for both scenarios.	62
E.14 NASA-TLX evaluation results for driver 14, for each driving mode, for both scenarios.	63
E.15 NASA-TLX evaluation results for driver 15, for each driving mode, for both scenarios.	64
E.16 NASA-TLX evaluation results for driver 16, for each driving mode, for both scenarios.	65
E.17 NASA-TLX evaluation results for driver 17, for each driving mode, for both scenarios.	66
E.18 NASA-TLX evaluation results for driver 18, for each driving mode, for both scenarios.	67
E.19 NASA-TLX evaluation results for driver 19, for each driving mode, for both scenarios.	68
E.20 NASA-TLX evaluation results for driver 20, for each driving mode, for both scenarios.	69
E.21 NASA-TLX evaluation results for driver 21, for each driving mode, for both scenarios.	70
E.22 NASA-TLX evaluation results for driver 22, for each driving mode, for both scenarios.	71
E.23 NASA-TLX evaluation results for driver 23, for each driving mode, for both scenarios.	72
E.24 NASA-TLX evaluation results for driver 24, for each driving mode, for both scenarios.	73

E.25 NASA-TLX evaluation results for driver 25, for each driving mode, for both scenarios.	74
E.26 NASA-TLX evaluation results for driver 26, for each driving mode, for both scenarios.	75
E.27 NASA-TLX evaluation results for driver 27, for each driving mode, for both scenarios.	76
E.28 NASA-TLX evaluation results for driver 28, for each driving mode, for both scenarios.	77
E.29 NASA-TLX evaluation results for driver 29, for each driving mode, for both scenarios.	78
E.30 NASA-TLX evaluation results for driver 30, for each driving mode, for both scenarios.	79
E.31 NASA-TLX evaluation results for driver 31, for each driving mode, for both scenarios.	80
E.32 NASA-TLX evaluation results for driver 32, for each driving mode, for both scenarios.	81

Nomenclature

Abbreviations

Abbreviation	Definition
ABS	Anti-lock Braking System
ADAS	Advanced Driver Assistance System
CoG	Center of Gravity
DYC	Direct Yaw Control
EPS	Electric Power Steering
GEMS	General Error-Modelling System
HMI	Human-Machine Interaction
HSC	Haptic Shared Control
MPC	Model Predictive Control
NLP	Nonlinear Programming
QP	Quadratic Programming
RMS	Root-Mean-Square
SAE	Society of Automotive Engineers
SbW	Steer-by-Wire
SD	Standard Deviation
SQP	Sequential Quadratic Programming
SRK	Skill-Rule-Knowledge
SRR	Steering Reversal Rate
TLX	Task Load Index
VSC	Vehicle Stability Control

Symbols

Symbol	Definition	Unit
A	State-space system matrix	[-]
A_{vib}	Haptic vibrations amplitude	[Nm]
B	State-space input matrix	[-]
C_{α}	Tire cornering stiffness	[N/rad]
C_M	Tire aligning stiffness	[Nm/rad]
d	State-space disturbance input	[-]
e	Error term	[rad]
f_{vib}	Haptic vibrations frequency	[Hz]
F_x	Longitudinal tire force	[N]
F_y	Lateral tire force	[N]
F_z	Vertical tire force	[N]
I_{zz}	Vehicle's moment of inertia	[kg/m ²]
k	Timestep	[-]
K	Haptic torque tuning factor	[-]
l_f	Distance from front axle to CoG	[m]
l_r	Distance from rear axle to CoG	[m]
L	Wheelbase length	[m]
m	Vehicle mass	[kg]
M_z	Tire self-aligning moment	[Nm]
N_c	Control horizon length	[-]
N_p	Prediction horizon length	[-]
Q_1	Weight on steering velocity	[-]
Q_2	Weight on steering velocity deviation	[-]
Q_3	Weight on steering angle deviation	[-]
r	Yaw rate	[rad/s]
t_p	Pneumatic trail	[m]
T_c	Controller sample time	[s]
u	Control input	[m/s]
v_x	Longitudinal velocity	[m/s]
v_y	Lateral velocity	[m/s]
w	Weighting term	[-]
x	Plant state vector	[-]
X	Distance the vehicle has travelled	[m]
Y	Vehicle lateral deviation	[m]
α	Tire slip angle	[rad]
α_{lim}	Tire slip angle at saturation	[rad]
$\alpha_{M,max}$	Self-aligning moment peak slip angle	[rad]
δ	Road-wheel angle	[rad]
δ_{lim}	Road-wheel angle safe boundary	[rad]
δ_{SW}	Steering wheel angle	[rad]
μ	Tire-road friction coefficient	[-]
τ_{hap}	Haptic torque	[Nm]
τ_s	Total support torque	[Nm]
τ_{SW}	Steering wheel torque	[Nm]
τ_{vib}	Haptic torque vibrations	[Nm]

1

Introduction

1.1. Motivation

New technologies are empowering modern vehicles like never before. With the introduction of ever more enhanced Advanced Driver Assistance Systems (ADAS), drivers are supported in a wider range of conditions which positively impacts safety and comfort [28]. In fact, a steady decline in road fatalities can be observed in Europe in recent years [8]. Although there are many contributing factors to this trend, part of the decrease is attributed to the popularisation of technologies like the anti-lock braking system (ABS) and the vehicle stability control (VSC) system [13].

Despite these technological improvements, statistics still show high rates of single-vehicle crashes: around 33% of all road fatalities reported in 2022 in EU involved a single vehicle [9]. Studies suggest that accidents of this type are mostly due to unintended lane or road departures, especially during cornering maneuvers [12]. This can be related to vehicle *understeer* when the vehicle speed is too high to negotiate the turn for the given road conditions [27][34]. This results in an unexpected deviation from the desired path, with potentially fatal consequences for all the occupants of the car.

1.2. Understeer Definition

Understeer is a handling characteristic present to some degree in all vehicles which prevents the vehicle from turning as sharply as intended by the driver. This natural, and often intentional, characteristic makes the vehicle handling inherently stable. However, when understeer happens at the grip limit of the front tires, the lateral acceleration cannot increase anymore and the vehicle is forced to follow a wider path than intended. This so called *terminal* understeer goes beyond the normal degree of handling imbalance found in all vehicles. It presents significant challenges to the drivers when it comes to negotiating turns effectively.

While many factors can regulate understeer in the vehicle setup, such as weight distribution, suspension geometry, and tire characteristics, these aspects are outside of the scope of this work. This study focuses instead of excessive understeer emerging from dynamic conditions, such as excessive entry speed into a corner, low tire-road friction, and incorrect driver reactions near the handling limits. In the rest of this work, the term understeer is used to designate the problematic and excessive understeer characteristic appearing near the saturation limits of the front tires.

1.3. Understeer Mitigation

1.3.1. Direct Yaw Control

Current state-of-the-art VSC can mitigate understeer to some degree through direct yaw control (DYC). By analogy to *oversteer* mitigation, understeer is detected by comparing the measured yaw rate with a reference model. If the measured yaw rate is significantly lower than desired, understeer is detected. The safety system then applies an additional yaw moment through differential braking which helps to align the vehicle heading angle with the reference value. The principle of operation of DYC is illustrated in Figure 1.1.

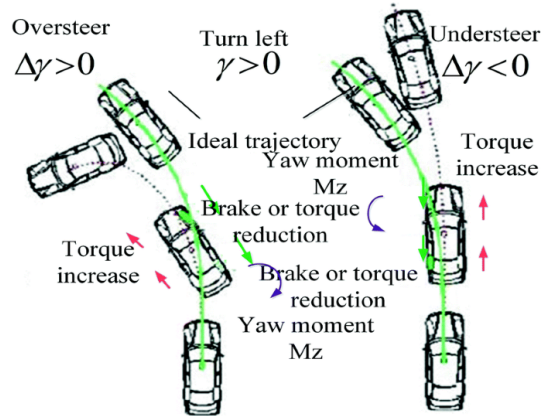


Figure 1.1: Schematic diagram of understeer and oversteer mitigation through DYC [52]

However, this approach has two major drawbacks. Firstly, understeer has to happen in order to be detected. This makes the safety system *reactive*. Secondly, although DYC can align the heading angle of the vehicle with the road direction, there is no guarantee that it will increase the path curvature [27]. On the contrary, differential braking can often make things worse by saturating the front tires when operating near the handling limits. This further decreases the cornering force and prevents the car from negotiating the turn. Therefore, the need for a more holistic understeer mitigation system, that takes into account path tracking and yaw control, is clear.

1.3.2. Integrated Understeer Mitigation Systems

Several understeer mitigation solutions have been proposed in literature that aim to limit excessive vehicle understeer without hindering path tracking capabilities. Integrated understeer mitigation systems aim to minimize understeer by (partially) overruling driver commands.

Gordon et al. [19] suggested the use of differential braking with an optimal control problem formulation to optimally solve the trade-off between path tracking and yaw rate correction. This solution was further improved through the addition of active front steering by Gao et al. [18] and the extension to independent front steering by Fors et al. [17]. However, all these approaches require prior knowledge of the desired trajectory. Studies on similar driver aids have shown that if the predicted path deviates substantially from the driver's intention, the results are an increased driver frustration, loss of trust, and a poor user acceptance [29].

Takahashi et al. [45] proposed an understeer mitigation method that does not need any knowledge of the trajectory. The study showed that by applying brakes proportionally to the lateral vehicle jerk, understeer can be reduced through a combination of deceleration and weight transfer to the front axle. Zhang et al. [54] went a step further and developed a torque vectoring control system for understeer mitigation. Without information about the desired path, the system infers the driver intention from the steering angle and steering rate. During cornering, it applies brakes in the entry phase of the turn and accelerates the vehicle during the exit phase,

essentially modifying the understeer characteristic of the vehicle. Although these approaches do not rely on knowledge of the desired trajectory, they can lead to dangerous situations with incoming traffic due to significant speed reductions when cornering.

1.3.3. Collaborative Understeer Mitigation Systems

Another type of safety systems employs a different approach when it comes to the level of human involvement. By promoting collaboration, these assistance systems work together with the driver to mitigate understeer and perform the maneuver successfully. Studies presented in this section all focus on limiting excessive steering input by the driver, which can further decrease the cornering force at the front tires and increase understeer. Nevertheless, they differ on the methods used to detect understeer, as well as on the type of feedback provided to the driver.

Katzourakis [26] was the first author to focus on understeer mitigation through haptic feedback on the steering wheel. The proposed control strategy emphasizes the drop of the self-aligning moment, a phenomenon inherently present in all vehicles, by further reducing the steering stiffness. This informs drivers about the incoming understeer in advance, such that they can avoid excessive steering angle inputs which would only further increase the slip of the front tires. The system detects understeer using a model-based approach using measurements of vehicle yaw rate and lateral acceleration. Experimental results showed a positive influence of the system on vehicle performance with a significant reduction in slip angles at the front tires. This indicates a better utilization of the tires and more optimal steering angle inputs.

As an alternative to Katzourakis' model-based approach, van Doornik [48] proposed an understeer mitigation support that relies on direct measurements of the tire lateral force and the self-aligning moment. The support system generates a haptic torque proportional to the ratio between the lateral force and the self-aligning moment of the front tires, which similarly decreases the perceived steering stiffness. Experimental results indicate a reduction in steering reversal rate (SRR) when driving with the support system compared to no support, which translates into a smoother steering input. However, the lateral tire force also decreases on average by 18% when participants drive with the assistance turned on, indicating that the support system reduces the cornering capabilities of the vehicle instead of improving them.

Hildenbrandt et al. [22] from the BMW Group developed an Intuitive Steering Assistance which increases the perceived steering torque when understeer is detected by an on-board VSC. Experimental results showed that drivers exhibit smaller steering inputs when driving with the support system, which results in smaller lateral deviations from the lane when cornering. Nevertheless, as the system relies on a classic VSC to detect understeer, it has the disadvantage of being reactive and only informing the driver once the situation has become critical.

1.4. Research Goal

From the above review of understeer mitigation systems, it becomes apparent that there is a lack of systems which include the driver in the control loop and that are simultaneously able to predict the approach of handling limits in advance. This thesis addresses this gap in research with a predictive haptic driver support system for understeer mitigation. The proposed system adheres to the following principles:

- the occurrence of understeer is predicted in advance;
- the driver is part of the control loop at all times;
- no knowledge of the desired path is required;

- the system intervenes only when necessary.

The main research goal of this graduation project is the design and evaluation of a novel predictive haptic driver support system that aims to mitigate understeer while obeying the above-mentioned principles. This goal can be further subdivided into the following research objectives:

1. review of the relevant scientific literature on understeer mitigation methods, human-machine interaction as well as model predictive control;
2. design and realization of a pilot study to evaluate the benefits of providing haptic steering support near the handling limits of the vehicle;
3. design and implementation of a model predictive control strategy for understeer mitigation while ensuring real-time performance;
4. design and realization of a driver-in-the-loop experimental simulator study to evaluate the impact of the designed driver support system on driving performance and user acceptance;
5. post-processing, interpretation and reporting of the recorded experimental data.

This work focuses exclusively on steady-state cornering conditions, during which the longitudinal vehicle speed is constant or slowly changing. However, the exclusion of other driving conditions does not diminish the significance of the findings presented in this study. The insights and methodologies introduced here can serve as a foundation for further research on understeer mitigation. Recommendations are provided on how the proposed solution can be extended to varying velocity conditions.

1.5. Organization

The remainder of this thesis is organized as follows. Chapter 2 presents the main contributions of this graduation project in the form of a research paper. More details are provided in the following appendices. Appendix A covers the theory of human-machine interaction. The design, realization and results of the pilot study are presented in Appendix B. Appendix C covers the design and implementation of the predictive haptic driver support system. Additional experimental results and discussions are shown in Appendix D, along individual results for each participant which are presented in Appendix E. The subjective evaluation form used during the experimental study is shown in Appendix F. Finally, the conference paper submitted to the 39th FISITA World Congress based on the present research can be consulted in Appendix G.

2

Research Paper

The content of this chapter presents the research paper summarizing the work done during this graduation project.

Predictive Haptic Driver Support Near Vehicle's Handling Limits

Kazimierz Dokurno

Abstract—This research presents a novel advanced driver assistance system (ADAS) that anticipates and mitigates understeer by delivering haptic support to the driver via the steering wheel. The proposed system calculates a safe steering envelope using a Model Predictive Control (MPC) framework, considering the saturation limits of the vehicle's front tires. If the predicted driver steering angle violates the safe envelope, haptic feedback is provided through the steering wheel in the form of an increased opposing torque with vibrations. Thus, the system aims to increase the driver's situational awareness and provide guidance to reduce the steering input if the safe steering limits are exceeded. To evaluate the effectiveness of the proposed support system, a total of 32 drivers participated in a driving simulator experiment at Toyota Motor Europe. The scenario involved an obstacle avoidance maneuver in the middle of a turn at high velocity. Two levels of automation were investigated: 1) haptic support where the additional haptic torque is provided at the steering wheel, and 2) no support which is equivalent to manual steering. The results demonstrate that haptic support has a positive impact on regular drivers, supporting them to mitigate understeer and significantly reducing lane deviation. No significant difference in performance was noted for expert drivers. Novice drivers report significantly reduced mental workload and lower frustration when the haptic support is active. Subjective evaluation indicates strong acceptance of the proposed assistance system.

Index Terms—Haptic shared control, model predictive control, human-machine interaction, handling limits, safety envelope

I. INTRODUCTION

RECENT developments in sensing, actuation, and computer processing technologies allow the introduction of more enhanced Advanced Driver Assistance Systems (ADAS). This enables the support of the driver in a wider range of conditions and improves driving safety [1]. Despite these advances, statistics still show high rates of accidents caused by unintended lane or road departures, especially during cornering maneuvers [2]. This can be related to excessive vehicle *understeer* when the vehicle speed is too high to negotiate the turn, resulting in an unexpected deviation from the desired path [3][4].

Understeer is a handling characteristic present in all vehicles to some extent. This intentional handling imbalance provides inherent yaw stability and is intuitive to the driver: an increase in the steering input results in a sharper turn. However, understeer becomes problematic when the vehicle approaches its handling limits. At this point, the front tires reach saturation, meaning they have already achieved their maximum lateral force capacity. When the driver attempts to compensate for insufficient turning by increasing the steering input, it causes the front tires to slip and generate even less lateral force. As a consequence, lateral acceleration is further reduced which leads to a wider turning radius than intended.

Several authors have observed a difference in response between novice and expert drivers when approaching the saturation point of the front tires [5][6][7]. Novice drivers exhibit a tendency to apply excessive steering input near the handling limits, which leads to understeer and a potential path deviation. Conversely, expert drivers reduce their steering input upon sensing the saturation of the front tires in order to maximize grip. Hildenbrandt et al. [5] associated the erroneous response of novice drivers with a phenomenon known as the *strong habit intrusion*. According to studies realized by Reason [8] and Rasmussen [9], strong habit intrusion occurs when individuals are faced with a novel problem but, due to the urgency of the situation, cannot use higher levels of cognition to find a solution. In such cases, individuals tend to instinctively rely on familiar patterns of behaviour that have proven successful in the past. Consequently, when understeer occurs, novice drivers tend to increase their steering angle input in an attempt to mitigate understeer, despite the fact that it only exacerbates the problem. This phenomenon is further explored in Appendix A.

An increasingly promising method to support the driver in difficult and unfamiliar situations is the shared control paradigm. According to Abbink et al. [10], in shared control both the human and the automation perform simultaneously a task that could be performed by either the human or the automation alone in ideal conditions. In a literature review done by Marcano et al. [11] which analysed over 100 contributions related to the field of shared vehicle control, haptic shared control (HSC) is reported as the most popular modality to combine the intentions of both the driver and the automation through the mutual exchange of force on the steering wheel. The most commonly found HSC use case in literature is lane keeping, which focuses on helping the driver with path tracking by providing haptic torque.

While continuous guidance has shown to reduce workload and increase driving comfort [11], a different set of driver support systems are specifically designed for sporadic interventions, activating only in emergency situations. This approach, also known as *envelope control*, was initially introduced by Beal and Gerdes [12] to vehicle stability control. It was later used by Balachandran et al. [13] who combined envelope control and HSC to design a predictive obstacle avoidance assistance. Such systems have proven to be effective in enhancing safety without causing annoyance or unnecessary interference with the driver's intentions.

The implementation of safe boundaries required for envelope control can be readily handled by the model predictive control (MPC) framework. The MPC algorithm takes into account these boundaries as constraints during the optimiza-

tion process, ensuring that the control inputs keep the vehicle within the predefined envelope. This enables the driver support system to proactively respond to changes in the driving conditions and mitigate understeer before it occurs. Several studies have demonstrated the practicality of MPC for ADAS [14], with applications such as driver-oriented lane-keeping [15], stability control at the limits of handling [12], or predictive haptic support for obstacle avoidance [13].

This work proposes a novel predictive haptic driver support for understeer mitigation by merging the MPC framework with the HSC approach. The proposed system predicts the future vehicle states and steering input using a single-track bicycle model with a nonlinear brush tire model. The predicted states are then used to compute a safe steering envelope for each instance of the prediction horizon. In case the predicted steering input violates the safe steering envelope, a low-level controller provides haptic feedback directly on the steering wheel. This alerts the driver about the incoming saturation of the front tires and offers guidance towards a safer steering input. The novelty of this approach is that the driver remains in the control loop at all times, while benefiting from the predictive capabilities of the system in an intuitive way.

The remainder of this paper is organized as follows. A literature review of related understeer mitigation methods is provided in Section II. Section III presents the model used to quantify the vehicle dynamics and develop the safe steering envelope, which is subsequently used in Section IV for the design of the haptic driver support system. The performed driving simulator experiment is presented in Section V and the study results are shown in Section VI. Conclusions are drawn in Section VII along with recommendations for future work.

II. RELATED WORK

Current state-of-the-art vehicle stability control (VSC) systems can mitigate understeer through direct yaw control (DYC), which employs differential braking to generate a yaw moment. If the vehicle starts to understeer, DYC can apply more braking force to the inner wheels to induce a yaw moment that counteracts the understeer. Although this approach is effective in aligning the vehicle's heading angle with the turn direction, differential braking can saturate the front tires (especially close to the handling limits). This reduces the cornering force and causes the vehicle to follow a wider path than desired.

Different understeer prevention techniques have been proposed that simultaneously aim to limit understeer and improve road holding. Gordon et al. [16] formulated the trade-off between path tracking and yaw rate correction as an optimal control problem. By efficiently using differential braking, the assistance system outperformed classic DYC in minimizing lateral path deviation during cornering. This solution was further improved through the addition of active front steering by Gao et al. [17] and the extension to independent front steering by Fors et al. [18]. However, all of these approaches require prior knowledge of the desired trajectory. If the predicted path deviates substantially from the driver's intention, it can result

in driver frustration, loss of trust, and lack of user acceptance [15].

Takahashi et al. [6] proposed a trajectory-agnostic method to understeer mitigation inspired by the driver longitudinal control model developed by Yamakado and Abe [19]. In the study, differential braking is applied proportionally to the lateral jerk, reducing understeer through a combination of deceleration and weight transfer to the front axle. Similarly inspired by professional drivers, Zhang et al. [7] developed a torque vectoring control system capable of modifying the understeer characteristic of the vehicle in real-time. The proposed controller supports the driver by modifying the torque distribution to each wheel, after inferring the driver intention from the steering angle and steering rate. Although these approaches do not rely on knowledge of the desired trajectory, they can lead to dangerous situations with the following traffic due to significant speed reductions when cornering.

While solutions mentioned so far (partially) overrule the driver in emergency situations, another type of systems relies on the concept of shared steering control [10]. Katzourakis [20] was the first to suggest haptic shared control as a method for understeer mitigation. The proposed system informs the driver about the front tires' saturation by emphasizing the drop of the self-aligning moment on the steering wheel. This is achieved by inferring the front axle slip angle, which is used to generate haptic torque in case the slip angle is close to the peak lateral slip. The experimental results showed a positive impact of the proposed system on vehicle performance with a reduction in slip angles indicating a better utilization of the front tires. Van Doornik [21] proposed an alternative to Katzourakis' model-based method. Instead of relying on a tire model, direct measurements of the tire lateral force and the self-aligning moment are used by load-sensing bearings [22]. The ratio between lateral force and self-aligning moment is used to generate haptic feedback which decreases the perceived steering wheel stiffness. Although the drop in self-aligning moment can be considered as an early indicator of tire saturation, the self-aligning moment itself is very sensitive to the vertical tire load, tire-road friction and even the type of tire compounds used [23]. Thus, detecting understeer from the self-aligning moment drop is not robust for dynamic and unknown operating conditions.

Hildebrandt et al. [5] developed a haptic driver understeer assistance which increases the perceived steering torque when understeer is detected by an on-board VSC. The system showed a positive impact on drivers, who used smaller steering inputs near handling limits, resulting in smaller lateral deviation from the lane. However, the system is reactive rather than proactive due to understeer detection by VSC, which relies on the comparison of yaw rate and lateral acceleration with a reference behaviour. Hence, significant understeer has to happen in order to be detected, informing the driver only after the situation has already become critical.

A common challenge faced by these systems is their inability to anticipate the approach of the handling limits of the vehicle, resulting in a delayed reaction to understeer. Alternatively, if they do predict the handling limits in advance, it comes at the cost of excluding drivers from the control loop

by largely overruling their commands.

This study addresses this gap with an intuitive haptic driver support system with predictive capabilities for understeer mitigation. Haptic torque is used to alert the driver about incoming handling limits and offers guidance for handling the situation in a safer manner. The proposed system adheres to the following principles:

- 1) the occurrence of understeer is predicted in advance,
- 2) the driver is part of the control loop at all times,
- 3) no knowledge of the desired path is required,
- 4) the system intervenes only when necessary.

The proposed system thus enables drivers to retain total control of the vehicle, while offering haptic support when their steering input is likely to result in understeer.

III. VEHICLE MODEL

The proposed predictive driver support relies on two models. The vehicle model is used to predict the lateral and rotational velocities of the car, while the tire model allows to calculate the forces at the tire-road contact patch.

A. Bicycle Model

The vehicle model used is a single-track bicycle model with two degrees of freedom [24]. The bicycle model, illustrated in Figure 1, considers the tires on each axle lumped together. Further assumptions include a constant longitudinal velocity v_x , no load transfers and no vertical motion of the vehicle. The equations of motion can be written in terms of the front and rear lateral tire forces, F_{yf} and F_{yr} , as

$$\dot{v}_y = \frac{F_{yf} + F_{yr}}{m} - r v_x, \quad (1)$$

$$\dot{r} = \frac{l_f F_{yf} - l_r F_{yr}}{I_{zz}}, \quad (2)$$

where v_y is the lateral velocity, r is the yaw rate, l_f and l_r are the distances from the center of gravity (CoG) to the front and rear axle, m is the vehicle mass and I_{zz} is the moment of inertia. From kinematics, the equations for the tire slip angles at the front (α_f) and at the rear (α_r) can be found as

$$\alpha_f = \frac{v_y + l_f r}{v_x} - \delta, \quad (3)$$

$$\alpha_r = \frac{v_y - l_r r}{v_x}, \quad (4)$$

where δ is the road-wheel steer angle.

B. Tire Brush Model

In this study, a nonlinear brush model proposed by Fiala [25] has been chosen due to its accurate description of tire behavior up to the tire saturation limits and light complexity ensuring real-time application (see Appendix B). An adapted version of the model formulated by Pacejka [23] is used. The model assumes a parabolic pressure distribution at the contact patch, a rigid tire carcass and a constant friction coefficient μ .

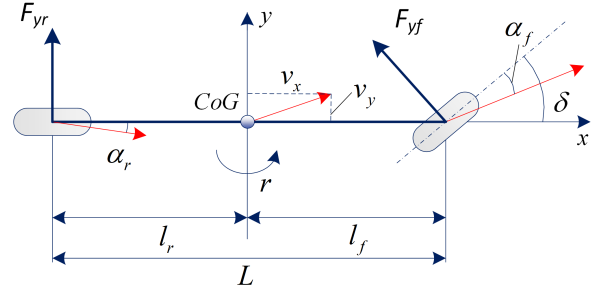


Fig. 1: Bicycle model

Given these assumptions, the relation between the lateral tire force $F_{y[f,r]}$ and $\alpha_{[f,r]}$ is described by

$$F_y = \begin{cases} C_\alpha \tan \alpha - \frac{C_\alpha^2}{3\mu F_z} |\tan \alpha| \tan \alpha \\ \quad + \frac{C_\alpha^3}{27\mu^2 F_z^2} \tan^3 \alpha, & \text{if } |\alpha| \leq \alpha_{lim} \\ \mu F_z \text{sgn} \alpha, & \text{else} \end{cases} \quad (5)$$

where C_α is the tire cornering stiffness, F_z is the normal load and α_{lim} is the slip angle at which the tire has reached the limits of friction, equal to

$$\alpha_{lim} = \tan^{-1} \left(\frac{3\mu F_z}{C_\alpha} \right). \quad (6)$$

C. Safe Steering Envelope

Following the approach of envelope control, steering angle limits can be defined to demarcate a safe region of operation. Substituting (6) into (3) and isolating δ yields an expression for the upper and lower boundary of the road-wheel angle δ_{lim} at which F_{yf} reaches its peak value, respectively:

$$\delta_{lim}^+ = \frac{v_y + l_f r}{v_x} + \tan^{-1} \left(\frac{3\mu F_z}{C_\alpha} \right), \quad (7)$$

$$\delta_{lim}^- = \frac{v_y + l_f r}{v_x} - \tan^{-1} \left(\frac{3\mu F_z}{C_\alpha} \right). \quad (8)$$

As long as δ remains within the bounds given in (7) and (8), the front tire slip angle will remain under its saturation value.

IV. HAPTIC SUPPORT SYSTEM DESIGN

The goal of the controller is to keep the vehicle within the handling limits, by restricting the road-wheel angle to the boundaries defined in (7) and (8). In order to achieve this objective while keeping the driver in the control loop, the following control architecture is proposed. A high-level MPC controller is designed for predicting the vehicle states and the road-wheel angle over a certain time horizon. These predictions serve as input to the low-level HSC controller which calculates the safe steering envelope for every predicted timestep and subsequently provides haptic feedback on the steering wheel in case the envelope is violated. The overall structure of the predictive haptic driver support system is shown in Figure 2. The complete design of the proposed system is treated in great detail in Appendix C.

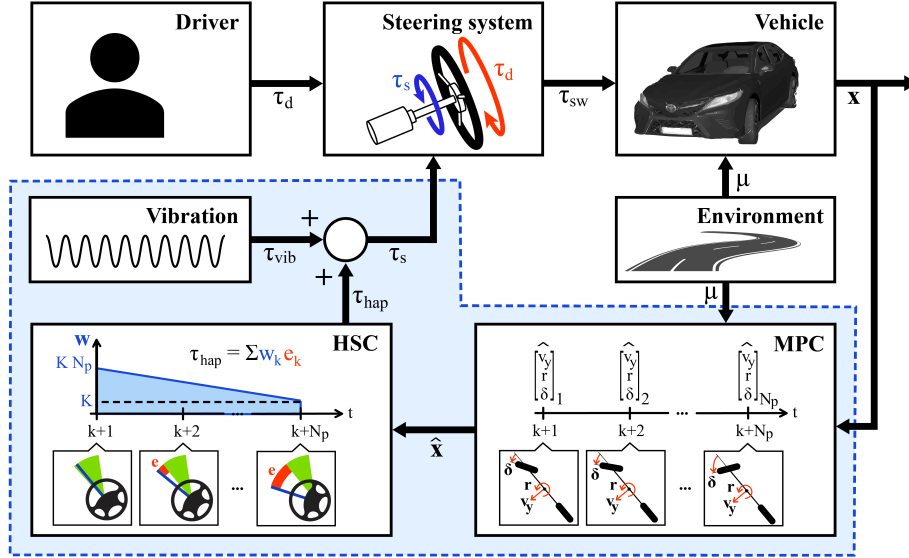


Fig. 2: Controller diagram: The MPC predicts the future vehicle states, which are then used to compute the safe steering envelope (in green) for each timestep of the prediction horizon. An error e (in red) is produced if the predicted steering angle leaves the envelope. The generated haptic torque τ_{hap} is equal to the weighted sum of the errors where the weighting function w is linearly decreasing. The total support torque τ_s is equal to the sum of τ_{hap} and τ_{vib} .

A. High-level Control

An optimization problem is solved over a receding time horizon, while taking into account modelled vehicle dynamics, constraints, and desired objectives. In this study, the state vector x is defined as $x = [v_y, r, \delta]$ and the control input u is the steering velocity $u = \dot{\delta}$. The goal of the controller is to predict the driver input as closely as possible, without *a priori* knowledge of the path. For short time intervals, the steering velocity can be assumed constant such that the future road-wheel angle is computed by integrating the steering velocity over time. Furthermore, the input $\dot{\delta}$ should not be too large and the resulting δ should not deviate significantly from the initial road-wheel angle at the start of the prediction. These requirements are reflected in the chosen least-squares cost function. The optimization problem that the MPC solves to predict the future vehicle states is formulated as follows:

$$\begin{aligned} \min_{\dot{\delta}} \quad & \sum_{k=1}^{N_p} \left(\|\dot{\delta}_k\|_{Q_1}^2 + \|\dot{\delta}_k - \dot{\delta}_0\|_{Q_2}^2 + \|\delta_k - \delta_0\|_{Q_3}^2 \right) \\ \text{s.t.} \quad & x[k+1] = Ax[k] + Bu[k] + d[k] \\ & -\frac{\pi}{2} \leq \delta \leq \frac{\pi}{2} \end{aligned} \quad (9)$$

In the cost function, δ_0 and $\dot{\delta}_0$ are the initial road-wheel angle and velocity, respectively, and Q_1 , Q_2 and Q_3 are the tuning weights. Furthermore, A , B and d are respectively the system matrix, the input matrix and the disturbance input associated with the current state from the discrete state-space vehicle model. The discrete state-space is obtained by discretizing the continuous bicycle model defined in (1) and (2), combined with the slip and tire model defined in (3), (4), (5) and (6). The constraint on δ reflects the actuation limits of the steering system.

B. Low-level Control

From the obtained predictions, the low-level controller calculates the safe steering envelope boundaries for each timestep of the prediction horizon using (7) and (8). If the predicted road-wheel angle exceeds the calculated limits at any point, an error term is generated for that particular timestep as follows:

$$e_k = \begin{cases} \delta_{lim,k}^- - \delta_k, & \text{if } \delta_k < \delta_{lim,k}^- \\ 0, & \text{if } \delta_{lim,k}^- \leq \delta_k \leq \delta_{lim,k}^+ \\ \delta_{lim,k}^+ - \delta_k, & \text{if } \delta_{lim,k}^+ < \delta_k \end{cases} \quad (10)$$

The error of each particular timestep k is multiplied by a decreasing weighting term $(N_p - k + 1)$ in order to assign more importance to imminent errors compared to errors further ahead in the horizon. The weighted sum is scaled by a tuning factor K in order to generate a haptic torque τ_{hap} which is noticeable but can also be overruled by the driver:

$$\tau_{hap} = K \sum_{k=1}^{N_p} (N_p - k + 1) e_k. \quad (11)$$

In addition to the increase in steering torque, torque vibrations τ_{vib} of fixed amplitude A_{vib} and frequency f_{vib} are also added to the steering wheel. These vibrations were perceived as a positive influence on user acceptance during the pilot study. The total support torque τ_s delivered by the system to the steering wheel is equal to $\tau_{hap} + \tau_{vib}$.

C. Implementation

The resulting optimization problem in (9) is nonlinear and requires the use of efficient solvers in order to guarantee real-time implementation. For this study, the problem is solved

using FORCES PRO NLP solver [26][27], using the real-time variant of the sequential quadratic programming method. The controller has been implemented in MATLAB Simulink, with a sample time of 0.01s. It was noted that without information about the incoming path, for normal driving conditions, predictions based on the current vehicle state and driver input are only accurate for around 0.5s. Beyond this time, steering velocity cannot be assumed to be approximately constant anymore and predictions deviate significantly from the actual states. Therefore, a prediction horizon of 0.5s was chosen as it results in good prediction accuracy while allowing enough margin for understeer to be detected ahead of time. MPC tuning weights were adjusted to improve the accuracy of the state prediction. The selection of the haptic torque tuning factor K was done during the pilot study with an expert driver to achieve a desired level of control authority. All relevant controller parameters are summarized in Table I.

Parameter	Description	Value
T_c	controller sample time in s	0.01
N_p	number of timesteps in prediction horizon	50
Q_1	weight on steering velocity	10
Q_2	weight on steering velocity deviation	2000
Q_3	weight on steering angle deviation	0.1
K	haptic torque tuning factor	0.05
A_{vib}	haptic vibration amplitude in Nm	0.5
f_{vib}	haptic vibration frequency in Hz	21

TABLE I: Controller parameters

Figure 3 illustrates the controller operation during one of the experimental trials described in the next section. The two uppermost plots show the predicted states, \hat{r} and \hat{v}_y , coming from the MPC at $t = 38.17$ s for the length of the prediction horizon, until $t = 38.67$ s. The predicted steering input $\hat{\delta}$ exceeds the calculated safe steering boundary around the 38.6s mark, as shown in the third plot. The support torque τ_s is provided as soon as the limit violation is predicted, as can be seen in the last plot. For reference, the recorded vehicle states and driver input are also shown.

V. EXPERIMENT DESIGN

In order to validate the proposed system, a driver-in-the-loop study was performed at Toyota Motor Europe on a high-fidelity driving simulator, which uses a static mock-up of a Toyota production vehicle in front of a 210° projection screen. The graphics were rendered with rFpro software based on an IPG CarMaker scenario. The simulator uses a vehicle dynamics model with a proprietary steer-by-wire model and a Toyota production vehicle parametrisation. The control loading system is used to measure the driver's steering input and provide realistic steering feedback during driving [28], alongside the additional torque provided by the haptic support system. The complete setup can be seen in Figure 4.

Two variations of the haptic support system have been investigated:

- *No support*: this case represents manual steering equivalent to a conventional vehicle with electric power assisted steering. There is no additional haptic torque added to the steering wheel. This variation is used as baseline.

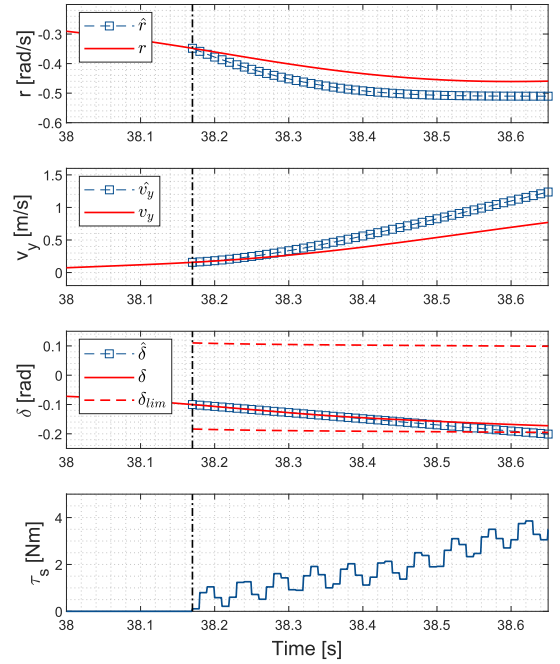


Fig. 3: State prediction at $t = 38.17$ s during a driver-in-the-loop experimental trial



Fig. 4: Driving simulator at Toyota Motor Europe, Belgium

- *Haptic support*: in this case, there is additional haptic torque together with vibrations added to the steering wheel when the controller predicts the violation of the safe steering envelope.

A. Driving Scenarios

The aim of the conducted experiment was to validate the proposed system under naturalistic driving conditions during which the vehicle approaches the limits of handling. A 1km long circuit was designed with straight sections as well as curves with a constant 50m cornering radius. The tire-road friction coefficient μ was set to 0.8. The vehicle velocity was set to 70km/h to recreate a situation in which the vehicle enters a corner with excessive speed and is close to the limits of handling. Similar to the study of Othman et al. [29] on overtaking maneuvers in curves, an obstacle was set to

obstruct the right lane on one of the corners. As a consequence, participants were forced to perform an avoidance maneuver in the middle of a turn. This situation is known to cause a large lateral acceleration peak which makes it even more difficult to negotiate the turn. The complete circuit can be seen in Figure 5.

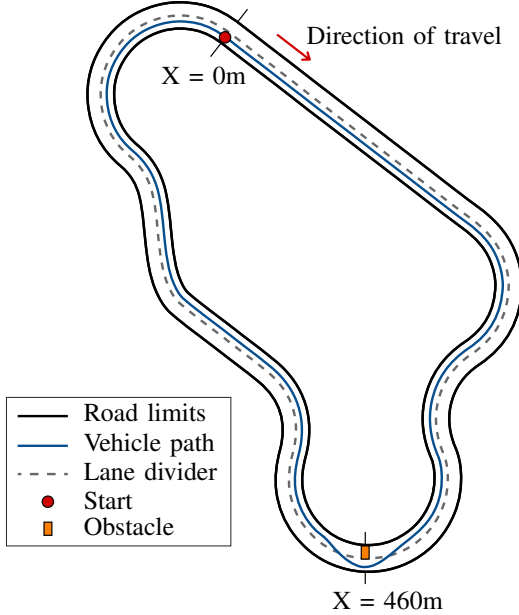


Fig. 5: Experimental circuit

B. Participants

In total, 32 participants conducted the experiment, all with a valid driving license. Among them, there were expert test drivers with professional experience in handling limit driving. Prior to conducting the experiment, each participant completed 6 practice runs on the same circuit, but without the obstacle: 3 runs without steering support and 3 runs with the haptic support enabled. This allowed them to become familiar with the driving simulator and the additional haptic torque on the steering wheel. The participants were instructed to remain in the right lane while driving, without using the gas or brake pedal. The practice runs without haptic support have been used to classify between regular and novice drivers. Those who managed to stay within the lane's boundaries were classified as regular drivers (N=15), while those who left the lane were classified as novice drivers (N=12). Expert drivers (N=5) were selected based on their professional qualifications.

From self-reported data, the mean age of an expert driver was 39.4 years (SD = 4.22), with an average driving license possession of 20.8 years (SD = 5.07). The average age of a regular driver was 28.53 years (SD = 7.12) with an average driving license possession of 10.4 years (SD = 7.11). Finally, the average age of a novice driver was 25.33 years (SD = 2.39) with an average driving license possession of 5.51 years (SD = 2.98).

C. Experimental Procedure

The experimental trials were performed immediately after the practice session. Each participant was instructed to keep the right lane as much as possible, with the gas and brake pedals deactivated. An obstacle was obstructing the right lane at the 460m mark, right in the middle of a corner. Participants were asked to avoid any obstacle by moving to the left lane and then returning to the right lane as fast as they could. Each test subject performed 6 runs on the circuit: 3 runs with the haptic support and 3 runs without any support. The runs were in random order (Randomised Latin Square Method) to mitigate the learning effect. The collected data includes information such as vehicle states, tire forces and slip angles, the position of the vehicle on the circuit, as well as the steering angle and torque. At the end of the experiment, participants were asked to complete the NASA task load index (TLX) evaluation form to assess the following subjective metrics: *mental demand*, *physical demand*, *performance* and *frustration*. Participants were asked to evaluate each metric on a scale from 1 to 21 (see Appendix F).

VI. RESULTS

The collected data from the runs with and without support of all 32 participants was averaged separately, first per participant and then across all participants of the same category. Statistical significance of the results is assessed using a two-tailed paired *t*-test, at 5% significance level.

The following section presents experimental results from the obstacle avoidance scenario only. The analysis of practice runs can be consulted in Appendix D, and the individual results for each participant are shown in Appendix E.

A. Objective Evaluation

Figure 6 presents the experimental results as a function of the distance for each of the three driver categories. The first row of plots (plots 6a to 6c) shows the vehicle lateral deviation from the center of the lane. As can be seen, the influence of haptic support on the vehicle path varies for different driver categories. In the case of expert drivers, the haptic support has no noteworthy effect with both trajectories largely overlapping. Novice drivers reduced their peak lateral deviation when driving with the haptic support. A significant change in trajectory is observed in the case of regular drivers. Table II presents a comparison of the means of the maximum lateral deviations calculated for each driver category. Regular drivers significantly reduced their peak lateral deviation by 11.28% when driving with haptic support compared to baseline.

Drivers	No support	Haptic support	p-value
Expert	6.63m (0.87)	6.60m (0.91)	0.9595
Regular	8.14m (1.51)	7.22m (1.52)	0.0113
Novice	8.55m (1.52)	8.30m (1.68)	0.4568

TABLE II: Averaged maximum lateral deviation for each driving mode, for each driver category (standard deviations in parentheses)

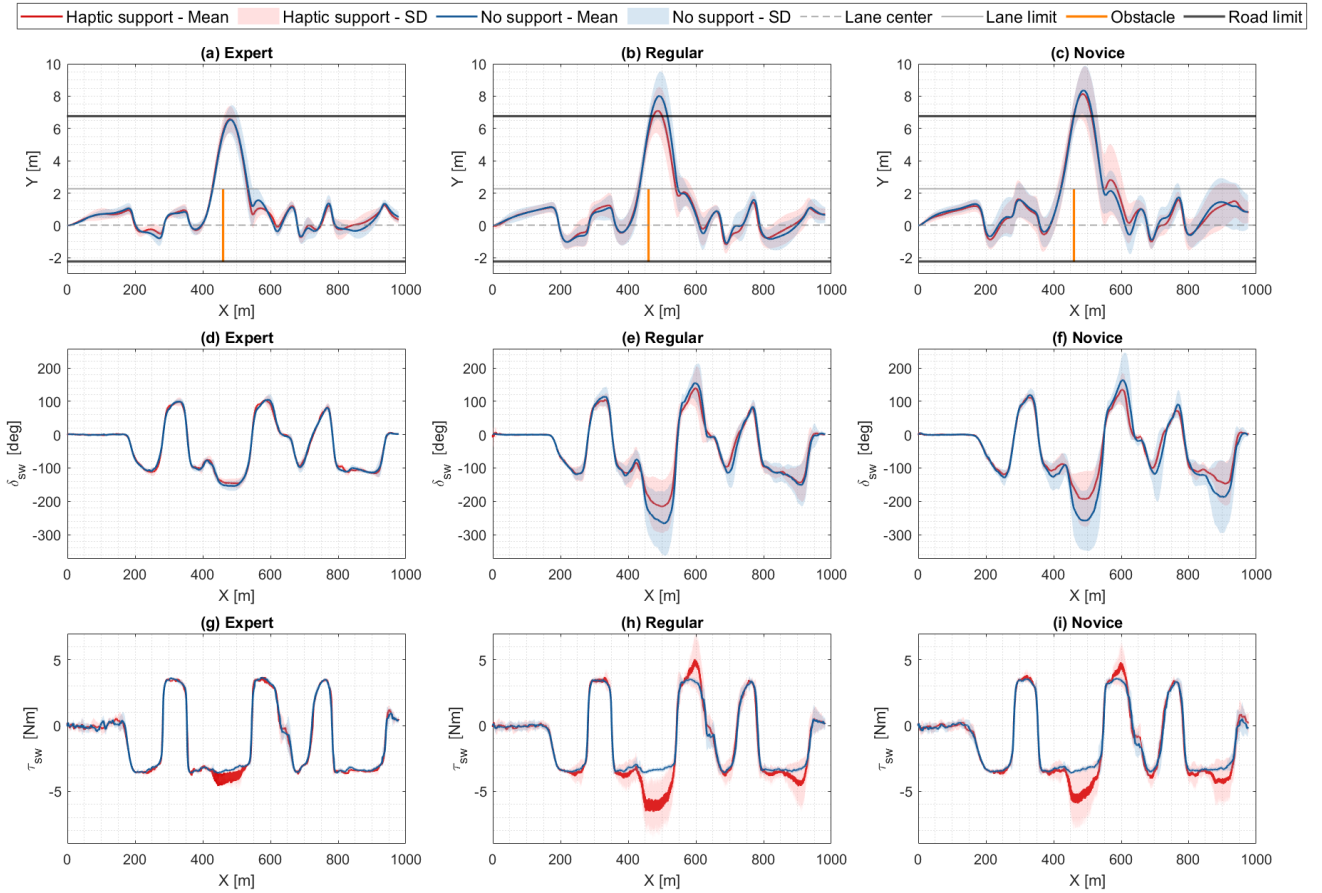


Fig. 6: Experimental results: mean values (solid lines), and standard deviations (shaded areas) for the 2 support cases, plotted for each driver group

The analysis of the averaged root-mean-square (RMS) value of the steering wheel angle in the vicinity of the obstacle, from $X=400\text{m}$ to $X=550\text{m}$, is shown in Table III. The haptic steering support significantly reduced the steering angle for regular and novice drivers, by 16.91% and 25.74% respectively. The difference in steering angle during the experiment can also be observed in Figure 6 (plots 6d to 6f).

Drivers	No support	Haptic support	p-value
Expert	125.15° (7.65)	121.28° (8.67)	0.3846
Regular	200.31° (61.33)	166.45° (56.69)	0.0025
Novice	195.24° (68.32)	144.99° (46.84)	0.0077

TABLE III: Averaged RMS values of steering wheel angle from $X=400\text{m}$ to $X=550\text{m}$ (around the obstacle) for each driving mode, for each driver category (standard deviations in parentheses)

Table IV presents the RMS values of the total torque on the steering wheel on the interval from $X=400\text{m}$ to $X=550\text{m}$. The difference in total steering torque between baseline and proposed system is significant for all categories of drivers, with an increase in torque of 10.23%, 38.83%, and 27.27% for expert, regular, and novice drivers, respectively. This indicates that the haptic support activated on average for all participants,

regardless of their driving skills. This is illustrated in Figure 6 (plots 6g to 6i), which shows an increase in the measured torque on the steering wheel between $X=400\text{m}$ and $X=550\text{m}$ for all drivers.

Drivers	No support	Haptic support	p-value
Expert	3.24N (0.03)	3.60N (0.30)	0.0390
Regular	3.20N (0.07)	4.98N (1.30)	<0.001
Novice	3.20N (0.08)	4.39N (1.28)	0.0095

TABLE IV: Averaged RMS values of steering wheel torque from $X=400\text{m}$ to $X=550\text{m}$ (around the obstacle) for each driving mode, for each driver category (standard deviations in parentheses)

Lastly, the RMS lateral force values for the front axle can be found in Table V, on the interval from $X=400\text{m}$ to $X=550\text{m}$. A significant difference can be noted for regular and novice drivers, who utilised respectively 1.00% and 1.03% additional lateral force during the obstacle avoidance maneuver when driving with haptic support.

B. Subjective Evaluation

The averaged results of the NASA-TLX evaluation form are summarized separately for expert, regular and novice

Drivers	No support	Haptic support	p-value
Expert	6896.5N (79.14)	6963.3N (101.44)	0.0965
Regular	6737.1N (204.39)	6804.9N (174.14)	0.0424
Novice	6758.2N (228.62)	6828.8N (204.15)	0.0106

TABLE V: Averaged RMS values of lateral force at the front axle from X=400m to X=550m (around the obstacle) for each driving mode, for each driver category (standard deviations in parentheses)

driver categories, in Tables VI, VII and VIII, respectively. A significant decrease in mental demand is reported by novice drivers. Regular drivers report a significant increase in self-assessed performance when driving with haptic support. Also, a significant decrease in perceived frustration can be observed for novice drivers when aided by haptic support compared to no support.

Metric	No support	Haptic support	p-value
Mental demand	6.80 (5.36)	6.60 (5.13)	0.3739
Physical demand	5.20 (5.02)	6.00 (4.47)	0.3739
Performance	15.40 (2.97)	16.00 (2.65)	0.2080
Frustration	8.6 (6.80)	9.8 (8.70)	0.3883

TABLE VI: NASA-TLX evaluation results for expert drivers, for each driving mode (standard deviations in parentheses)

Metric	No support	Haptic support	p-value
Mental demand	12.00 (4.50)	11.60 (4.24)	0.6044
Physical demand	9.60 (3.81)	10.07 (4.48)	0.5892
Performance	12.47 (3.56)	14.67 (3.58)	0.0176
Frustration	9.33 (4.81)	9.13 (4.75)	0.8003

TABLE VII: NASA-TLX evaluation results for regular drivers, for each driving mode (standard deviations in parentheses)

Metric	No support	Haptic support	p-value
Mental demand	14.50 (4.03)	11.58 (5.00)	0.0431
Physical demand	12.08 (5.79)	10.67 (4.77)	0.3474
Performance	10.58 (3.94)	11.33 (5.16)	0.6975
Frustration	11.58 (4.56)	8.33 (4.33)	0.0310

TABLE VIII: NASA-TLX evaluation results for novice drivers, for each driving mode (standard deviations in parentheses)

After the experiment, participants were also asked about their interest in having the haptic support system in their own personal vehicle, should such technology become available on the market. The results revealed that 3 out of 5 expert drivers are interested in having such a system installed. In the case of regular drivers, a vast majority of 13 out of 15 participants expressed their desire for its implementation. Similarly, among novice drivers, 10 out of 12 participants showed interest in having haptic support installed in their vehicles.

C. Discussion

The results show that haptic driver support does impact the drivers, however, the degree to which a driver is influenced

greatly depends on their driving skills. Regular drivers seem to particularly benefit from the haptic support, which allows them to deviate significantly less from the road. This is also reflected by the increase in self-assessed performance for regular drivers in the NASA-TLX form. This improvement in performance can be linked to the decrease in steering wheel angle during obstacle avoidance, which allows more lateral force to be generated at the front axle. It should be noted that regular drivers exhibit similarities with expert drivers in terms of steering wheel angle, front axle lateral force and lateral deviation when driving with the haptic support system.

Novice drivers also show a significant reduction in their steering input, along with a significant increase in lateral force on the front axle. However, no significant decrease in lane deviation is noticed. More research is needed in this area, however, factors like reaction time and how early a driver starts the evasive maneuver could be of importance. Nevertheless, novice drivers scored significantly lower on the reported frustration metric and mental demand. Hence, the proposed system also has a positive influence on less experienced drivers and can help reduce the perceived workload during an emergency maneuver.

Lastly, no significant differences can be found for expert drivers in terms of objective or subjective metrics other than the total measured torque on the steering wheel. While driving with both controller variations, expert drivers outperformed all the other drivers in terms of minimizing lane deviation. On average, they generated the largest lateral force at the front axle while using the smallest steering input to perform the evasive maneuver. Furthermore, they scored the lowest on both mental and physical demand metrics. Therefore, haptic support systems have no significant influence on expert drivers, who can reliably assess the situation by themselves. In fact, haptic support could be linked with a slight increase in frustration reported by expert drivers, however the difference is not statistically significant. More research should be done on identifying relevant differences between expert and regular/novice drivers in emergency scenarios that could be linked with safer maneuvers.

VII. CONCLUSION

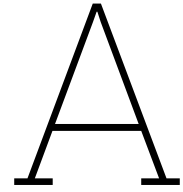
In this study, a predictive haptic driver support system was proposed with the aim of mitigating vehicle understeer. The system operates by intuitively alerting the driver about incoming front tire saturation limits in advance. In order to validate the system, a driving simulator study was performed involving an obstacle avoidance maneuver in the middle of a turn. Results demonstrate that haptic support has a positive impact on regular drivers' behavior, characterized by a reduced RMS steering angle value compared to manual steering. This results in higher lateral force at the front axle which translates to a smaller lateral deviation from the lane. The proposed system also positively influenced novice drivers in reducing their steering input during the maneuver, and significantly increased the lateral force at the front tires. However, no significant decrease in lane deviation has been observed for novice drivers. Subjective evaluation indicates a significant

increase in self-assessed performance for regular drivers who drove with haptic support. Similarly, novice drivers report significantly reduced mental demand and frustration when haptic support is active. Expert drivers are the least affected by the haptic support system and show no significant difference in performance or reported subjective metrics.

Future research focuses on adapting the proposed haptic driver support to scenarios with varying vehicle speeds. The system could be extended to provide support in adjusting the speed and the steering input at the same time with integrated vehicle control. The combination of the haptic driver support with differential braking offers an interesting direction for further investigation.

REFERENCES

- [1] M. Kyriakidis, C. van de Weijer, B. van Arem, and R. Happee, "The deployment of advanced driver assistance systems in Europe," in *Proceedings of 22nd ITS World Congress, Bordeaux, France*, 2015.
- [2] R. Elvik, "International transferability of accident modification functions for horizontal curves," *Accident Analysis & Prevention*, vol. 59, pp. 487–496, 2013.
- [3] M. Klomp, M. Lidberg, and T. Gordon, "On optimal recovery from terminal understeer," *Proceedings of the Institution of Mechanical Engineers, Part D: Journal of Automobile Engineering*, vol. 228, no. 4, pp. 412–425, 2014.
- [4] S. Othman, R. Thomson, and G. Lannér, "Identifying critical road geometry parameters affecting crash rate and crash type," in *Annals of advances in automotive medicine/annual scientific conference*, vol. 53, 2009, pp. 155–165.
- [5] C. Hildebrandt, M. Schmidt, M. Sedlmayr, O. Pion, G. Büyükyildiz, and F. Küçükay, "Intuitive steering assistance in critical understeer situations," *Traffic injury prevention*, vol. 16, no. 5, pp. 484–490, 2015.
- [6] J. Takahashi, M. Yamakado, S. Saito, and A. Yokoyama, "A hybrid stability-control system: combining direct-yaw-moment control and g-vectoring control," *Vehicle system dynamics*, vol. 50, no. 6, pp. 847–859, 2012.
- [7] L. Zhang, H. Chen, Y. Huang, P. Wang, and K. Guo, "Human-centered torque vectoring control for distributed drive electric vehicle considering driving characteristics," *IEEE Transactions on Vehicular Technology*, vol. 70, no. 8, pp. 7386–7399, 2021.
- [8] J. Reason, *Human error*. Cambridge University Press, 1990.
- [9] J. Rasmussen, "Skills, rules, and knowledge; signals, signs, and symbols, and other distinctions in human performance models," in *IEEE Transactions on Systems, Man, and Cybernetics*, vol. SMC-13, 1983, pp. 257–266.
- [10] D. Abbink, T. Carlson, M. Mulder, J. De Winter, F. Aminravan, T. Gibo, and E. Boer, "A topology of shared control systems—finding common ground in diversity," *IEEE Transactions on Human-Machine Systems*, vol. 48, no. 5, pp. 509–525, 2018.
- [11] M. Marciano, S. Diaz, J. Perez, and E. Irigoyen, "A review of shared control for automated vehicles: Theory and applications," *IEEE Transactions on Human-Machine Systems*, vol. 50, no. 6, p. 475–491, 2020.
- [12] C. E. Beal and J. Gerdes, "Model predictive control for vehicle stabilization at the limits of handling," *IEEE Transactions on Control Systems Technology*, vol. 21, no. 4, pp. 1258–1269, 2012.
- [13] A. Balachandran, M. Brown, S. M. Erlien, and J. C. Gerdes, "Predictive haptic feedback for obstacle avoidance based on model predictive control," *IEEE Transactions on Automation Science and Engineering*, vol. 13, no. 1, pp. 26–31, 2015.
- [14] D. Hrovat, S. Di Cairano, H. E. Tseng, and I. V. Kolmanovsky, "The development of model predictive control in automotive industry: A survey," in *2012 IEEE International Conference on Control Applications*, 2012, pp. 295–302.
- [15] A. Lazcano, T. Niu, X. Akutain, D. Cole, and B. Shyrokau, "Mpc-based haptic shared steering system: A driver modeling approach for symbiotic driving," *IEEE/ASME Transactions on Mechatronics*, vol. 26, no. 3, pp. 1201–1211, 2021.
- [16] T. Gordon, M. Klomp, and M. Lidberg, "Strategies for minimizing maximum off-tracking resulting from over-speed in curves," in *Proceedings of 11th International Symposium on Advanced Vehicle Control, Seoul, South Korea*, 2012.
- [17] Y. Gao and T. Gordon, "Optimal control of vehicle dynamics for the prevention of road departure on curved roads," *IEEE Transactions on Vehicular Technology*, vol. 68, no. 10, pp. 9370–9384, 2019.
- [18] V. Fors, B. Olofsson, and L. Nielsen, "Yaw-moment control at-the-limit of friction using individual front-wheel steering and four-wheel braking," *IFAC-PapersOnLine*, vol. 52, no. 5, pp. 458–464, 2019.
- [19] M. Yamakado and M. Abe, "An experimentally confirmed driver longitudinal acceleration control model combined with vehicle lateral motion," *Vehicle System Dynamics*, vol. 46, no. S1, pp. 129–149, 2008.
- [20] D. Katzourakis, "Driver steering support interfaces near the vehicle's handling limits," Ph.D. dissertation, Faculty of Mechanical, Maritime and Materials Engineering, Delft University of Technology, 2012.
- [21] J. Van Doornik, "Haptic feedback on the steering wheel near the vehicle's handling limits using wheel load sensing," MSc thesis, Faculty of Mechanical, Maritime and Materials Engineering, Delft University of Technology, 2014.
- [22] S. Kerst, B. Shyrokau, and E. Holweg, "A model-based approach for the estimation of bearing forces and moments using outer ring deformation," *IEEE Transactions on Industrial Electronics*, vol. 67, no. 1, pp. 461–470, 2019.
- [23] H. B. Pacejka, *Tire and Vehicle Dynamics, 3rd ed.* Oxford, U.K.: Butterworth-Heinemann, 2012.
- [24] R. Rajamani, *Vehicle dynamics and control*. Springer Science & Business Media, 2011.
- [25] E. Fiala, "Lateral forces on rolling pneumatic tires," *Zeitschrift VDI*, vol. 96, no. 29, pp. 973–979, 1954.
- [26] A. Domahidi and J. Jerez, "Forces professional," Embotech AG, url=https://embotech.com/FORCES-Pro, 2014–2019.
- [27] A. Zanelli, A. Domahidi, J. Jerez, and M. Morari, "Forces nlp: an efficient implementation of interior-point methods for multistage nonlinear nonconvex programs," *International Journal of Control*, pp. 1–17, 2017.
- [28] M. Damian, B. Shyrokau, X. C. Akutain, and R. Happee, "Experimental validation of torque-based control for realistic handwheel haptics in driving simulators," *IEEE Transactions on Vehicular Technology*, vol. 71, no. 1, pp. 196–209, 2021.
- [29] S. Othman, R. Thomson, and G. Lannér, "Are driving and overtaking on right curves more dangerous than on left curves?" in *Annals of Advances in Automotive Medicine/Annual Scientific Conference*, vol. 54, 2010, pp. 253–264.



Human-Machine Interaction

This chapter covers different approaches for human-machine interaction design, with a focus on driver assistance systems. The importance of considering the human in the design process is discussed, along the main points of attention for designing a human-machine interface. The theory discussed in this chapter serves as a basis for the design of the haptic driver support system.

A.1. Background

Human-machine interaction (HMI) is the study of the communication between humans and machines during task-oriented interactions, especially in physical environments [2]. The first mathematical models of the human operator were proposed in the 1940s [47], consisting of simple linear transfer functions that described human performance during a tracking task. In the 1960s, the mathematical human pilot model developed by McRuer [33] attempted to describe the human operator in terms of a closed-loop transfer function. McRuer noted that humans adapt to the process being controlled by changing their behaviour. Contemporary works from this period by Rashevsky et al. [40] demonstrated that the car and the driver form a complex feedback system with no clear distinction between purely “mechanical” and purely “human” aspects when it comes to system dynamics. This introduced the idea that the stability of the vehicle-driver system depends on the system as whole, not on the stability of its isolated components.

The growing research interest in this field, combined with rapid advances in sensing and computing technology allowed to deepen the understanding of the human-vehicle interaction with the emergence of ever more sophisticated driver models [31][38]. The state-of-the-art driver models today incorporate cognitive, neuromuscular and sensory dynamics which are combined into a single holistic model and allow to predict the behaviour of the driver and the vehicle together. Examples of such driver models have been developed at the Delft University of Technology [26][29] in recent years. However, it is important to note that there is no consensus in the scientific community about *the* correct driver modelling approach at the time of writing this thesis. Due to the nonlinearity and unpredictability of the human physical and mental processes, driver modelling remains an ongoing topic of research.

Nevertheless, the growing understanding of human behaviour influenced the development of control systems in the automotive industry. Originally, the goal of vehicle stability systems was to align the behavior of the vehicle with the intention of the driver. Examples of such systems include the ABS and the VSC. These systems infer the intended vehicle behaviour based on the velocity, acceleration and the angle of the steering wheel [49]. If the movement of

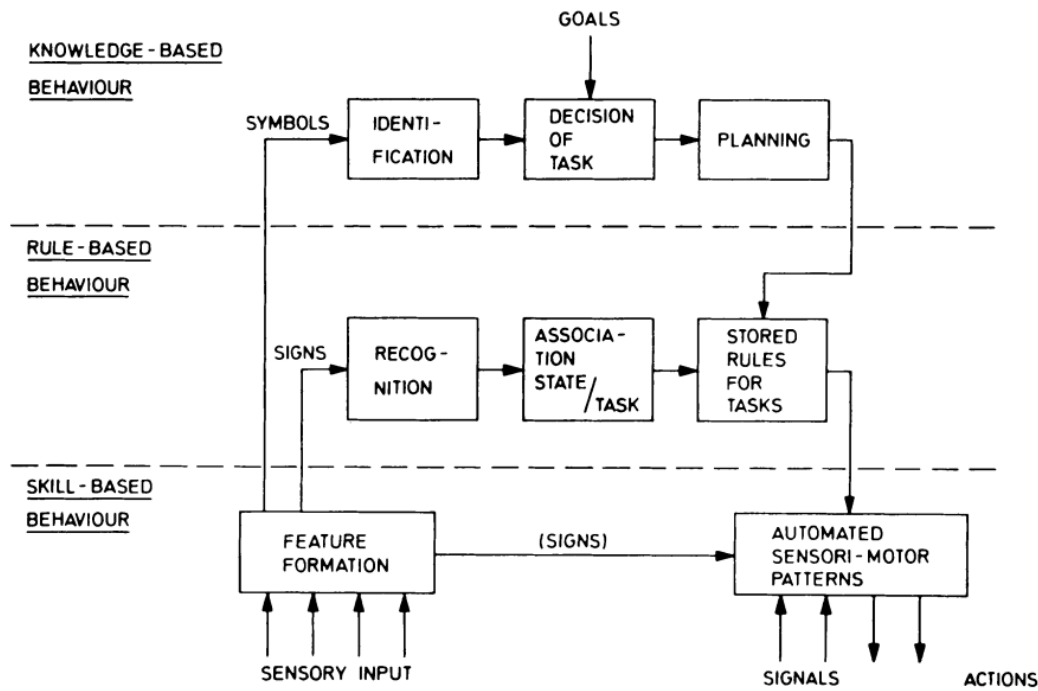


Figure A.1: Skill-based, rule-based and knowledge-based levels of performance of human operators according to Rasmussen [41]

the vehicle deviates from this intended course, the ABS and VSC can take corrective actions by applying or releasing the brakes on one or more wheels or by reducing engine power. This helps the driver regain control and brings the vehicle back in line with the intended course. However, as noted by Beal and Gerdes [5], this approach may be insufficient if the driver's intention itself is unsafe or exceeds the handling limits of the vehicle. Hence, control systems cannot simply enforce the driver's intention, they should also evaluate its feasibility in real-time. To address this issue, new safety systems have been developed that incorporate drivers in the control loop to shape their behavior in a way that promotes safety. This new generation of ADAS can support drivers by augmenting their situational awareness, provide assistance for specific control tasks or even fully take over control in case of an emergency [6][21].

A.2. Human Modes of Operation

Each driver assistance system is designed to help the driver perform a specific task in a faster, safer or in a more comfortable way. The nature of the task determines the most suitable type of interface between the human and the system. In order to have a better understanding of the sorts of tasks in which drivers engage, the skill-rule-knowledge (SRK) classification is introduced next.

Rasmussen developed the SRK classification in the 1980s [41]. This classification is based on information processing and provides a framework for understanding human performance in complex systems. According to Rasmussen, human performance can be divided into three categories: *skill-based*, *rule-based*, and *knowledge-based*. These three levels of performance are shown in Figure A.1.

Skill-based performance refers to the use of perceptual and motor skills to perform an task. In this mode of performance, the operator relies on well-learned, automatic responses and habitual actions that require minimal conscious thought. This allows to perform a task quickly and efficiently, without need for any extensive cognitive processing. Task executions at this

level are smooth and intuitive, as the person relies mainly on their muscle memory, reflexes and instinctive reactions.

Rule-based performance involves the use of explicit rules and procedures to achieve a desired goal. In rule-based performance, the operator relies on established routines that form an internal model of the situation. This allows individuals to leverage their past experience and knowledge to handle familiar tasks more efficiently and consistently.

Knowledge-based performance refers to the use of abstract knowledge, reasoning and planning to perform a task. When operating at the knowledge-based level, the operator needs to rely on his/her knowledge, logic and interpretation of the situation to make informed decisions and adapt to changing situations. This level of processing happens in novel contexts, when the operator is not yet familiar with the rules required to operate at the skill- or rule-based processing level.

According to Rasmussen [41], humans have a tendency to prefer performing at the lowest cognition level necessary to complete a task. This phenomenon to minimize the conscious effort and limit cognitive processing is also called *cognitive economy*. Only when the lower level performance mode is insufficient, humans will resort to a more effortful cognitive process and shift to a higher level of performance. Individuals can also practice to perform a task at a lower level of performance through repetition. With enough training, the task gradually shifts to a lower performance level, and can be executed accurately with little conscious thought.

When it comes to vehicle control, drivers have to simultaneously perform different tasks at different performance levels [2]. For instance, route planning over a long period of time might require the driver to operate at the knowledge-based level, whereas a successful lane-change maneuver requires the driver to perform a specific sequence of actions, distinct for rule-based performance. For the majority of drivers, steering is associated with skill-based performance [46]. It is an intuitive process relying on the driver's sensory-motor skills, which allows for rapid decision-making required for stable performance in highly dynamical situations.

According to Vicente et al. [50], automation can intuitively support the human operator only when the assistance system acts at an appropriate performance level, without pushing the process to a higher level than required by the demands of the task. For instance, providing driving direction in a visual way can be helpful for the driver because reading and interpreting symbols is related to knowledge-based processes, same as the navigation task. However, relying on purely visual signals for an emergency obstacle avoidance assistance might not be the most suitable method. Knowledge-based tasks are mentally demanding and require processing time, which does not go well with the urgency of the potential impact in the immediate future. Instead, a driver assistance system that operates at the skill-based level and supports the steering task fits better with the demands of the task. Such a system could provide intuitive guidance requiring the lowest levels of cognition, which would translate into lower driver reaction time, and thus a higher chance of a successful maneuver.

A.3. Human Error

According to Reason [42], human error mechanisms and human performance mechanisms are closely interconnected: errors are a natural aspect of human performance and can be caused by several different factors. Reason formulated the general error-modelling system (GEMS) based on Rasmussen's skill-rule-knowledge classification of human performance. He proposed the following dichotomy for the types of human errors encountered at each performance level:

- Skill-based level: Slips and lapses;
- Rule-based level: Rule-based mistakes;

- Knowledge-based level: Knowledge-based mistakes.

Slips and lapses are related to an execution failure: the desired outcome was not achieved because the performed actions did not go as planned. Even when the intention is correct, this type of error is often due to a sudden loss of attention, memory failure or mode confusion. Mistakes, either rule-based or knowledge-based, are related to a planning failure where the intention itself is not appropriate. The key difference between rule-based and knowledge-based mistakes lies in the source of the planning failure: rule-based mistakes arise either from the application of the wrong rules or from the application of the correct rules in the wrong situation, while knowledge-based mistakes are more complex and stem from a lack of understanding of the situation. The former can happen when the individual follows an established yet inadequate routine due to a misinterpretation of the problem or due to attentional lapses. The latter reflects an incomplete or inaccurate internal model of the situation at hand.

When considering the case of driving near the handling limits, the situation becomes inherently risky and prone to errors. Given the fact that such conditions are not encountered daily, drivers typically lack established rules or guidelines to rely on when approaching the limits of handling. In similar situations, humans are expected to switch to a higher level of performance in order to solve the problem. However, due to the urgency during an emergency maneuver, there is insufficient time to rely on higher levels of cognition to find a solution. Previous studies have shown that individuals under stress tend to react instinctively, relying on familiar patterns of behavior that have worked in the past [23]. Consequently, when understeer occurs, drivers tend to increase their steering angle input in an attempt to mitigate understeer. Unfortunately, applying this rule when the tires are already saturated only exacerbates the problem. This phenomenon, known as a *strong habit intrusion*, has been extensively studied in the literature by Rasmussen [41] and Reason [42]. It was also observed by Hildenbrandt et al. [22] during their own study on the intuitive steering assistance in critical understeer situations. This pattern of behaviour can be summarized in a driver error model shown in Figure A.2.

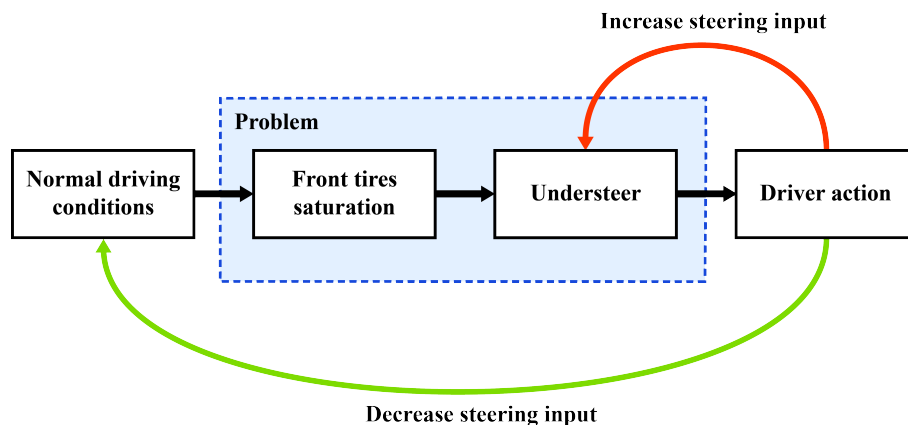


Figure A.2: Driver error model: the expected pattern of behaviour when encountering understeer

A.4. Shared Control

A successful implementation of driver steering assistance systems requires a combination of control inputs coming both from the driver and from the assistance system. An attractive approach to promote cooperation between humans and automation is the shared control paradigm. Shared control emerged from the field of HMI in the 1970's when the concept was first formulated by Sheridan and Verplank to categorize control tasks in which the human and the robot are active at the same time [43]. A formal definition of shared control was introduced

by Abbink et al.:

“In shared control, human(s) and robot(s) are interacting congruently in a perception-action cycle to perform a dynamic task that either the human or the robot could execute individually under ideal circumstances.” - Abbink et al.[2]

Shared control has become an interesting alternative to full automation in the automotive field. It enables the utilization of advanced sensing and computing capabilities of onboard computer systems while keeping the human driver in the control loop. By doing so, shared control mitigates the numerous pitfalls of full automation such as overreliance on the system, complacency, loss of situational awareness by the driver or degradation of driving skills [36][51].

According to Marcano et al. [32] who reviewed over 100 papers related to shared control for automotive applications, most studies focus on shared control of the steering task, with common use-cases being lane keeping, obstacle avoidance or control resumption. Furthermore, there are two different control frameworks for shared control of the steering task: *coupled* control and *uncoupled* control. In the coupled control framework, the wheels remain mechanically connected to the steering wheel and the controller interacts with the driver by applying haptic torque on the steering wheel. This allows drivers to always overrule the haptic guidance in case of disagreement with the automation by simply increasing their torque input. Alternatively, the uncoupled control framework relies on mixed-input control in which the driver input can be closely followed, modified or even fully ignored if it is deemed unsafe. This control framework requires a lack of mechanical linkage between the front wheels and the steering wheel and is thus only possible to implement on Steer-by-Wire (SbW) systems.

Haptic shared control (HSC) has been gaining in popularity thanks to its ability to be implemented on both coupled and uncoupled steering configurations [1][32]. According to Petermeijer et al. [37], who investigated the reported effects of HSC on driver performance, two distinct forms of haptic support can be found in literature. On the one hand, there are *warning* systems relying on vibrations, whereas on the other hand there are *guidance* systems which rely on continuous force application. From empirical studies in real or simulated driving conditions, it appears that warning systems are effective in reducing the reaction time of drivers compared to no warning systems. Haptic warnings also show a larger reduction in the number of collisions with a lead vehicle compared to auditory or visual warnings. However, they are also prone to cause annoyance in case of excessively early or false alarms. Guidance systems appear to improve driving performance compared to no guidance, with a significant decrease in control activity, as well as mental and visual demand. On the other side, drivers that use such systems often report higher physical workload compared to no guidance, due to the increase in force necessary to operate the control interface. They also suffer from after-effects, meaning that their driving performance is negatively affected when the haptic guidance is switched off after a prolonged period of exposure to it.

A.5. Summary

Following an extensive investigation into the development of driver assistance systems, there appears to be a paradigm shift in the design of new ADAS to include drivers in the loop, question their intentions and shape them accordingly to promote safety on the road. This has been largely facilitated by the emergence of new driver modelling approaches which allow to better understand and predict driver behaviour. However, driver modelling remains an active area of research due to the inherent nonlinearity, complexity and unpredictability of the human physical and mental processes. This makes it difficult for driver models to match the accuracy of other models in vehicle system dynamics. Nevertheless, several factors have been identified in literature to promote successful cooperation between humans and automation

systems, such as the skill-rule-knowledge classification by Rasmussen [41], which advocates driver steering assistance systems to act at the skill-based level. Furthermore, from the review of human error mechanisms, it becomes apparent that the driver support system should aim to resolve the strong-habit intrusion problem. A promising approach for such a system is the shared control paradigm, in which HSC appears to be the most popular modality for combining intentions of the driver and of the assistance system through the mutual exchange of forces on the steering wheel. From the literature survey done by Petermeijer et al. [37], haptic vibrations on the steering wheel are effective in reducing the reaction time of the drivers, and yield better results than equivalent auditory or visual warning systems. Haptic torque can also be applied continuously on the steering wheel to provide guidance. This has shown positive effects on reducing mental and visual demand.

B

Pilot Study

This chapter outlines the design, implementation and validation of a simple haptic driver support system for understeer mitigation. The aim of this study is to evaluate the benefits of providing different kinds of haptic torque feedback on the steering wheel when approaching the handling limits of the car. Methods for detecting the onset of understeer as well as the tire model used for this purpose are outlined first.

B.1. Understeer Detection

B.1.1. Principle of Operation

Forces that govern the handling of the vehicle depend on the relative motion of the vehicle with respect to the road. As the contact point of this interaction, the tires are of crucial importance for vehicle control. In this pilot study, an understeer detection method based on monitoring the self-aligning moment is chosen. This method relies on detecting a drop in the self-aligning moment of the front tires, which is indicative of the incoming tire saturation. In order to better understand the predictive nature of the self-aligning moment, an overview of the relevant tire mechanics is provided next.

This work uses a tire axis convention proposed by the Society of Automotive Engineers (SAE) as used by Pacejka in [35] which can be seen in Figure B.1. All forces and moments acting on the tire are shown in their positive orientation.

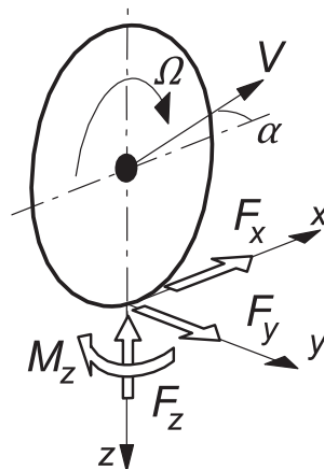


Figure B.1: Forces and moments acting on the tire [44]

There are three forces acting on the tire, namely the longitudinal force F_x , the lateral force F_y and the vertical force F_z alongside three moments, one around each respective axis. For the purpose of this study, only the self-aligning moment M_z acting around the z-axis is relevant. The x-axis is aligned with the plane of rotation of the wheel. The wheel heading direction is represented by the velocity vector V . The angle between the plane of rotation and the heading direction of the wheel is the slip angle α . The wheel rotates with an angular velocity Ω .

In general, the lateral force and the self-aligning moment are both nonlinear functions of the slip angle. Many other factors influence F_y and M_z such as the type of the tire used, the tire-road friction coefficient μ , the vertical tire load F_z , the camber angle, the temperature, etc. [35][44]. The lateral force acts at the interface between the tire and the road, which is not a single point but rather an area called the contact patch. In essence, F_y is the resultant of the lateral force distribution at the contact patch which is due to the elastic deformation of the tire [20]. Moreover, F_y does not act at the center of the contact patch. Due to the vehicle motion and deformation of the rubber treads, the force is applied at a certain distance away from the center. This distance is called the pneumatic trail t_p and it acts as a moment arm. This causes the lateral force to produce the self-aligning moment around the vertical axis of rotation. For a parabolic pressure distribution in the contact patch, the tire deflection begins on the edge opposite to the direction of motion called the trailing edge. This results in a large initial pneumatic trail value. As the slip angle increases, the tire deflects more and the lateral force distribution grows in area. This causes the pneumatic trail to shrink such that the resulting lateral force F_y is applied closer to the center of the contact patch. Eventually, the pneumatic trail vanishes completely and the self-aligning moment goes to zero, indicating that the tire reached its friction limit and is in pure side slip.

This effect is also widely used by expert drivers to feel the approaching handling limits so that they can react appropriately before it is too late. The self-aligning moment of the front tires is passed on to the steering rack and is then transmitted through the steering column to the steering wheel. A sudden drop in the self-aligning moment will translate into a drop of the steering wheel stiffness which can be perceived by a skilled driver. This pilot study attempts to use the information provided by the drop of the self-aligning moment to detect vehicle understeer, and provide intuitive haptic feedback to the driver in order to avoid excessive front wheel slip.

B.1.2. Tire Model

In order to quantify the behaviour of the tire, a mathematical tire model must be chosen. Such a model should be elaborate enough to capture all the tire dynamics of interest while avoiding unnecessary complexity which could make simulations computationally expensive. For this work, the nonlinear Fiala tire brush model [15] is chosen as it is able to accurately capture the tire behaviour up to, and including, the saturation limits [3]. In this model, the tire is portrayed as a single row of compliant bristles that deform when in contact with the road, as shown in Figure B.2. The tire brush model assumes steady-state cornering conditions such that the longitudinal tire force is equal to zero. Since only steady-state vehicle lateral motions are considered in this work, the simplified brush model is sufficiently accurate. Furthermore, the model assumes a parabolic pressure distribution at the contact patch, a rigid tire carcass and a constant friction coefficient [35]. Given these assumptions, the lateral force F_y can be described by equation (B.1) and the self-aligning moment M_z by equation (B.2). The complete derivation of the model is outlined in [35].

$$F_y = \begin{cases} C_\alpha \tan \alpha - \frac{C_\alpha^2}{3\mu F_z} |\tan \alpha| \tan \alpha + \frac{C_\alpha^3}{27\mu^2 F_z^2} \tan^3 \alpha, & \text{if } |\alpha| \leq \alpha_{lim} \\ \mu F_z \operatorname{sgn} \alpha, & \text{else} \end{cases} \quad (\text{B.1})$$

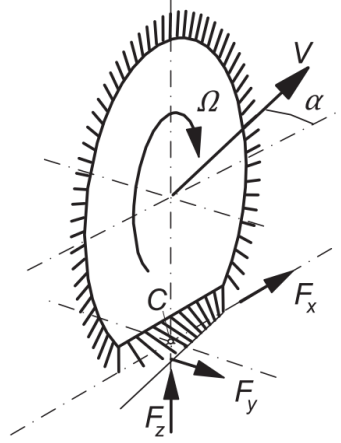


Figure B.2: Fiala tire brush model [35]

$$M_z = \begin{cases} -C_M \tan \alpha + \frac{C_M C_\alpha}{\mu F_z} |\tan \alpha| \tan \alpha - \frac{C_M C_\alpha^2}{\mu^2 F_z^2} \tan^3 \alpha \\ + \frac{C_M C_\alpha^3}{27 \mu^3 F_z^3} |\tan^3 \alpha| \tan \alpha, & \text{if } |\alpha| \leq \alpha_{lim} \\ 0, & \text{else} \end{cases} \quad (\text{B.2})$$

where α_{lim} is the slip angle at which the tire has reached the limits of friction, given by:

$$\alpha_{lim} = \tan^{-1} \left(\frac{3\mu F_z}{C_\alpha} \right). \quad (\text{B.3})$$

From equations (B.1) and (B.2) it can be noticed that for very small values of α (using small angle approximation, we can assume that $\tan(\alpha) \approx \alpha$), both F_y and M_z vary approximately linearly with the slip angle. In this linear region, the rate of change of F_y with respect to α is called the cornering stiffness C_α . Similarly, the rate of change of M_z with respect to α is called the aligning stiffness C_M . As the slip angle increases, the higher order terms become more and more important and the tire enters the nonlinear regime of motion. Once the slip angle reaches α_{lim} , the tire is in pure side slip and the lateral force remains constant at the maximum saturation value whereas the self-aligning moment goes to zero. A plot of F_y , M_z and t_p as a function of the slip angle is shown in Figure B.3. In this plot, a is the tire contact patch length and θ_y has been defined for convenience as:

$$\theta_y = \frac{C_\alpha}{3\mu F_z}. \quad (\text{B.4})$$

From the nonlinear tire brush model given in equations (B.1) and (B.2), a relation can be obtained for the slip angle $\alpha_{M,max}$ at which the self-aligning moment reaches its peak value:

$$\alpha_{M,max} = \tan^{-1} \left(\frac{1}{4\theta_y} \right) = \tan^{-1} \left(\frac{3\mu F_z}{4C_\alpha} \right) \approx \frac{1}{4} \alpha_{lim}. \quad (\text{B.5})$$

As can be seen, if the slip angle at which the self-aligning moment peaks is known, the slip angle at which the lateral force peaks can be found using small angle approximation. Since the self-aligning moment always peaks before the lateral force, equation B.5 can be used to detect the front tire saturation in advance.

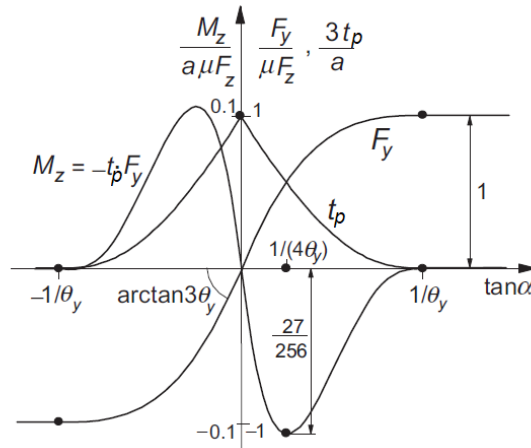


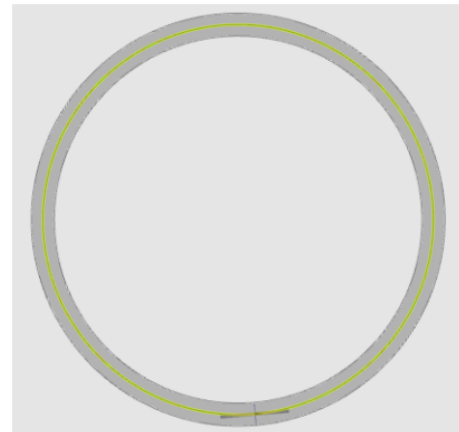
Figure B.3: Lateral force F_y , self-aligning moment M_z and the pneumatic trail t_p as a function of the slip angle α [35]

B.1.3. Validation

In order to validate the accuracy of the tire brush model, the calculated lateral force is compared with the high-fidelity vehicle model from the IPG CarMaker simulation software [7]. The simulated scenario is a steady-state constant radius cornering motion of a typical passenger vehicle (see Figure B.4a). The track has a constant radius of 42m and can be seen in Figure B.4b.



(a) IPG CarMaker vehicle model



(b) Steady-state constant radius circular track ($r=42m$)

Figure B.4: IPG CarMaker simulation scenario

In the simulated scenario, the vehicle starts from standstill and slowly accelerates until the limits of lateral adhesion are reached. Once the front tires are saturated, the vehicle is unable to negotiate the turn due to terminal understeer and eventually leaves the track. As the velocity changes slowly, the longitudinal load transfer as well as the longitudinal tire forces are negligible and the steady-state assumption is valid. The lateral force calculated using the tire brush model as a function of the slip angle is compared with simulation results from IPG CarMaker in Figure B.5 for different values of the tire-road friction coefficient. As can be seen, the lateral force fits closely to the simulation data. Furthermore, the slip angle at which the self-aligning moment peaks can be used to calculate the slip angle at which the lateral force will peak using equation (B.5). The instance at which the slip angle α is equal to the predicted

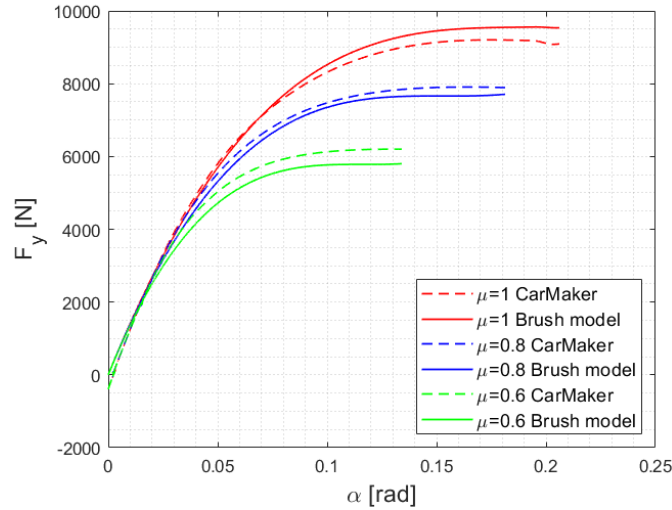


Figure B.5: Comparison between the tire brush model and the IPG CarMaker tire model in steady-state cornering for different values of μ

α_{lim} during the maneuver is represented by the red dotted line in the plots of Figure B.6, for several tire-road friction coefficient values.

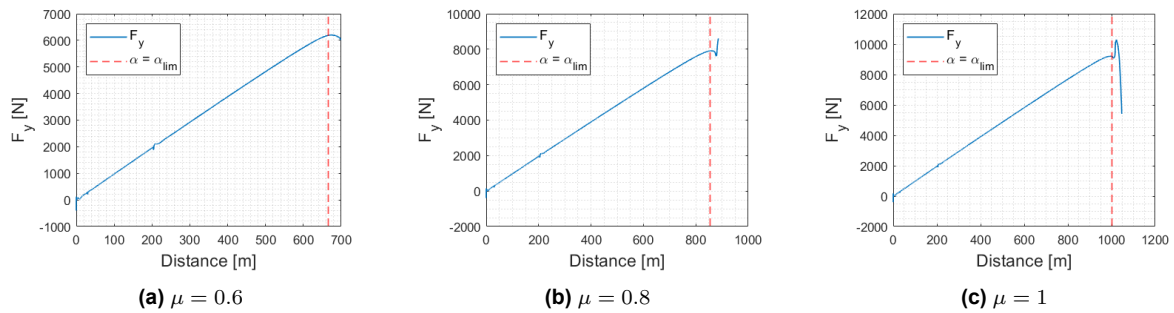


Figure B.6: Lateral tire force as a function of distance in steady-state cornering for different values of μ

The lateral force at the predicted slip angle instance is close to the actual maximum lateral force $F_{y,max}$ as can be seen from Figure B.6. The estimation is marginally conservative, in the sense that the predicted F_y peaks sooner than the actual F_y reaches its maximum. However, this should not be a problem for the design of a haptic driver support, as it will notify the driver sooner and therefore give the driver more time to react.

The above-mentioned results show that the tire brush model is capable of capturing the tire dynamics of interest, and this for different tire-road friction coefficients. If the self-aligning moment peak value is known, α_{lim} can be accurately predicted. Next section outlines the design of a simple haptic driver support system utilizing the predictive capabilities of the tire brush model.

B.2. Controller

B.2.1. Objective

The objective of the controller is two-fold. First, it should detect the self-aligning moment peak value. Using the corresponding slip angle measurement, this will allow to calculate the slip angle at saturation α_{lim} using equation B.5. Second, it should provide haptic guidance to the

drivers and guide them towards a safer steering input once the front slip angle reaches α_{lim} .

From the previously developed driver error model (see Appendix A), it is apparent that the type of human error that needs to be addressed is the strong-habit intrusion. Haptic support can help resolve this problem in two ways:

- **Awareness:** haptic torque on the steering wheel can signal to the driver that the vehicle is approaching its handling limits. This will promote a correct assessment of the regime of motion.
- **Guidance:** haptic torque can guide the driver towards a safer steering input in case of understeer. An increasing steering stiffness will promote a reduction of the steering angle, which will minimize the front tire slip.

In this way, the driver is more likely to interpret the situation correctly and react appropriately to minimize understeer.

B.2.2. Design

The controller diagram can be seen in Figure B.7. The controller takes as input the slip angle and the self-aligning moment from the front left and the front right tire, and the steering torque exerted by the driver on the steering wheel. The three main steps of the control algorithm are outlined as follows:

I. Self-aligning moment peak detection

The front axle self-aligning moment is calculated by taking the average of the self-aligning moments on the front left and right tires. Next, the averaged self-aligning moment is low-pass filtered with a cut-off frequency of 0.5Hz. By comparing the filtered signal with a delayed version of itself by 0.5s, the peak value can be detected. If the difference between the two is larger than the threshold of 1Nm, the peak detection block outputs 1. Otherwise, it outputs 0.

II. Lateral force peak prediction

The second step of the algorithm consists in monitoring the state of the M_z peak prediction block. When a peak is detected, the current slip angle at the front axle α_f is registered as $\alpha_{M,max}$. Next, using equation B.5, the slip angle α_{lim} at which the front tires saturate is calculated. This slip angle is then kept in memory and passed on to the next block.

III. Haptic torque generation

The calculated α_{lim} is continuously compared with the current slip angle of the front axle α_f . If α_f exceeds α_{lim} , the haptic steering support is activated. The added haptic torque is proportional to the driver input torque on the steering wheel, and opposite in sign. It can be tuned using a tuning gain which allows to set the degree of authority of the haptic support system. A value of 0.7 was chosen based on preliminary tests.

B.3. Experiment

In order to evaluate the effectiveness of the proposed haptic steering support, a driving simulator experiment was performed at Toyota Motor Europe. The dynamics were simulated using a high-fidelity vehicle model with a proprietary nonlinear steering system. The model was run on the IPG CarMaker physics engine [7] accessible through a MATLAB/Simulink interface. The graphics were rendered with rFpro software and displayed on a 210° projection screen. An actuated steering wheel was used to read the driver's steering input and provide realistic steering feedback during driving, alongside the additional haptic torque provided by the steering support system. The simulator setup can be seen in figure B.8.

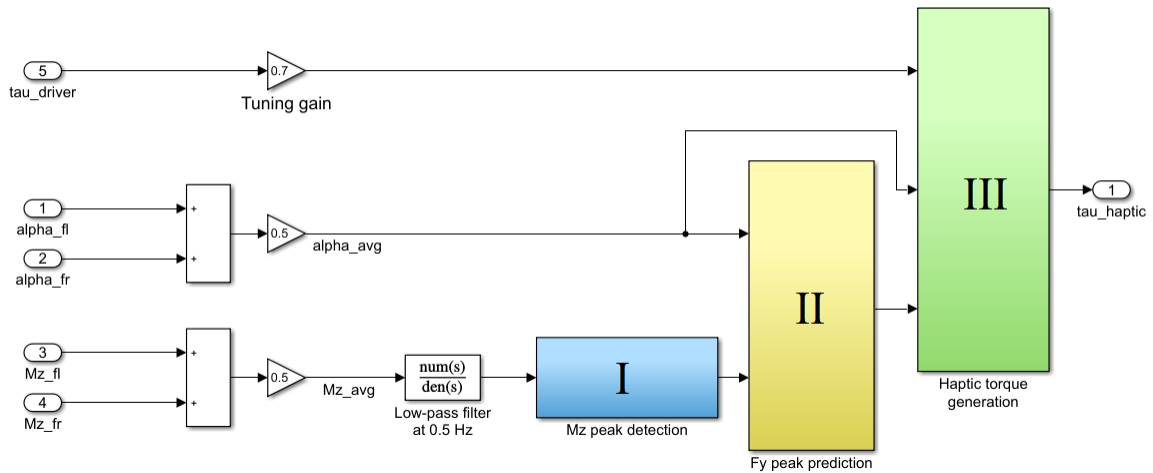


Figure B.7: Haptic controller block diagram



Figure B.8: Driving simulator at Toyota Motor Europe, Belgium

The driving scenario is a steady-state cornering maneuver on a circular track with a constant 42m radius. The tire-road friction coefficient has been set to $\mu = 0.6$ to replicate a low-grip wet surface. The task of the participants was to control the lateral motion of the vehicle to stay on the track at all times. The longitudinal velocity of the car was programmed to gradually increase at a slow rate such that the steady-state assumption remained valid. The vehicle speed would eventually get too high to negotiate the turn in which case the car would be forced to leave the road due to terminal understeer. The participants were instructed to keep the vehicle on the road as long as possible. Three variations of the haptic support system were investigated:

1. *No support*: this case is equivalent to manual steering on a normal car. There is no additional haptic torque added to the steering wheel. This variation is used as baseline for comparison with the other two haptic steering support variations.
2. *Haptic torque*: in this case there is additional haptic torque added to the steering wheel when the front axle slip angle α_f reaches α_{lim} . The torque is proportional to the steering torque input by the driver multiplied by a tuning gain.
3. *Haptic torque with vibration*: this case is similar to the above-mentioned variation with the addition of vibration with a frequency of 80 Hz. This communicates the limits of handling to the driver in a characteristic way for understeer situations.

In total, 4 participants took part in the pilot study. All participants were engineers at Toyota Motor Europe, with an average age of 24.5 years and 2.75 years of average driving experience. Each subject has been instructed to perform 3 trials with each variation of haptic support, after which the trials were averaged to get rid of intra-individual variability. Furthermore, the order in which the haptic support variations were presented was randomized for each participant in order to minimize human bias and learning effects. The specific version of the haptic guidance system used was communicated to the driver only after the completion of all 3 trials. The collected simulation data includes information about the vehicle states, tire forces, slip angles, as well as the steering angle and torque. After all the trials with one variation were finished, participants were also asked to fill-in a subjective evaluation form based on the NASA task load index (TLX) questionnaire (see Appendix F). The questionnaire is based on a 21-point scale with a total of 4 questions designed to subjectively assess the perceived workload by the driver. The metrics that were evaluated in this study are: *mental demand*, *physical demand*, *performance* and *frustration*. At the end of the experiment, participants were also asked to state which of the controller variation they prefer the most.

B.4. Preliminary Results

B.4.1. Objective Evaluation

The objective evaluation is based on metrics relevant for vehicle lateral stability. The difference between the 3 studied variations can be observed in Figure B.9 which depicts the average steering wheel torque τ_{sw} measured for each version of the haptic support.

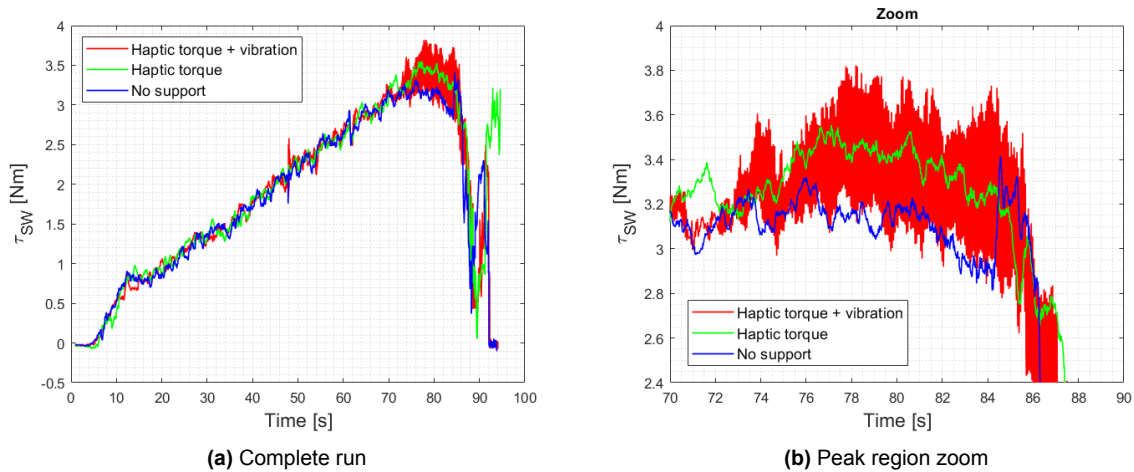


Figure B.9: Average steering wheel torque for each variation of haptic support

The steering wheel torque across the 3 cases in Figure B.9 is mostly the same in the time period between $t = 0s$ and $t = 70s$. During this time, the steering wheel torque increases as the vehicle gradually requires a larger roadwheel steer angle to negotiate the turn at increasing speed. The steering wheel torque measurements begin to differ around $t = 75s$. The added haptic torque by the controller acts in the opposite direction to the driver input torque, which requires an increase in torque from the driver to maintain the same steering angle. This effect is visible for both versions of the haptic support controller which resulted in an average increase of torque of 0.5Nm. Furthermore, the vibrations induced by the last controller variant can be noticed on the plot as well (in red).

Figure B.10 shows the average steering wheel angle δ_{sw} measured for each variation of the haptic support. In this plot, a uniform steering wheel angle can be noted across the studied variations from the beginning of the maneuver up until $t = 80s$. The steering angle starts to

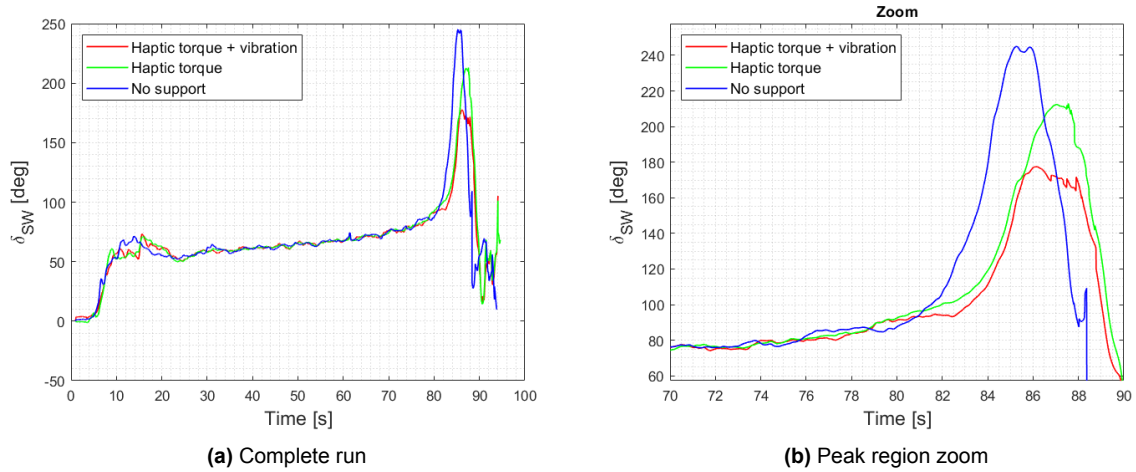


Figure B.10: Average steering wheel angle for each variation of haptic support

show a large disparity between the haptic support versions as the vehicle approaches the handling limits near $t = 80s$. Participants without haptic support exhibit the largest peak value for the steering angle (245.1°) and they also start increasing their steering input earlier than the two haptic support variations. Results from the runs in which participants drove with the haptic torque support enabled show a smaller peak steering angle of 213.1° . Participants also start increasing their steering input later compared to no support. Lastly, runs in which participants drove aided by the haptic torque and the vibrations show on average the smallest peak steering angle value (177.5°) and their increase in steering angle input happens the latest from the three variations. Consequently, it can be seen that the haptic steering support has a considerable effect on the steering behaviour of the drivers.

Finally, Figure B.11 shows the average lateral force F_y exerted by the front wheels for each variation of the haptic support.

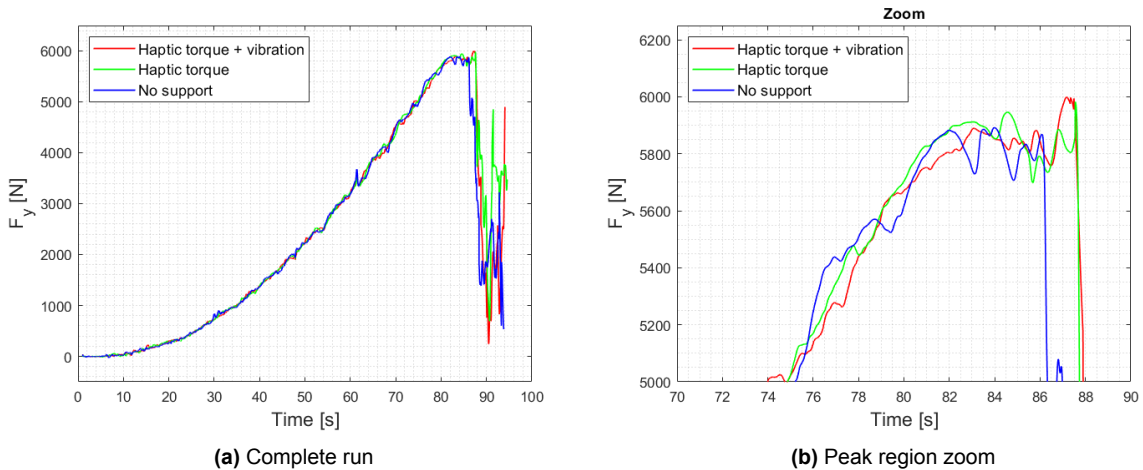


Figure B.11: Average lateral force for each variation of haptic support

The lateral tire force increases through out the maneuver for all three variations of haptic support, as the vehicle develops more speed which causes the front tires to generate higher slip angles. Eventually, the front tires saturate for large slip angle values and the vehicle reaches terminal understeer at which it goes off the road and the lateral force reduces rapidly. However, the peak lateral force value differs across the studied configurations. The maximum

average lateral force achieved by participants driving without any haptic support is 5891 N. Subjects driving with haptic torque developed on average a maximum lateral force of 5983 N. In the case of haptic steering support with vibration, the average peak lateral force achieved was 5999 N. Moreover, with both versions of the haptic support controller, participants managed to maintain the front tires around their maximum lateral force level for almost 2 seconds longer than participants who drove with no support at all.

B.4.2. Subjective Evaluation

The results of the subjective evaluation are summarized in Table B.1, with the average score of each subjective metric shown for each haptic support variation. For each metric, the best score is indicated in bold font.

Metric	No support	Haptic torque	Haptic torque with vibration
Mental demand	7.50	8.25	5.50
Physical demand	6.75	9.00	4.75
Performance	12.75	13.75	10.75
Frustration	6.75	7.50	4.50

Table B.1: NASA-TLX evaluation results for each driving mode (best results in bold)

It can be seen that the mental and physical demand are perceived the lowest when participants drive with haptic torque and vibration enabled. The self-reported performance is deemed the highest when using haptic torque. The lowest level of frustration when driving is reported for the haptic torque with vibration controller. Furthermore, 3 out of 4 participants consider driving with haptic torque and vibration as their favorite controller version.

B.5. Discussions

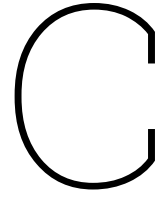
The positive impact of the designed haptic support is reflected by both objective and subjective experimental results. From Figure B.9 it can be seen that the haptic steering assistance works as expected by increasing the torque on the steering wheel when approaching the peak lateral tire force. When the haptic torque is applied, drivers need to apply more torque themselves in order to maintain a given steering angle or to increase the steering angle further. This has an effect on the resulting steering angle which can be seen in Figure B.10, with participants steering on average less when the haptic steering support is active compared to no support. As this is the correct action to prevent understeer, it can be concluded that the haptic steering support positively influences drivers to apply a more optimal steering input when approaching the handling limits. This is further confirmed in Figure B.11 by the additional lateral force generated by the front tires in cases when the haptic support was activated. The system not only helps the drivers to find the steering angle which maximizes the front axle grip, it also helps the drivers to maintain the optimal steering angle in order to generate the maximum lateral force for a longer period of time. The additional 2 seconds during which the car maintains maximum lateral force on the front tires can make the difference between successfully negotiating a curve or causing an accident in a real-world scenario.

From the subjective evaluation, the haptic steering assistance appears to be widely accepted by the majority of participants. Drivers also exhibit the lowest mental demand, physical demand and frustration when driving with the haptic support with vibrations. A common remark made by the participants was that they could “feel the handling limits” when this controller variant was active. Interestingly, although participants performed the best when driving

with the haptic torque and vibrations enabled, the self-reported performance is the lowest for this controller variation. This could be due to the fact that vibrations provide a clear warning to the drivers that there is something wrong with their steering input, which alters their perception of what the correct steering input is. This indicates an improved awareness of the changed handling conditions, one of the objectives of the haptic driver support system.

B.6. Summary

This pilot study investigated the design and implementation of a simple haptic driver support system for understeer mitigation. A model-based approach for detecting the front tire saturation has been proposed based on the nonlinear Fiala tire model. The tire model has been successfully validated using IPG CarMaker simulation software, and was able to accurately capture the tire behaviour up to, and including, the tire saturation limits. The proposed system was evaluated in a driving simulator experiment at Toyota Motor Europe, during steady-state cornering at the limits of handling. Three variants of haptic feedback were investigated: 1) no support, 2) haptic torque, and 3) haptic torque with vibrations. Preliminary results indicate that haptic torque and haptic torque with vibrations positively influence the drivers, supporting them to reduce their steering input near the saturation limits of the front tires. Both controller variants supported the drivers in maintaining the front tires at their maximum lateral force for a longer period of time. Furthermore, subjective evaluation indicates strong acceptance of the haptic support system, with the haptic torque with vibrations being the favorite controller variant among participants.



Haptic Support System Design

This chapter covers the theoretical background behind model predictive control (MPC) and presents a strategy to combine it with the haptic shared control (HSC) framework to form a predictive haptic support system for understeer mitigation. The mathematical models used for state prediction, the optimization problem formulation as well as the software implementation of the complete system are discussed in details.

C.1. MPC Background

Model predictive control is a model-based control strategy that is used to optimally control a system based on predictions about its future behaviour. While MPC has been widely used in the process control field since the 1980's [30], in recent years it has gained interest in the automotive field thanks to advancements in optimization algorithms and the increase in processing speed of modern on-board computers [24]. With its ability to handle nonlinear dynamics as well as multiple constraints on system inputs, states and outputs, MPC has quickly become an attractive approach for many automotive applications like engine control, energy management and even vehicle stability control [24].

MPC is predominantly implemented in discrete form, with a certain controller sample frequency T_c . It relies on a mathematical model of the plant to predict how the system will behave over a limited time window. Based on these predictions, the control input can be optimized in a way that minimizes the defined cost function while satisfying a set of constraints. The time window over which the optimization problem is solved is called the prediction horizon, denoted by N_p . Solving the optimization problem yields an optimal control input $u(k)$, defined for the length of the control horizon N_c . By applying only the first control input from the calculated control sequence, and then repeating the optimization process again, the MPC is able to account for changing operating conditions in an approach called *receding horizon control*. Figure C.1 illustrates the principle of operation of MPC for an arbitrary system in case where $N_p = N_c$.

MPC provides several advantages over other control methods when considering a predictive driver support system. Firstly, the field of model predictive control has seen significant advancements over the years, resulting in well-established methodologies and refined optimization algorithms tailored specifically to real-time applications. This enables rapid development and configuration, while also ensuring timely convergence of the optimization process. Secondly, MPC is well-suited for control problems involving multiple variables with complex dynamics. This is representative of a vehicle approaching its handling limits, in which multiple factors like the velocity, steering angle and the available tire-road friction all influence the vehicle's behaviour. Lastly, multiple studies have demonstrated the practicality of MPC for

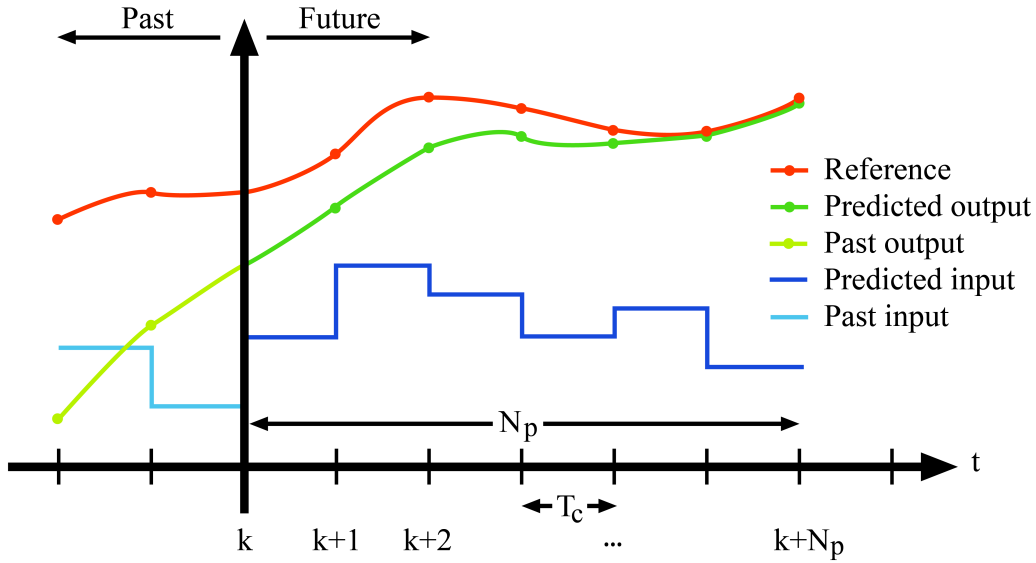


Figure C.1: A general discrete MPC scheme

automotive applications, thanks to its ability to predict vehicle states in the near future [24]. Several studies showcased the effectiveness of MPC in steering-related ADAS applications like driver-oriented lane-keeping [29], stability control at the limits of handling [5], and predictive haptic support for obstacle avoidance [4].

This iterative, finite-horizon, optimization process requires an accurate plant model. The model should be accurate enough to yield precise predictions, while avoiding unnecessary complexities which could negatively impact computational efficiency, and impede real-time operation. Therefore, the next section presents the mathematical model used to capture the relevant vehicle dynamics up to the limits of handling.

C.2. Vehicle Model

Two separate models are necessary to capture all the dynamics of interest. The bicycle model is used to predict the lateral and rotational velocities of the car, while the tire model allows to calculate the forces at the tire-road contact patch.

C.2.1. Bicycle Model

In order to model the vehicle motion, a planar single track bicycle model is chosen. Such a model has been extensively used by several studies for its simplicity and ability to capture the main system dynamics up to and including the lateral handling limits [5][14][25]. The model assumes a constant longitudinal velocity v_x , no load transfers, no rolling, no pitching and no vertical motion of the vehicle. This model has two degrees of freedom as both front tires and both rear tires are lumped together as shown in figure C.2. The complete derivation can be consulted in [39]. The equations of motion can be written in terms of the front and rear tire forces, F_{yf} and F_{yr} , as

$$\dot{v}_y = \frac{F_{yf} + F_{yr}}{m} - r v_x, \quad (\text{C.1})$$

$$\dot{r} = \frac{l_f F_{yf} - l_r F_{yr}}{I_{zz}}, \quad (\text{C.2})$$

where v_y is the lateral velocity, r is the yaw rate, l_f and l_r are the distances from the center of gravity (CoG) to the front and rear axle, m is the vehicle mass and I_{zz} is the moment of inertia. From kinematics, the equations for the tire slip angles at the front (α_f) and at the rear (α_r) can be found as

$$\alpha_f = \frac{v_y + l_f r}{v_x} - \delta, \quad (\text{C.3})$$

$$\alpha_r = \frac{v_y - l_r r}{v_x}, \quad (\text{C.4})$$

where δ is the road-wheel steer angle.

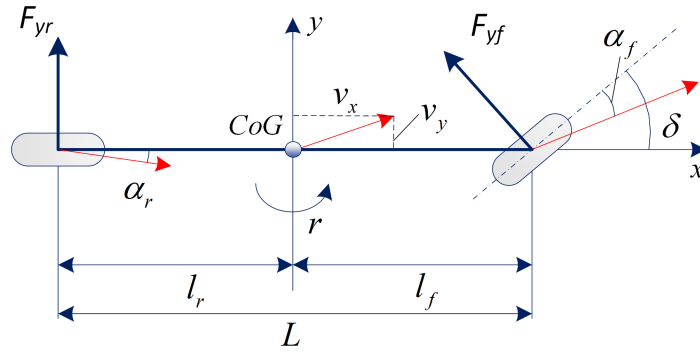


Figure C.2: Bicycle model

C.2.2. Tire Model

Following the insights obtained from the pilot study (see Appendix B), a nonlinear Fiala brush tire model is chosen. Such a model has been successfully validated using IPG CarMaker simulation software and proved to be sufficiently accurate to predict the tires' saturation limit. For convenience, the tire model equation is repeated below:

$$F_y = \begin{cases} C_\alpha \tan \alpha - \frac{C_\alpha^2}{3\mu F_z} |\tan \alpha| \tan \alpha + \frac{C_\alpha^3}{27\mu^2 F_z^2} \tan^3 \alpha, & \text{if } |\alpha| \leq \alpha_{lim} \\ \mu F_z \text{sgn} \alpha, & \text{else} \end{cases} \quad (\text{C.5})$$

where α_{lim} is the slip angle at which the tire has reached the limits of friction, given by:

$$\alpha_{lim} = \tan^{-1} \left(\frac{3\mu F_z}{C_\alpha} \right). \quad (\text{C.6})$$

C.2.3. Safe Steering Envelope

Following the approach of envelope control, steering angle limits can be defined to demarcate a safe region of operation. Substituting (C.6) into (C.3) and isolating δ yields an expression for the upper and lower boundary of the road-wheel angle δ_{lim} at which F_{yf} reaches its peak value, respectively:

$$\delta_{lim}^+ = \frac{v_y + l_f r}{v_x} + \tan^{-1} \left(\frac{3\mu F_z}{C_\alpha} \right), \quad (\text{C.7})$$

$$\delta_{lim}^- = \frac{v_y + l_f r}{v_x} - \tan^{-1} \left(\frac{3\mu F_z}{C_\alpha} \right). \quad (\text{C.8})$$

As long as δ remains within the bounds given in (C.7) and (C.8), the front tire slip angle will remain under its saturation value.

C.3. Predictive Haptic Driver Support System

In order to design a predictive haptic driver support system, this study relies on the predictive capabilities of MPC to detect the vehicle handling limits in advance, which are then communicated to the driver using haptic shared control. The support system aims to notify drivers of potential understeer and guide them in reducing the steering angle if they exceed the safe steering limits. An outline of the proposed control framework is shown in Figure C.3.

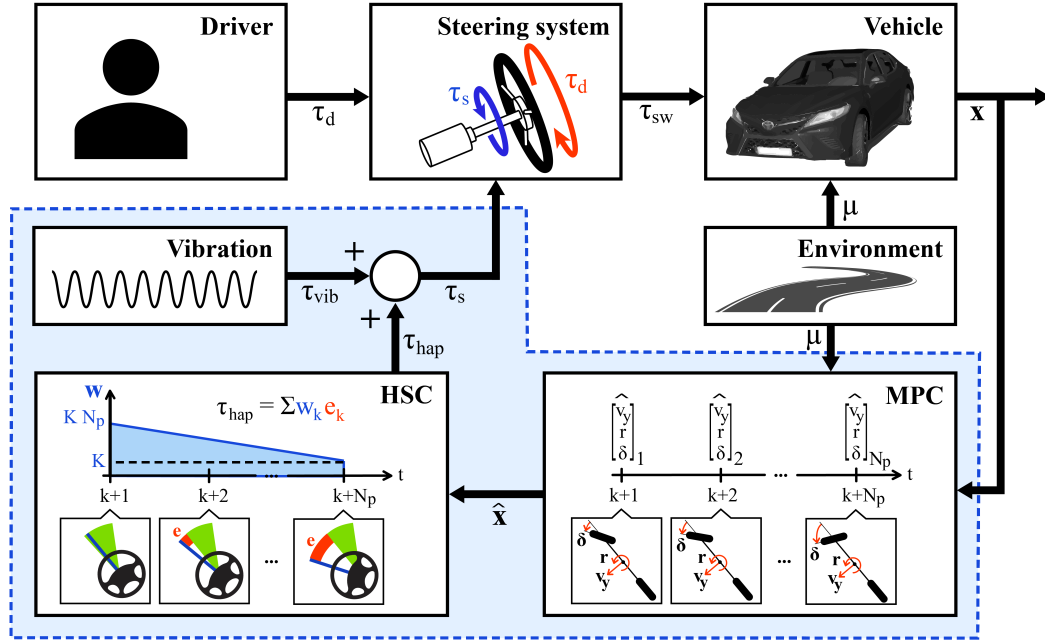


Figure C.3: Control framework: The MPC predicts the future vehicle states, which are then used to compute the safe steering envelope (in green) for each timestep of the prediction horizon. An error e (in red) is produced if the predicted steering angle leaves the envelope. The generated haptic torque τ_{hap} is equal to the weighted sum of the errors where the weighting function w is linearly decreasing. The total support torque τ_s is equal to the sum of τ_{hap} and τ_{vib} .

C.3.1. MPC Formulation

The goal of the MPC is to accurately predict the vehicle states which allow to calculate the safe steering envelope defined in (C.8) and (C.7), namely v_y and r . This in turn requires knowledge of the future road-wheel angle δ . Accurate predictions of these variables over the prediction horizon will allow to detect understeer in advance. The MPC state vector x is therefore defined as $x = [v_y, r, \delta]$.

While v_y and r can be predicted using the bicycle model, road-wheel angle prediction is problematic as it requires knowledge of the driver's intention. This requires an accurate driver model for predicting the steering command in real-time which is a complex endeavour (see Appendix A). Although there has been progress in driver modelling approaches for normal driving conditions [29], no driver model able to predict the driver's behaviour at the vehicle's handling limits was found at the time of this work. As an alternative, the proposed system uses a road-wheel angle prediction method without *a priori* knowledge of the driver's objective. This approach relies on the assumption that for a short prediction horizon, the steering velocity $\dot{\delta}$ can be assumed to be approximately constant. This allows to compute the future road-wheel angle by integrating $\dot{\delta}$ over time. Furthermore, the predicted steering velocity should not be too large and the resulting δ should not deviate significantly from the initial road-wheel angle

at the start of the prediction.

By defining the steering velocity $\dot{\delta}$ as the control input u , a cost function can be constructed to reflect the objective of the prediction algorithm. This study uses a least-squares cost function for its ease of implementation and low computational complexity. The lengths of the control horizon N_c and the prediction horizon N_p are assumed equal. The total optimization problem that the MPC solves in order to predict future vehicle states is formulated as follows:

$$\begin{aligned} \min_{\delta} \quad & \sum_{k=1}^{N_p} \left(\|\dot{\delta}_k\|_{Q_1}^2 + \|\dot{\delta}_k - \dot{\delta}_0\|_{Q_2}^2 + \|\delta_k - \delta_0\|_{Q_3}^2 \right) \\ \text{s.t.} \quad & x[k+1] = Ax[k] + Bu[k] + d[k] \\ & -\frac{\pi}{2} \leq \delta \leq \frac{\pi}{2} \end{aligned} \quad (\text{C.9})$$

In the cost function, δ_0 and $\dot{\delta}_0$ are the initial road-wheel angle and velocity, respectively, and Q_1 , Q_2 and Q_3 are the tuning weights. Furthermore, A , B and d are respectively the system matrix, the input matrix and the disturbance input associated with the current state from the discrete state-space vehicle model. The discrete state-space is obtained by discretizing the continuous bicycle model defined in (C.1) and (C.2), combined with the slip and tire model defined in (C.3), (C.4), (C.5) and (C.6). The constraint on δ reflects the actuation limits of a typical steering system.

C.3.2. HSC Design

With predictions for v_y , r and δ available, the safe steering envelope boundaries given by equations (C.7) and (C.8) can be computed for each timestep of the prediction horizon, which allows to detect front tires saturation in advance. The goal of the HSC is to communicate the approach of these handling limits to the drivers in an intuitive way, and support them in decreasing their steering input in case of predicted limit violation.

From the previously developed driver error model in Appendix A, haptic support should aim to resolve the issue of strong-habit intrusion by increasing situation awareness and guiding the driver towards a safer steering input in case of understeer. Preliminary results from the pilot study presented in Appendix B indicate that these control objectives can be achieved through an increasing haptic torque with vibrations provided directly on the steering wheel. The proposed HSC builds on top of the haptic driver support developed during the pilot study by providing a similar kind of haptic feedback. If the predicted road-wheel angle exceeds the calculated limits at any point, an error term e_k is computed for that particular timestep k :

$$e_k = \begin{cases} \delta_{lim,k}^- - \delta_k, & \text{if } \delta_k < \delta_{lim,k}^- \\ 0, & \text{if } \delta_{lim,k}^- \leq \delta_k \leq \delta_{lim,k}^+ \\ \delta_{lim,k}^+ - \delta_k, & \text{if } \delta_{lim,k}^+ < \delta_k \end{cases} \quad (\text{C.10})$$

To leverage the predictive capabilities of the support system, the haptic feedback should convey the notion of urgency of the situation in a comprehensible way to the driver. In other words, drivers should be able to intuitively understand how far away their steering input currently is from the safe steering boundaries. Imminent safe steering envelope incursions should be penalized more than violations further ahead in the horizon. This can be implemented by introducing a weighting term which linearly decreases as a function of subsequent timesteps in the prediction horizon. For each timestep k , the weighting term w_k is defined as:

$$w_k = K(N_p - k + 1), \quad (\text{C.11})$$

where K is a tuning factor allowing to tune the haptic authority of the support torque. The error of each particular timestep e_k can thus be multiplied by w_k in order to assign more importance to imminent errors compared to errors further ahead. The haptic torque τ_{hap} is equal to the sum of the weighted errors for the length of the prediction horizon N_p :

$$\tau_{hap} = \sum_{k=1}^{N_p} w_k e_k. \quad (\text{C.12})$$

In addition to the increase in steering torque, torque vibrations τ_{vib} of fixed amplitude A_{vib} and frequency f_{vib} are also added to the steering wheel. These vibrations were perceived as a positive influence on user acceptance during the pilot study. The total support torque τ_s delivered by the system to the steering wheel is equal to $\tau_{hap} + \tau_{vib}$.

C.4. Implementation

The proposed haptic support system has been implemented in MATLAB Simulink. The following section covers the configuration of the MPC and HSC controllers, along the settings and tuning parameters used.

C.4.1. MPC Settings

The optimization problem defined in (C.9) is non-convex due to the nonlinearity of the tire model. Finding a solution to this optimization problem requires the use of efficient solvers which guarantee real-time performance. In this study, the numerical software package FORCES PRO has been used to generate and configure the solver [11][53]. FORCES PRO is a software environment designed for optimization-based control which is able to handle nonlinear optimization problems while being readily compatible with MATLAB.

The continuous vehicle dynamics are discretized with a controller sample time T_c of 0.01s. System states are then evaluated at discrete grid points using the explicit Runge-Kutta 4 as the numerical integration method. This integration scheme has shown to be sufficiently accurate for this application, while also being efficient enough to ensure real-time performance.

There is a trade-off regarding the length of the prediction horizon N_p . In order for the constant steering velocity assumption to remain valid, the chosen time horizon should be short. In the contrary, the predicted steering velocity might deviate too much from the initial steering velocity at the beginning of the prediction process, leading to a decrease in prediction accuracy. On the other hand, a long prediction horizon is interesting because it allows to look further ahead into the future, thus offering the driver more time to react in case of safe handling limits violation. The length of the prediction horizon has also a major influence on the computational efficiency and therefore real-time operation of the system. During preliminary driving simulator tests conducted under normal driving conditions, vehicle states predictions based on the assumption of constant steering velocity within the prediction horizon were accurate for approximately 0.5s. Beyond this time, the predictions deviated significantly from the actual states as the constant steering velocity assumption could not hold for longer periods of time. As a consequence, the proposed system adopts a prediction horizon of 0.5s as it results in good prediction accuracy while allowing enough margin for understeer to be detected ahead of time.

To solve the optimization problem, the FORCES PRO nonlinear programming (NLP) solver is used with the sequential quadratic programming (SQP) method. This algorithm transforms the non-convex NLP problem into a sequence of quadratic programming (QP) problems, which are less computationally expensive. By iteratively solving these QP problems, and using the solution of one iteration as the initial condition of the next iteration, the algorithm converges to

a solution satisfying the original NLP problem. In order to decrease the computation time, the real-time variant of the SQP method is used in this work, which constrains the solver to only one SQP iteration per timestep. Finally, the Gauss-Newton Hessian approximation is used to increase the convergence speed of the solution. Further information on the real-time implementation of the SQP algorithm, along an extensive review of the most common numerical methods for nonlinear optimization problems, is provided by Diehl et al. [10]. More details about the available solver configurations are provided in the FORCES PRO user manual [16]. For the proposed haptic support system, the MPC parameters are shown in Table C.1, and a summary of the solver settings is presented in Table C.2.

Parameter	Description	Value
T_c	controller sample time in s	0.01
N_p	number of timesteps in prediction horizon	50
Q_1	weight on steering velocity	10
Q_2	weight on steering velocity deviation	2000
Q_3	weight on steering angle deviation	0.1

Table C.1: MPC parameters

Variable	Value
<code>codeoptions.nlp.integrator.type</code>	ERK4
<code>codeoptions.solvemethod</code>	SQP_NLP
<code>codeoptions.nlp.hessian_approximation</code>	gauss-newton
<code>codeoptions.sqp_nlp.maxqps</code>	1

Table C.2: FORCES PRO NLP solver settings

C.4.2. HSC Settings

The HSC was tuned in close collaboration with an expert test driver with professional experience in driving at the vehicle's handling limits.

First, the haptic authority K has been tuned in a way which makes the haptic torque τ_{hap} noticeable while giving the driver the ability to overrule it if needed. This allows the driver to remain in total control of the vehicle at all times.

Next, the magnitude and frequency of the haptic vibrations τ_{vib} have been tuned to replicate the steering wheel vibrations felt by a driver when the car experiences understeer on a high friction surface in the real-world. This notifies the driver of incoming understeer in an insightful and realistic way. The HSC parameters are summarised in Table C.3.

Parameter	Description	Value
K	haptic torque tuning factor	0.05
A_{vib}	haptic vibration amplitude in Nm	0.5
f_{vib}	haptic vibration frequency in Hz	21

Table C.3: HSC parameters

C.5. Operation

Figure C.4 demonstrates the operation of the complete haptic driver support system. The figure shows the recorded data from one of the experimental trials performed on a driving simulator with a driver-in-the-loop. The two uppermost plots show the predicted states, \hat{r} and \hat{v}_y , coming from the MPC at $t = 38.17$ s for the length of the prediction horizon, until $t = 38.67$ s. The predicted steering input $\hat{\delta}$, shown on the third plot from the top, breaches the safe steering envelope around the 38.6s mark. The support torque τ_s , consisting of haptic torque with vibrations, is provided as soon as the limit violation is predicted, as can be seen in the last plot. For reference, the true vehicle states (r, v_y) and driver input (δ) recorded during the driving simulator run are also shown.

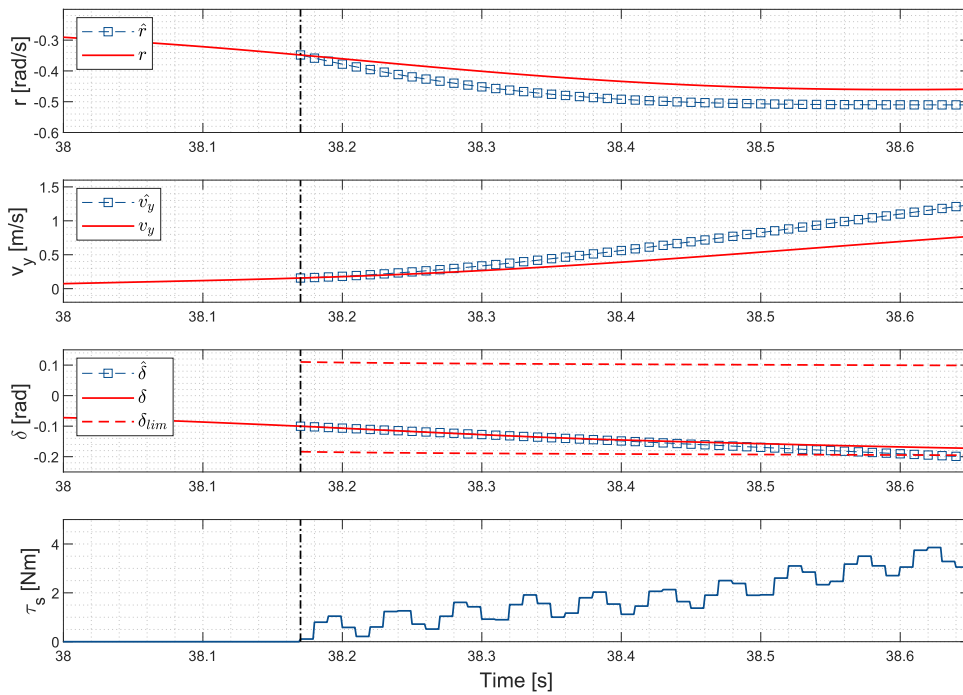


Figure C.4: State prediction at $t = 38.17$ s during a driver-in-the-loop experimental trial

D

Results and Discussions

D.1. Participants

In total, 32 participants took part in the experiment, all with a valid driving license. Participants were split into 3 groups in order to gain insight into the influence of haptic support on drivers with different levels of experience. The classification was done based on the drivers' average maximum lateral deviation during the practice runs, when driving without any support. Drivers who's averaged maximum lateral deviation was above the lane limit of 2.25m were classified as *novice* drivers (N=12). *Regular* drivers were drivers who managed to stay within the limits of the lane (N=15). *Expert* drivers were selected based on their professional qualifications in handling limit driving (N=5).

Figure D.1 presents a scatter plot of the average maximum lateral deviation during practice runs (no support) as a function of the driving license possession years. The three driver categories are color-coded. As can be seen, all novice drivers had their driving license for less than 10 years. Furthermore, the correlation coefficient between the maximum lateral deviation and the driving license possession is equal to -0.56 ($p\text{-value} < 0.001$).

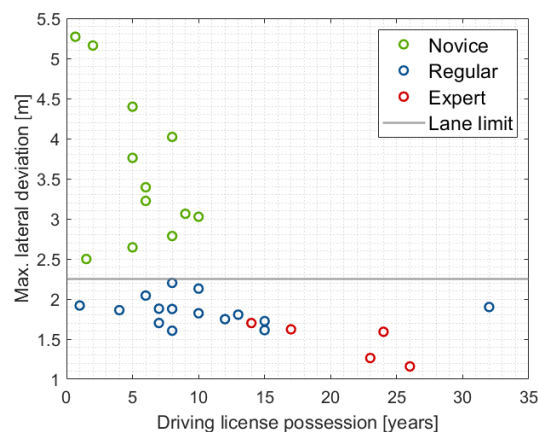


Figure D.1: Average maximum lateral deviation during scenario 1 when driving without support, plotted as a function of the driving license possession years

D.2. Results

Scenario 1 and scenario 2 are analysed apart. The collected data from the runs with and without support of all 32 participants was averaged separately, first per participant and then

across all participants of the same category. Statistical significance of the results is assessed using a two-tailed paired t-test, at 5% significance level.

D.2.1. Objective Evaluation

Scenario 1: Practice Runs

Figure D.2 shows the experimental results from scenario 1 as a function of the distance for each of the three driver groups.

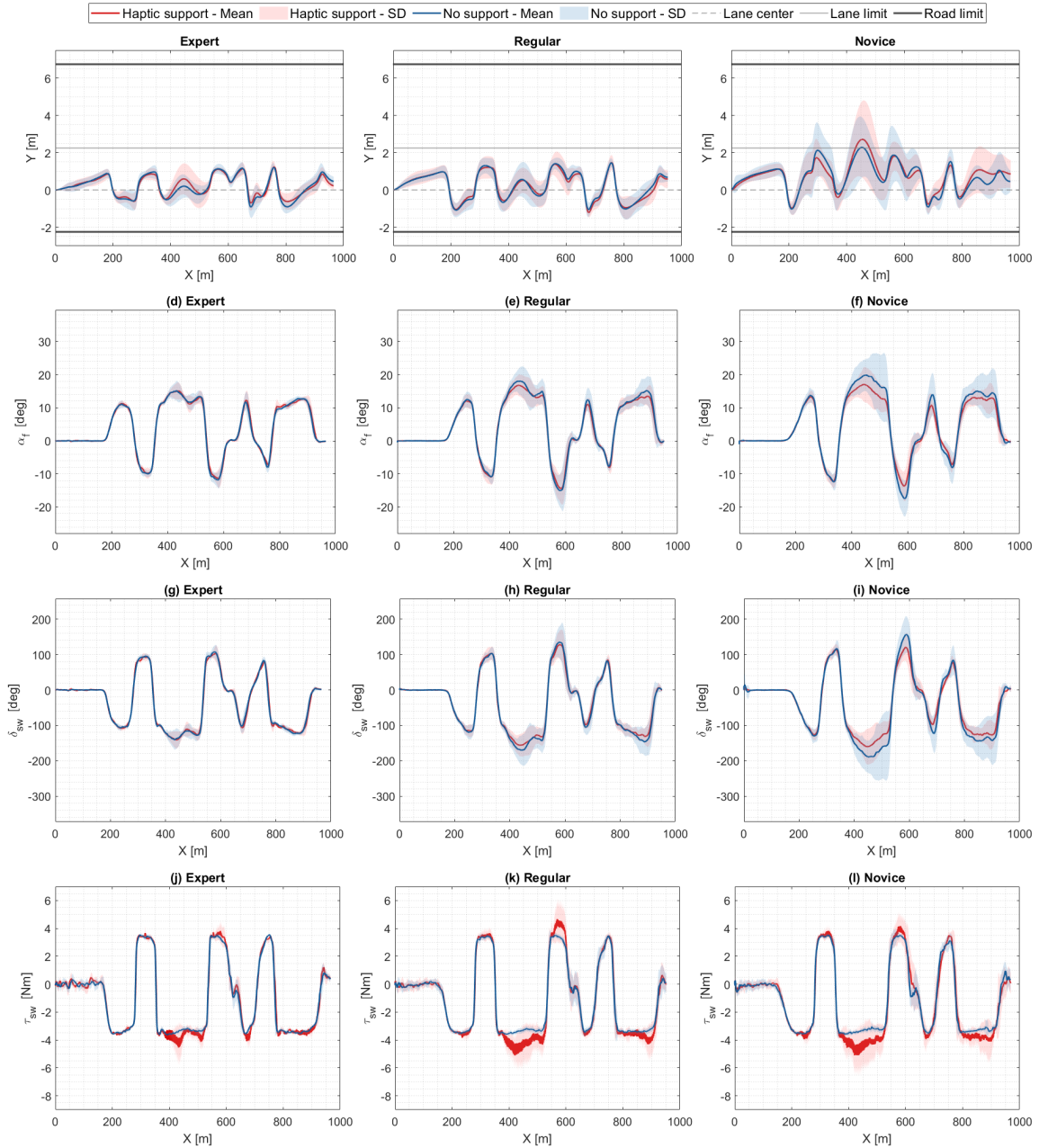


Figure D.2: Experimental results from scenario 1: mean values (solid lines), and standard deviations (shaded areas) for the 2 support cases, plotted for each driver category

Plots D.2a to D.2c show the vehicle lateral deviation from the center of the lane as a function of the distance. The average trajectories with and without haptic support closely align

for all driver categories. Similarly, no significant difference in maximum lateral deviation was observed between the two support variations across driver groups (see Table D.1).

Drivers	No support	Haptic support	p-value
Expert	1.47m (0.24)	1.52m (0.22)	0.2112
Regular	1.86m (0.17)	1.81m (0.45)	0.6755
Novice	3.60m (0.94)	3.55m (1.37)	0.9055

Table D.1: Averaged maximum lateral deviation during scenario 1 for each driving mode, for each driver category (standard deviations in parentheses)

The averaged maximum slip angle values at the front tires are presented in Table D.2. Both regular and novice drivers significantly reduced their slip angle when aided by the haptic support, by 8.94% and 20.95% respectively, which can also be seen in the plots D.2e and D.2f.

Drivers	No support	Haptic support	p-value
Expert	15.91° (2.93)	15.49° (2.62)	0.2563
Regular	19.53° (4.47)	17.79° (3.40)	0.0056
Novice	23.57° (8.34)	18.63° (5.73)	0.0336

Table D.2: Averaged maximum slip angle at the front axle during scenario 1 for each driving mode, for each driver category (standard deviations in parentheses)

Table D.3 presents the averaged maximum front lateral force. The increase in lateral force when driving with haptic support is not statistically significant for any driver category.

Drivers	No support	Haptic support	p-value
Expert	7314.3N (234.88)	7357.6N (172.02)	0.6050
Regular	7372.5N (202.37)	7422.5N (177.07)	0.2841
Novice	7438.4N (136.97)	7490.7N (94.41)	0.2805

Table D.3: Averaged maximum lateral force at the front axle during scenario 1 for each driving mode, for each driver category (standard deviations in parentheses)

The averaged maximum steering wheel angle values are shown in Table D.4, for each driver group. Novice drivers show a significant decrease of 21.05% in their steering angle when driving with haptic support, which can also be seen in Figure D.2i.

Drivers	No support	Haptic support	p-value
Expert	113.54° (17.97)	110.69° (18.74)	0.5412
Regular	150.09° (51.65)	136.25° (39.71)	0.1199
Novice	171.82° (47.34)	135.65° (39.48)	0.0052

Table D.4: Averaged maximum steering wheel angle during scenario 1 for each driving mode, for each driver category (standard deviations in parentheses)

Lastly, Table D.5 presents the averaged maximum steering wheel torque. Regular and novice drivers significantly increased their steering torque respectively by 29.10% and 21.96% when driving with the haptic support. This is also illustrated by the plots D.2k and D.2l.

Drivers	No support	Haptic support	p-value
Expert	3.62N (0.03)	4.16N (0.71)	0.1618
Regular	3.65N (0.01)	5.15N (1.39)	< 0.001
Novice	3.64N (0.01)	4.67N (1.08)	0.0069

Table D.5: Averaged maximum steering wheel torque during scenario 1 for each driving mode, for each driver category (standard deviations in parentheses)

Scenario 2: Obstacle Avoidance

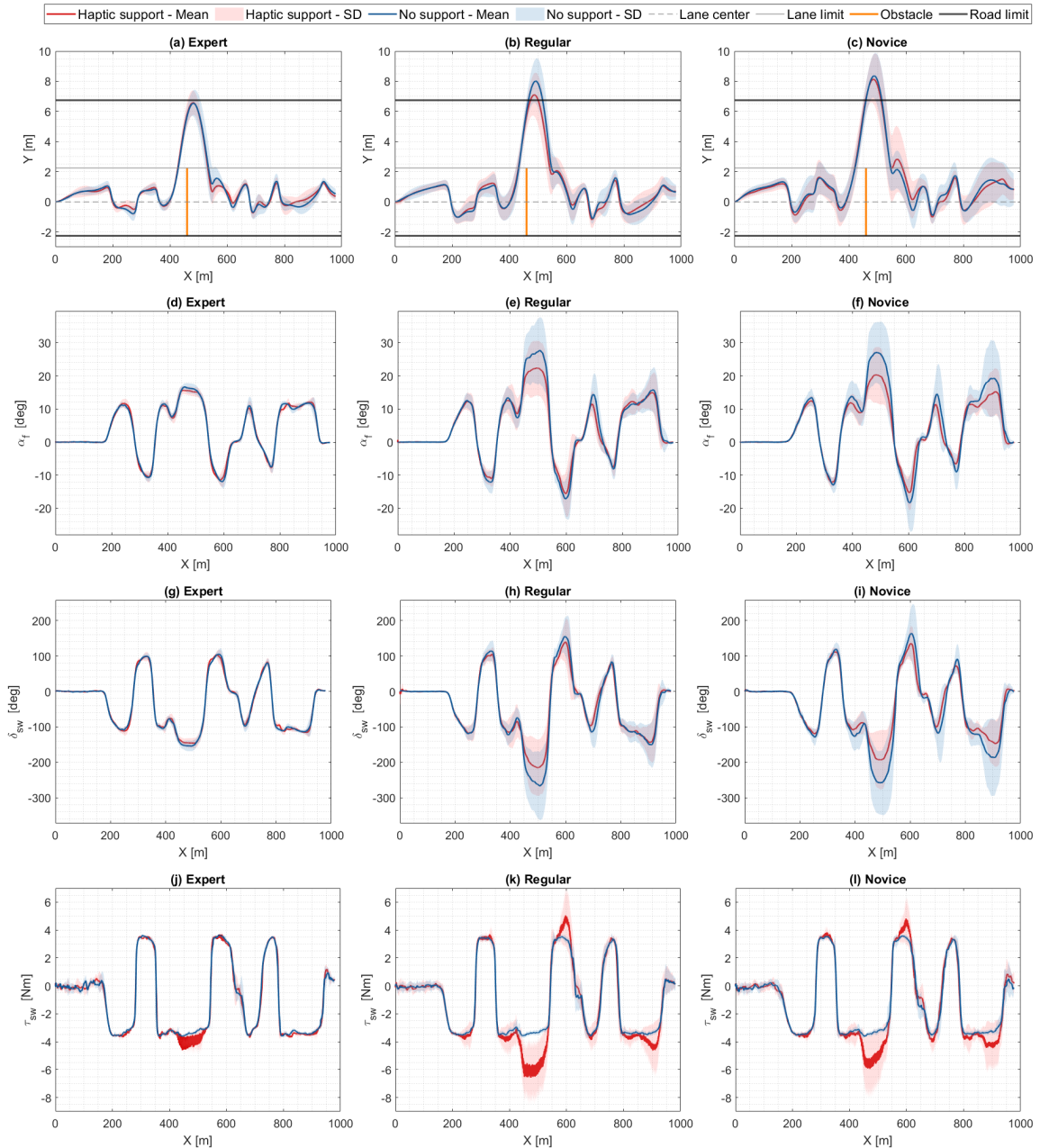


Figure D.3: Experimental results from scenario 2: mean values (solid lines), and standard deviations (shaded areas) for the 2 support cases, plotted for each driver category

Figure D.3 presents the experimental results from scenario 2 as a function of the distance for each of the three driver groups. The emphasis during the following analysis is put on the obstacle avoidance maneuver, specifically on the interval between $X=400\text{m}$ and $X=550\text{m}$. Plots D.3a to D.3c show the vehicle lateral deviation from the center of the lane as a function of the distance. As can be seen, the influence of haptic support on the vehicle path varies for the different driver groups. In the case of expert drivers, the haptic support has no noteworthy effect with both trajectories largely overlapping. Regular drivers significantly reduced their lateral deviation around the obstacle when driving with the haptic support. A small change in trajectory is also observed in the case of novice drivers.

Table D.6 presents a comparison of the means of the maximum lateral deviations calculated for each driver category. Regular drivers significantly reduced their peak lateral deviation by 11.28% when driving with haptic support compared to baseline.

Drivers	No support	Haptic support	p-value
Expert	6.63m (0.87)	6.60m (0.91)	0.9595
Regular	8.14m (1.51)	7.22m (1.52)	0.0113
Novice	8.55m (1.52)	8.30m (1.68)	0.4568

Table D.6: Averaged maximum lateral deviation during scenario 2 for each driving mode, for each driver category (standard deviations in parentheses)

The analysis of the averaged root-mean-square (RMS) slip angle at the front tires on the interval from $X=400\text{m}$ to $X=550\text{m}$ is presented in Table D.7. Both regular and novice drivers significantly reduced their slip angle when aided by the haptic support, by 16.82% and 25.67% respectively. The decrease in the front tires' slip angle on the interval from $X=400\text{m}$ to $X=550\text{m}$ is also clearly visible in the plots D.3e and D.3f.

Drivers	No support	Haptic support	p-value
Expert	13.18° (0.79)	12.78° (0.91)	0.4134
Regular	21.03° (6.38)	17.49° (5.89)	0.0026
Novice	20.51° (7.10)	15.25° (4.85)	0.0076

Table D.7: Averaged RMS slip angle at the front axle from $X=400\text{m}$ to $X=550\text{m}$ (around the obstacle) for each driving mode, for each driver category (standard deviations in parentheses)

A difference in slip angle has also a direct influence on the front axle lateral force. Table D.8 presents the RMS lateral force values for the front axle, on the interval from $X=400\text{m}$ to $X=550\text{m}$. A significant difference can be noted for regular and novice drivers, who utilised respectively 1.00% and 1.03% additional lateral force during the obstacle avoidance maneuver when driving with haptic support.

Drivers	No support	Haptic support	p-value
Expert	6896.5N (79.14)	6963.3N (101.44)	0.0965
Regular	6737.1N (204.39)	6804.9N (174.14)	0.0424
Novice	6758.2N (228.62)	6828.8N (204.15)	0.0106

Table D.8: Averaged RMS values of lateral force at the front axle from $X=400\text{m}$ to $X=550\text{m}$ (around the obstacle) for each driving mode, for each driver category (standard deviations in parentheses)

The averaged RMS steering wheel angles from $X=400\text{m}$ to $X=550\text{m}$ are shown in Table

D.9, for each driver group. The haptic steering support significantly reduced the steering angle for regular and novice drivers, by 16.91% and 25.74% respectively. The difference in steering angle during the experiment can also be observed in the plots D.3h and D.3i.

Drivers	No support	Haptic support	p-value
Expert	125.15° (7.65)	121.28° (8.67)	0.3846
Regular	200.31° (61.33)	166.45° (56.69)	0.0025
Novice	195.24° (68.32)	144.99° (46.84)	0.0077

Table D.9: Averaged RMS values of steering wheel angle from X=400m to X=550m (around the obstacle) for each driving mode, for each driver category (standard deviations in parentheses)

Lastly, Table D.10 presents the RMS values of the total torque on the steering wheel on the interval from X=400m to X=550m. The difference in total steering torque between baseline and proposed system is significant for all categories of drivers, with an increase in torque of 10.23%, 38.83%, and 27.27% for expert, regular, and novice drivers, respectively. This indicates that the haptic support activated on average for all participants, regardless of their driving skills. This is illustrated in Figure D.3 (plots D.3j to D.3l), which shows an increase in the measured torque on the steering wheel between X=400m and X=550 for all drivers.

Drivers	No support	Haptic support	p-value
Expert	3.24N (0.03)	3.60N (0.30)	0.0390
Regular	3.20N (0.07)	4.98N (1.30)	<0.001
Novice	3.20N (0.08)	4.39N (1.28)	0.0095

Table D.10: Averaged RMS values of steering wheel torque from X=400m to X=550m (around the obstacle) for each driving mode, for each driver category (standard deviations in parentheses)

D.2.2. Subjective Evaluation

Scenario 1: Practice Runs

The averaged results of the NASA-TLX evaluation form filled after completion of scenario 1 are summarized separately for expert, regular and novice driver categories, in Tables D.14, D.15 and D.16, respectively. A significant increase in self-assessed performance is reported by novice drivers when driving with haptic support compared to baseline. No other significant differences were found in the subjective evaluation results from scenario 1.

Metric	No support	Haptic support	p-value
Mental demand	5.80 (5.07)	5.60 (4.77)	0.3739
Physical demand	6.00 (4.58)	6.80 (3.77)	0.3739
Performance	14.8 (4.02)	16.60 (2.61)	0.1210
Frustration	7.40 (6.19)	8.40 (8.23)	0.4734

Table D.11: NASA-TLX evaluation results for expert drivers during scenario 1, for each driving mode (standard deviations in parentheses)

Metric	No support	Haptic support	p-value
Mental demand	9.07 (3.94)	8.60 (3.27)	0.7152
Physical demand	6.73 (3.20)	8.73 (4.99)	0.0755
Performance	14.73 (3.08)	15.73 (3.01)	0.3409
Frustration	7.47 (4.70)	7.13 (4.20)	0.7678

Table D.12: NASA-TLX evaluation results for regular drivers during scenario 1, for each driving mode (standard deviations in parentheses)

Metric	No support	Haptic support	p-value
Mental demand	11.50 (3.87)	9.58 (4.56)	0.1504
Physical demand	9.42 (4.62)	10.42 (4.10)	0.4877
Performance	11.92 (3.50)	15.17 (2.69)	0.0124
Frustration	9.00 (4.77)	6.67 (4.46)	0.1924

Table D.13: NASA-TLX evaluation results for novice drivers during scenario 1, for each driving mode (standard deviations in parentheses)

Scenario 2: Obstacle Avoidance

The averaged results of the NASA-TLX evaluation form for scenario 2 are summarized in Tables D.14, D.15 and D.16, respectively. A significant decrease in mental demand is reported by novice drivers. Regular drivers report a significant increase in self-assessed performance when driving with haptic support. Also, a significant decrease in perceived frustration can be observed for novice drivers when aided by haptic support compared to no support.

Metric	No support	Haptic support	p-value
Mental demand	6.80 (5.36)	6.60 (5.13)	0.3739
Physical demand	5.20 (5.02)	6.00 (4.47)	0.3739
Performance	15.40 (2.97)	16.00 (2.65)	0.2080
Frustration	8.6 (6.80)	9.8 (8.70)	0.3883

Table D.14: NASA-TLX evaluation results for expert drivers during scenario 2, for each driving mode (standard deviations in parentheses)

Metric	No support	Haptic support	p-value
Mental demand	12.00 (4.50)	11.60 (4.24)	0.6044
Physical demand	9.60 (3.81)	10.07 (4.48)	0.5892
Performance	12.47 (3.56)	14.67 (3.58)	0.0176
Frustration	9.33 (4.81)	9.13 (4.75)	0.8003

Table D.15: NASA-TLX evaluation results for regular drivers during scenario 2, for each driving mode (standard deviations in parentheses)

Metric	No support	Haptic support	p-value
Mental demand	14.50 (4.03)	11.58 (5.00)	0.0431
Physical demand	12.08 (5.79)	10.67 (4.77)	0.3474
Performance	10.58 (3.94)	11.33 (5.16)	0.6975
Frustration	11.58 (4.56)	8.33 (4.33)	0.0310

Table D.16: NASA-TLX evaluation results for novice drivers during scenario 2, for each driving mode (standard deviations in parentheses)

Post-experiment

After the completion of both scenarios, participants were asked which controller variations did they prefer to drive with during the experiment. The results showed that 2 out of 5 expert drivers preferred driving with the haptic support, compared to 11 out of 15 regular drivers and 11 out of 12 novice drivers with the same preference for haptic support. Participants were also asked about their interest in having the haptic support system in their own personal vehicle, should such technology become available on the market. The results revealed that 3 out of 5 expert drivers are interested in having such a system installed. In the case of regular drivers, a vast majority of 13 out of 15 participants expressed their desire for its implementation. Similarly, among novice drivers, 10 out of 12 participants showed interest in having haptic support installed in their vehicles.

D.3. Discussions

The results show that haptic driver support does impact the drivers, however, the degree to which a driver is influenced greatly depends on the situation at hand. In scenario 1, novice drivers aided by haptic support reduced their steering angle input, which resulted in a significantly lower front tires' slip angle. However, neither the front tires' lateral force nor the lateral vehicle deviation changed significantly in the case of novice drivers. Further results from scenario 1 show that the only significant difference in the case of regular drivers is an increase in the steering torque when driving with the haptic support, while expert drivers did not show any significant differences between the two controller variations.

The impact of the proposed system is more noticeable in scenario 2. Regular drivers experienced a significant improvement with a 11.28% decrease in maximum lane deviation when driving with the haptic support. This could be linked to a reduction in the steering angle input by 16.91% following the engagement of the haptic support, which in turn considerably lowered the slip angle and allowed to generate additional lateral force at the front tires. All in all, regular drivers reduced their deviation by almost 1m around the obstacle when aided by the proposed system, which can make the difference between a successfully negotiated turn or a potentially fatal accident in a real-world situation.

Novice drivers also seem to benefit from the haptic support. During the obstacle avoidance maneuver, novice drivers reduced their steering angle input by 25.74% compared to baseline, by far the most of the three driver groups. This resulted in a significantly reduced slip angle and an increased lateral force at the front axle when driving with the haptic support. This indicates a better utilization of the tires. Moreover, novice drivers reported significantly reduced mental demand and frustration during scenario 2, as well as an increased self-reported performance during scenario 1. This indicates that novice drivers like the proposed system and find it helpful. However, no significant decrease in their lateral deviation was noted in either scenarios.

It is important to note that the lack of reduction in lateral deviation in the case of novice drivers is not necessarily a failure of the haptic support itself. After all, novice drivers exhibited smaller steering input angles, and lower front tires' slip angles in both experimental scenarios.

This even resulted in a significant increase in lateral force in scenario 2. All of this indicates that the proposed support system helped to mitigate the front tires saturation by positively influencing the driver. Nonetheless, preventing tire saturation does not necessarily guarantee good path tracking. More research is needed in this area, however, factors like driver's reaction time and how early the evasive maneuver is started could be of importance.

Lastly, no significant differences can be found for expert drivers in either scenarios other than the total measured torque on the steering wheel in scenario 2. While driving with both controller variations, expert drivers outperformed all the other drivers in terms of minimizing lane deviation. On average, they generated the largest lateral force at the front axle while using the smallest steering input to perform the evasive maneuver. Furthermore, they scored the lowest on mental and physical demand metrics. Therefore, haptic support systems have no significant influence on expert drivers, who can reliably assess the situation by themselves. More research should be done on identifying relevant differences between expert and regular/novice drivers in emergency scenarios that could be linked with safer maneuvers. An in-depth analysis of their behaviour could be beneficial for the design of future driver-oriented ADAS systems. Such an endeavor would require a large sample size of expert drivers, and their performance should be assessed on a wide range of emergency situations.

E

Individual Results

This chapter presents the experimental results of each participant individually. For each scenario, the collected data from the 3 runs with the support and the 3 runs without the support was averaged separately.

Driver 1

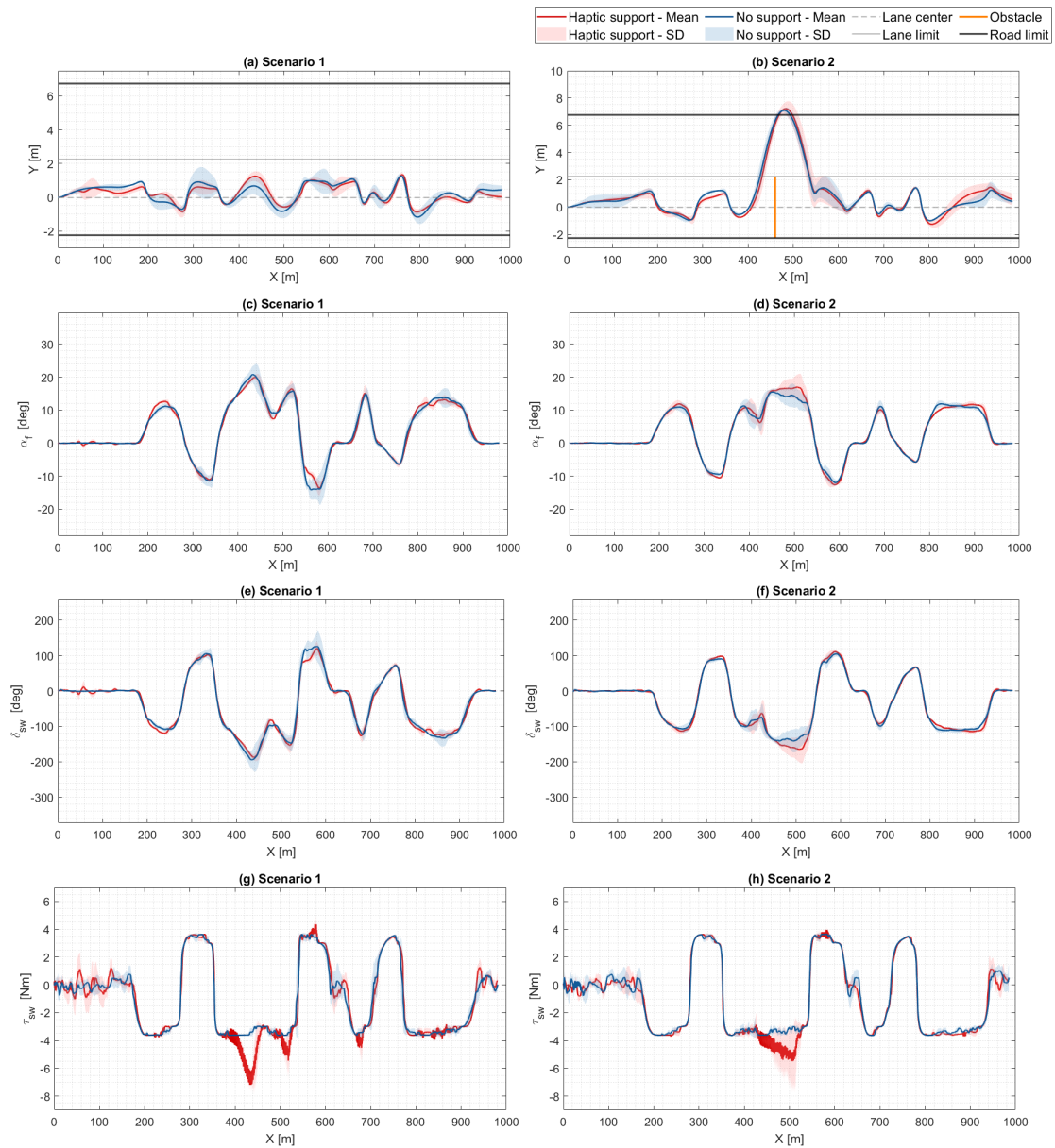


Figure E.1: Experimental results of driver 1: mean values (solid lines), and standard deviations (shaded areas) for the 2 support cases, plotted for both scenarios.

Metric	Scenario 1		Scenario 2	
	No support	Haptic support	No support	Haptic support
Mental demand	1	1	1	1
Physical demand	1	5	1	5
Performance	10	15	15	15
Frustration	15	21	15	21

Table E.1: NASA-TLX evaluation results for driver 1, for each driving mode, for both scenarios.

Driver 2

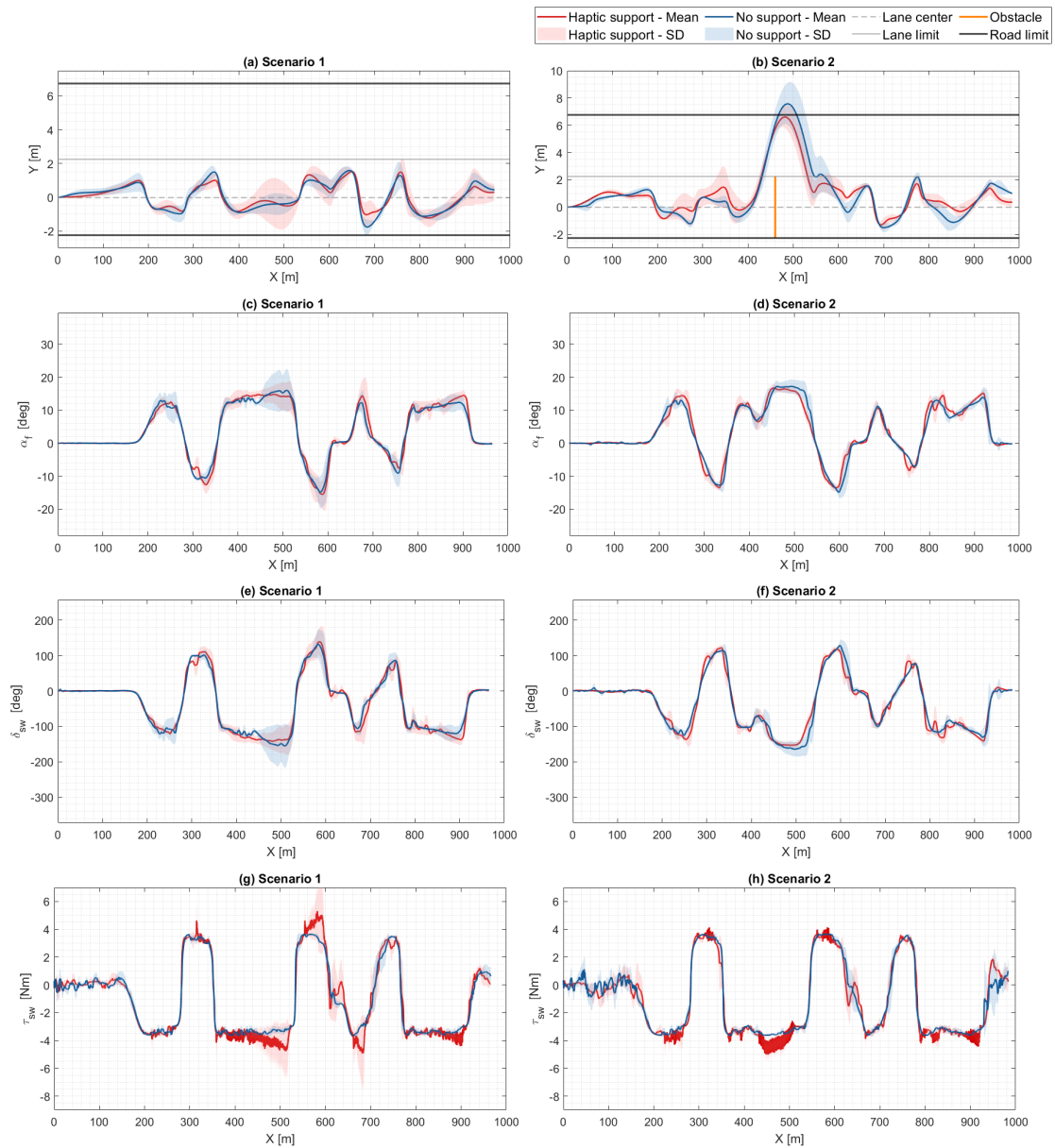


Figure E.2: Experimental results of driver 2: mean values (solid lines), and standard deviations (shaded areas) for the 2 support cases, plotted for both scenarios.

Metric	Scenario 1		Scenario 2	
	No support	Haptic support	No support	Haptic support
Mental demand	1	1	1	1
Physical demand	1	1	1	1
Performance	21	21	19	19
Frustration	1	1	1	1

Table E.2: NASA-TLX evaluation results for driver 2, for each driving mode, for both scenarios.

Driver 3

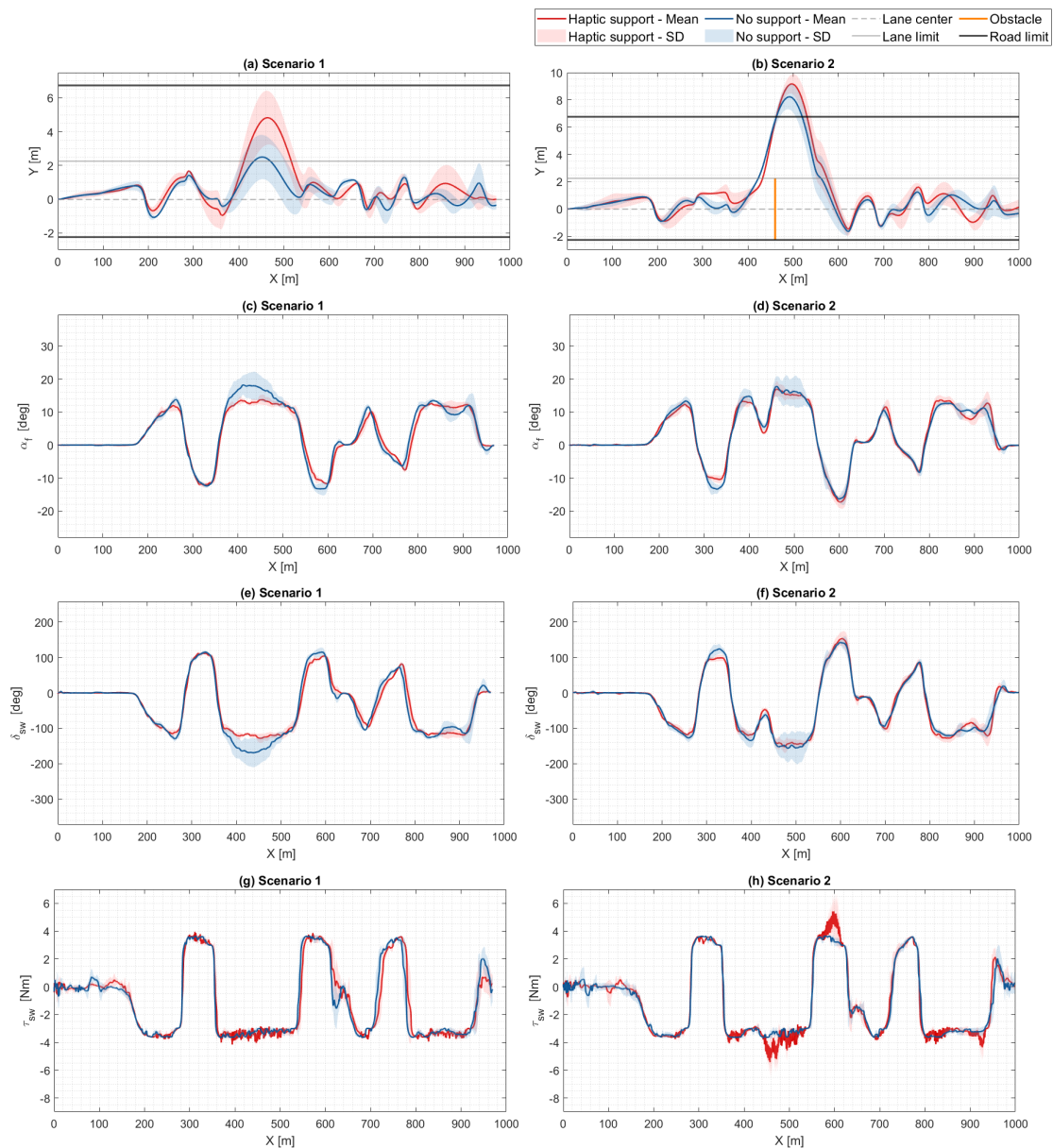


Figure E.3: Experimental results of driver 3: mean values (solid lines), and standard deviations (shaded areas) for the 2 support cases, plotted for both scenarios.

Metric	Scenario 1		Scenario 2	
	No support	Haptic support	No support	Haptic support
Mental demand	14	10	18	15
Physical demand	16	14	20	15
Performance	7	12	5	8
Frustration	10	5	14	11

Table E.3: NASA-TLX evaluation results for driver 3, for each driving mode, for both scenarios.

Driver 4

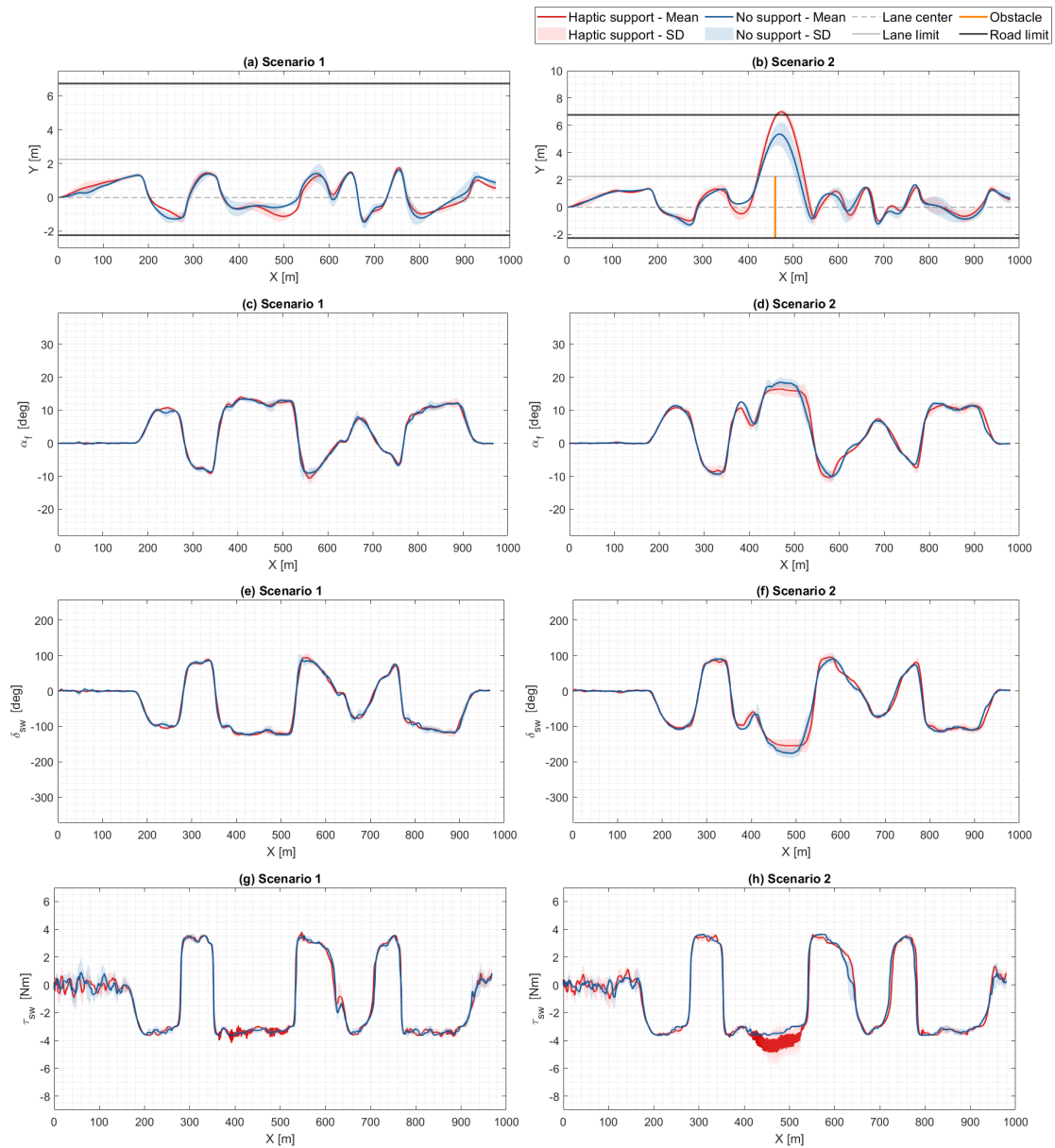


Figure E.4: Experimental results of driver 4: mean values (solid lines), and standard deviations (shaded areas) for the 2 support cases, plotted for both scenarios.

Metric	Scenario 1		Scenario 2	
	No support	Haptic support	No support	Haptic support
Mental demand	10	10	10	10
Physical demand	10	10	3	3
Performance	15	15	17	17
Frustration	1	1	2	2

Table E.4: NASA-TLX evaluation results for driver 4, for each driving mode, for both scenarios.

Driver 5

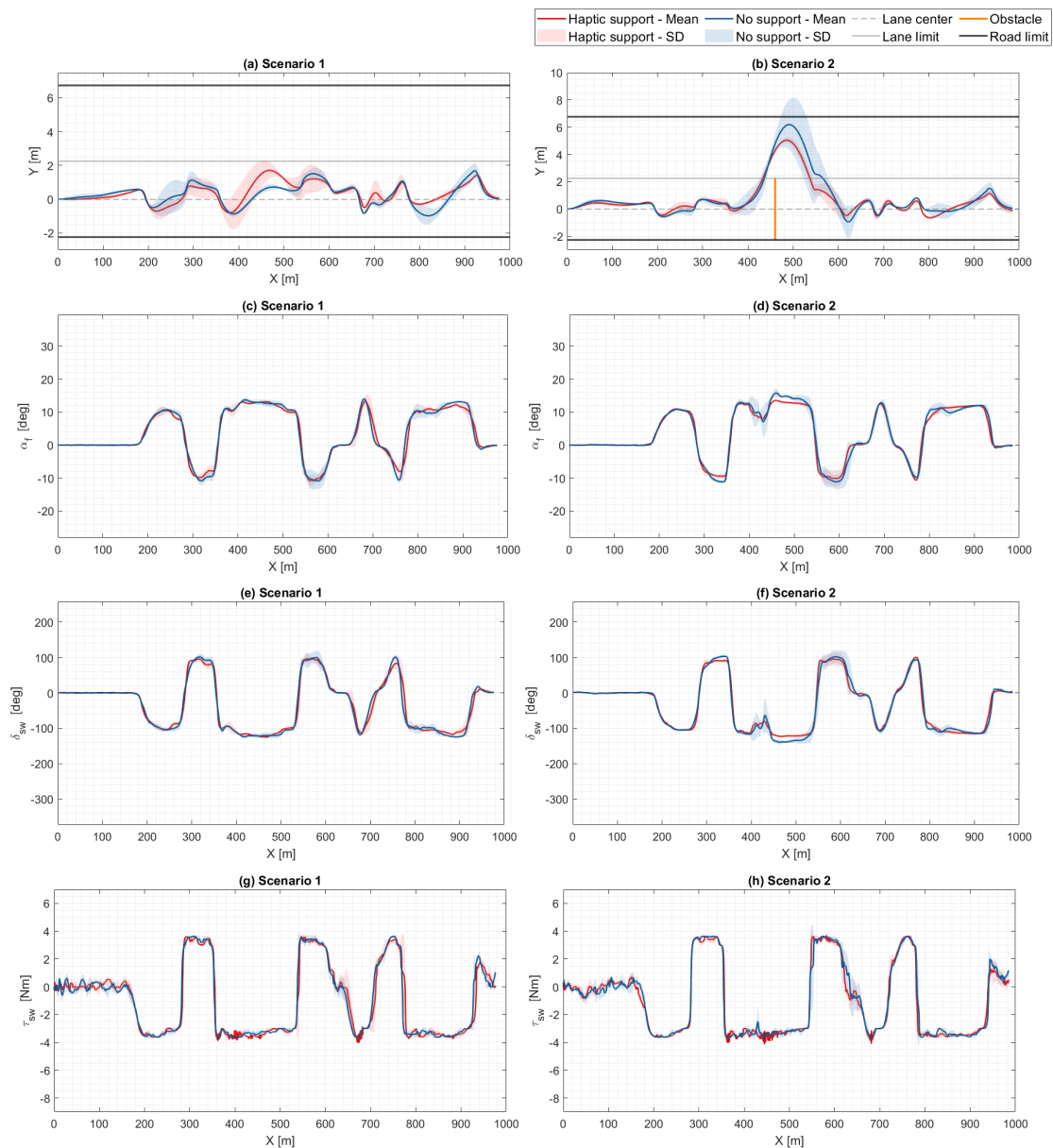


Figure E.5: Experimental results of driver 5: mean values (solid lines), and standard deviations (shaded areas) for the 2 support cases, plotted for both scenarios.

Metric	Scenario 1		Scenario 2	
	No support	Haptic support	No support	Haptic support
Mental demand	5	5	10	10
Physical demand	9	9	12	12
Performance	13	15	11	12
Frustration	10	10	15	16

Table E.5: NASA-TLX evaluation results for driver 5, for each driving mode, for both scenarios.

Driver 6

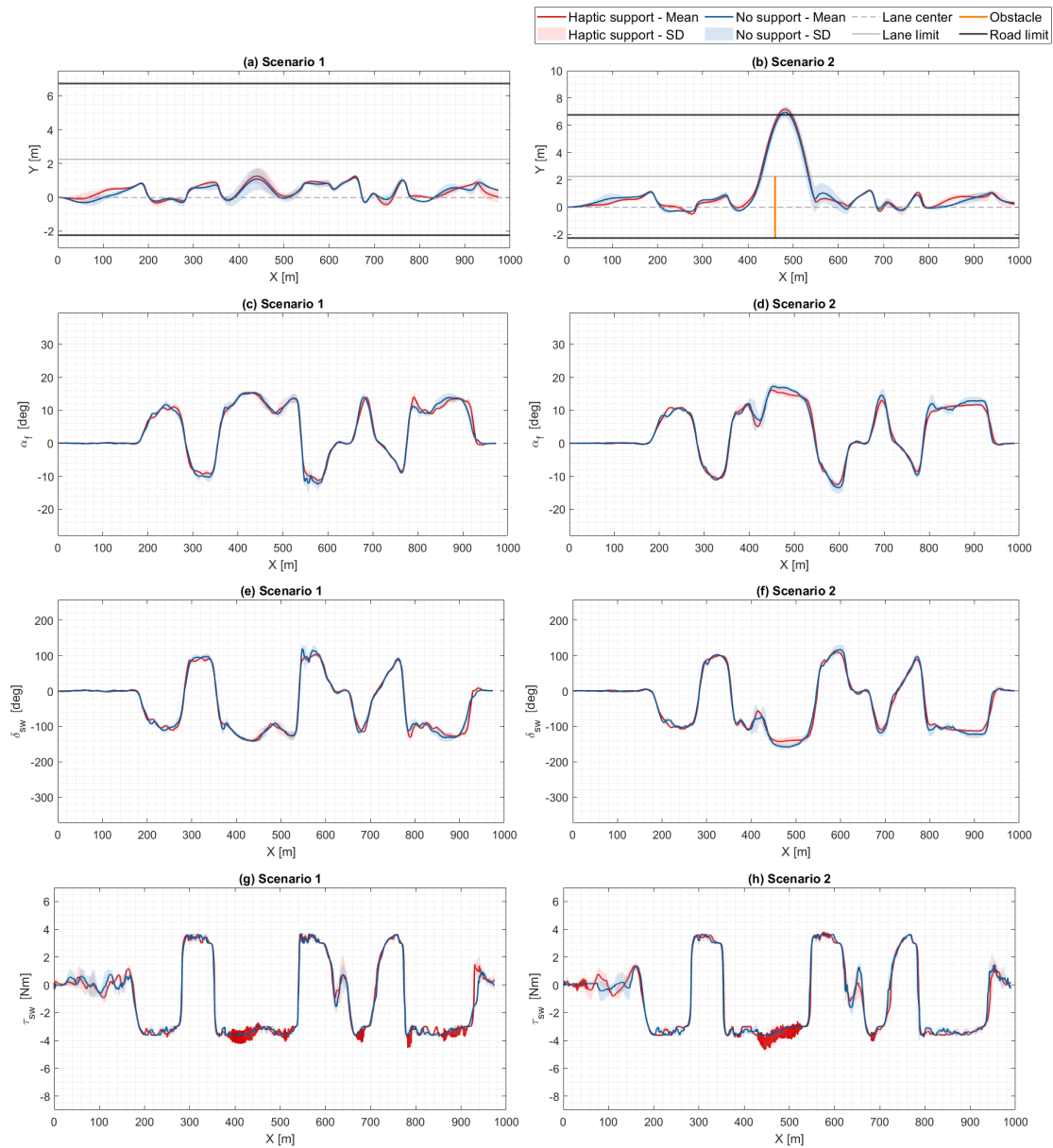


Figure E.6: Experimental results of driver 6: mean values (solid lines), and standard deviations (shaded areas) for the 2 support cases, plotted for both scenarios.

Metric	Scenario 1		Scenario 2	
	No support	Haptic support	No support	Haptic support
Mental demand	12	11	12	11
Physical demand	9	9	9	9
Performance	15	17	15	17
Frustration	10	9	10	9

Table E.6: NASA-TLX evaluation results for driver 6, for each driving mode, for both scenarios.

Driver 7

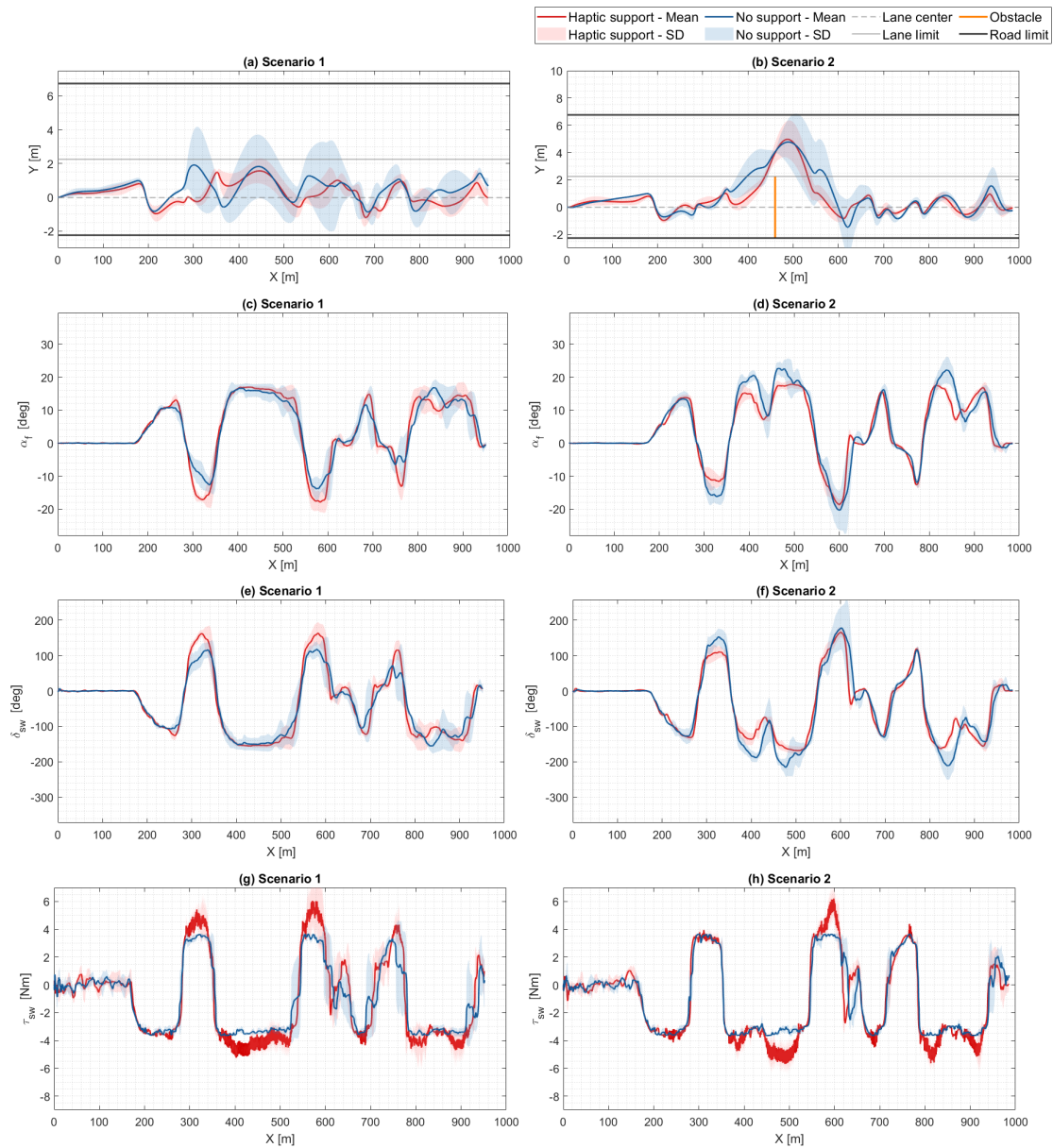


Figure E.7: Experimental results of driver 7: mean values (solid lines), and standard deviations (shaded areas) for the 2 support cases, plotted for both scenarios.

Metric	Scenario 1		Scenario 2	
	No support	Haptic support	No support	Haptic support
Mental demand	11	9	14	13
Physical demand	12	12	13	10
Performance	14	16	16	18
Frustration	8	9	12	13

Table E.7: NASA-TLX evaluation results for driver 7, for each driving mode, for both scenarios.

Driver 8

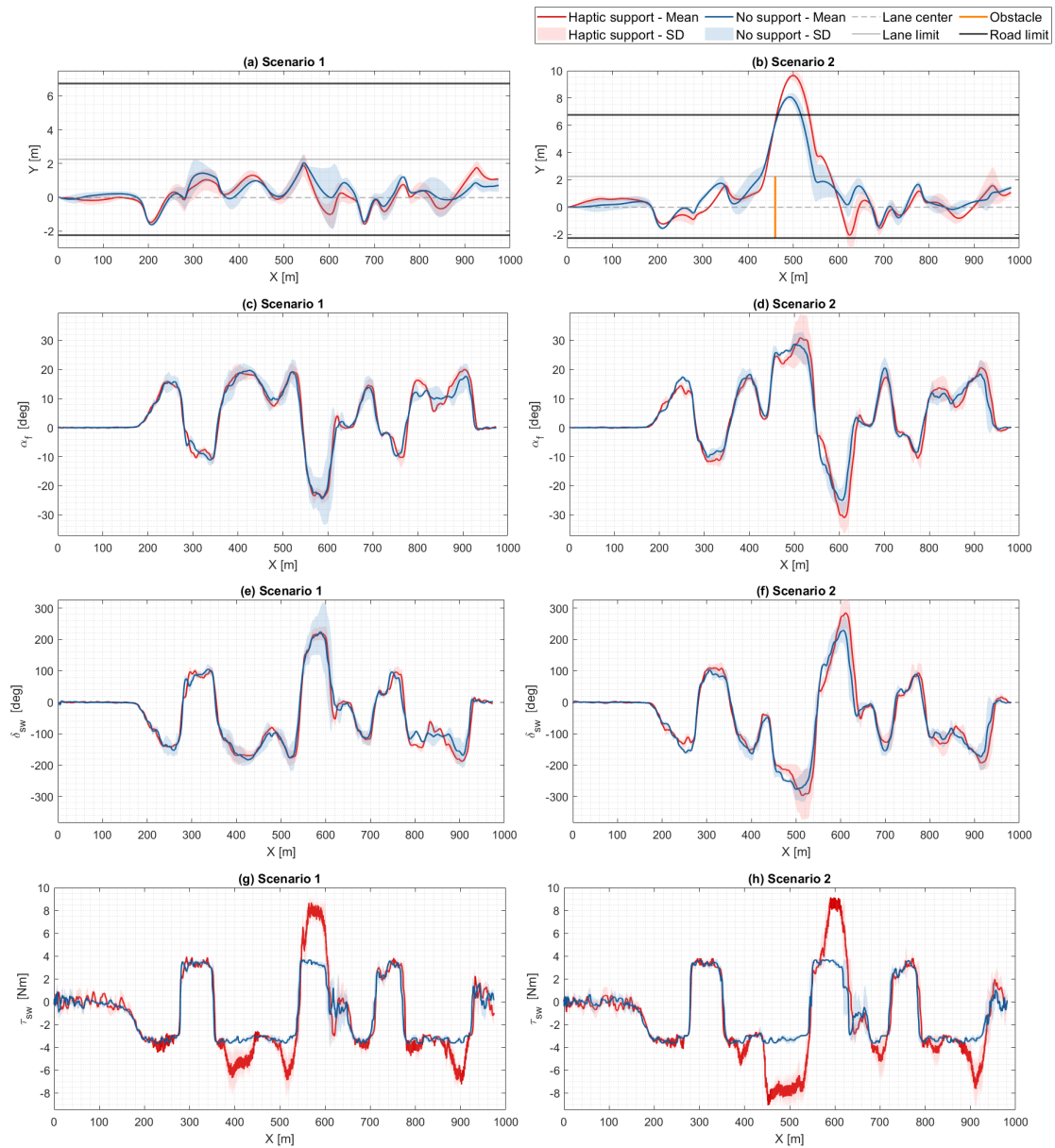


Figure E.8: Experimental results of driver 8: mean values (solid lines), and standard deviations (shaded areas) for the 2 support cases, plotted for both scenarios.

Metric	Scenario 1		Scenario 2	
	No support	Haptic support	No support	Haptic support
Mental demand	11	7	15	15
Physical demand	3	4	6	9
Performance	14	16	9	8
Frustration	13	12	15	17

Table E.8: NASA-TLX evaluation results for driver 8, for each driving mode, for both scenarios.

Driver 9

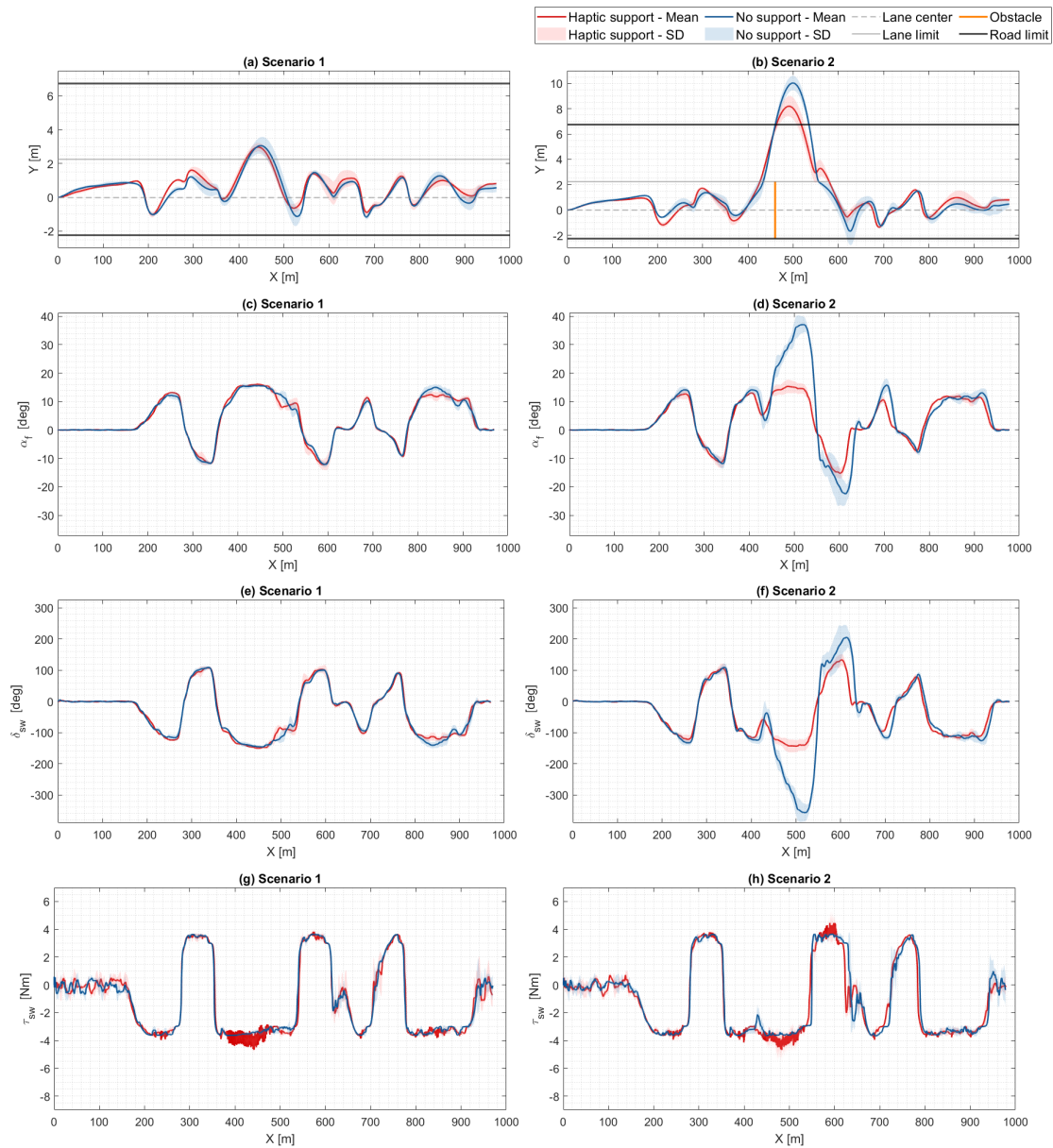


Figure E.9: Experimental results of driver 9: mean values (solid lines), and standard deviations (shaded areas) for the 2 support cases, plotted for both scenarios.

Metric	Scenario 1		Scenario 2	
	No support	Haptic support	No support	Haptic support
Mental demand	14	11	15	4
Physical demand	14	10	14	2
Performance	10	14	17	1
Frustration	14	8	15	4

Table E.9: NASA-TLX evaluation results for driver 9, for each driving mode, for both scenarios.

Driver 10

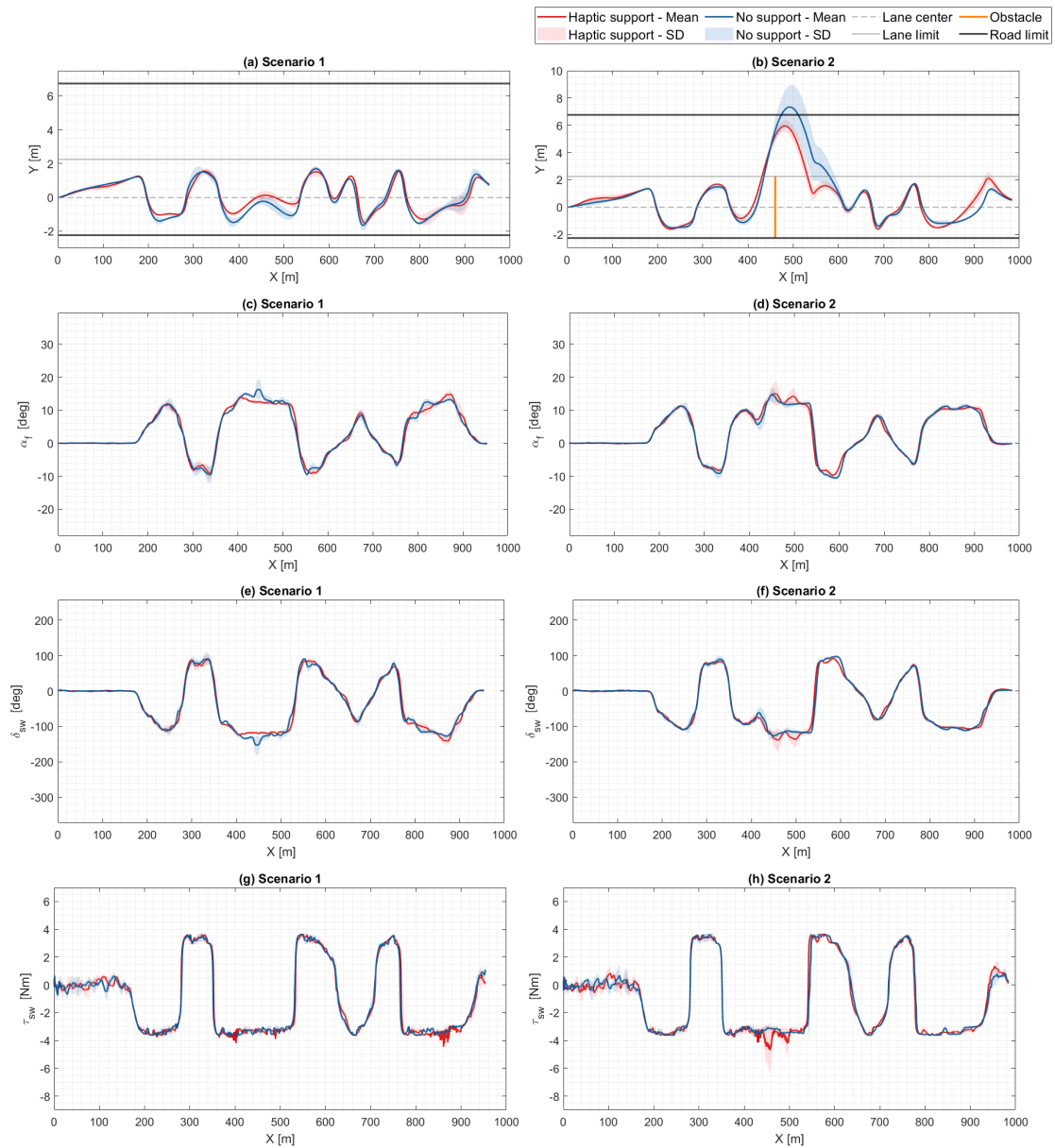


Figure E.10: Experimental results of driver 10: mean values (solid lines), and standard deviations (shaded areas) for the 2 support cases, plotted for both scenarios.

Metric	Scenario 1		Scenario 2	
	No support	Haptic support	No support	Haptic support
Mental demand	7	7	7	7
Physical demand	4	4	6	6
Performance	19	20	19	20
Frustration	1	1	1	1

Table E.10: NASA-TLX evaluation results for driver 10, for each driving mode, for both scenarios.

Driver 11

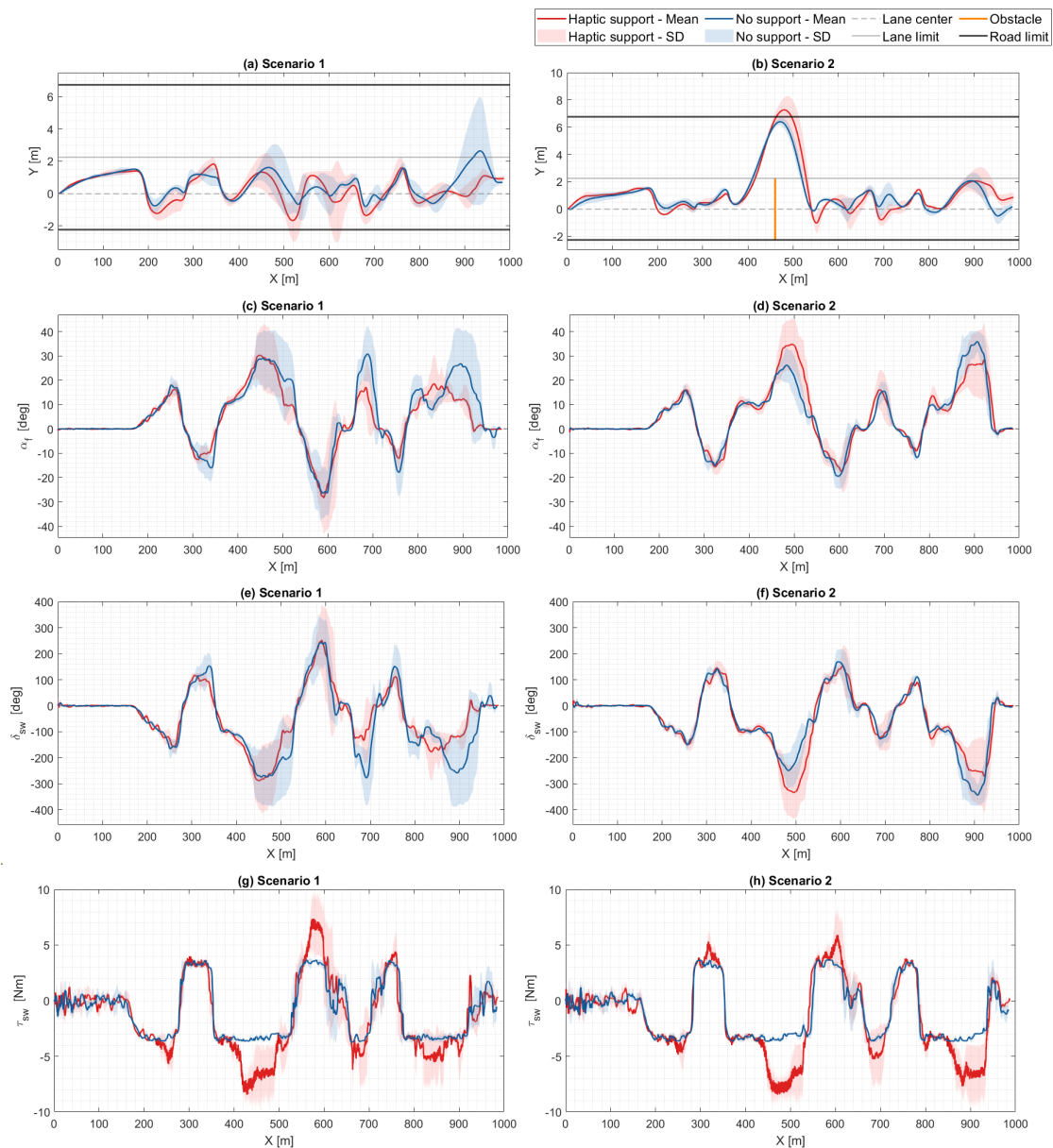


Figure E.11: Experimental results of driver 11: mean values (solid lines), and standard deviations (shaded areas) for the 2 support cases, plotted for both scenarios.

Metric	Scenario 1		Scenario 2	
	No support	Haptic support	No support	Haptic support
Mental demand	13	15	13	15
Physical demand	6	9	6	9
Performance	15	16	15	16
Frustration	1	1	1	1

Table E.11: NASA-TLX evaluation results for driver 11, for each driving mode, for both scenarios.

Driver 12

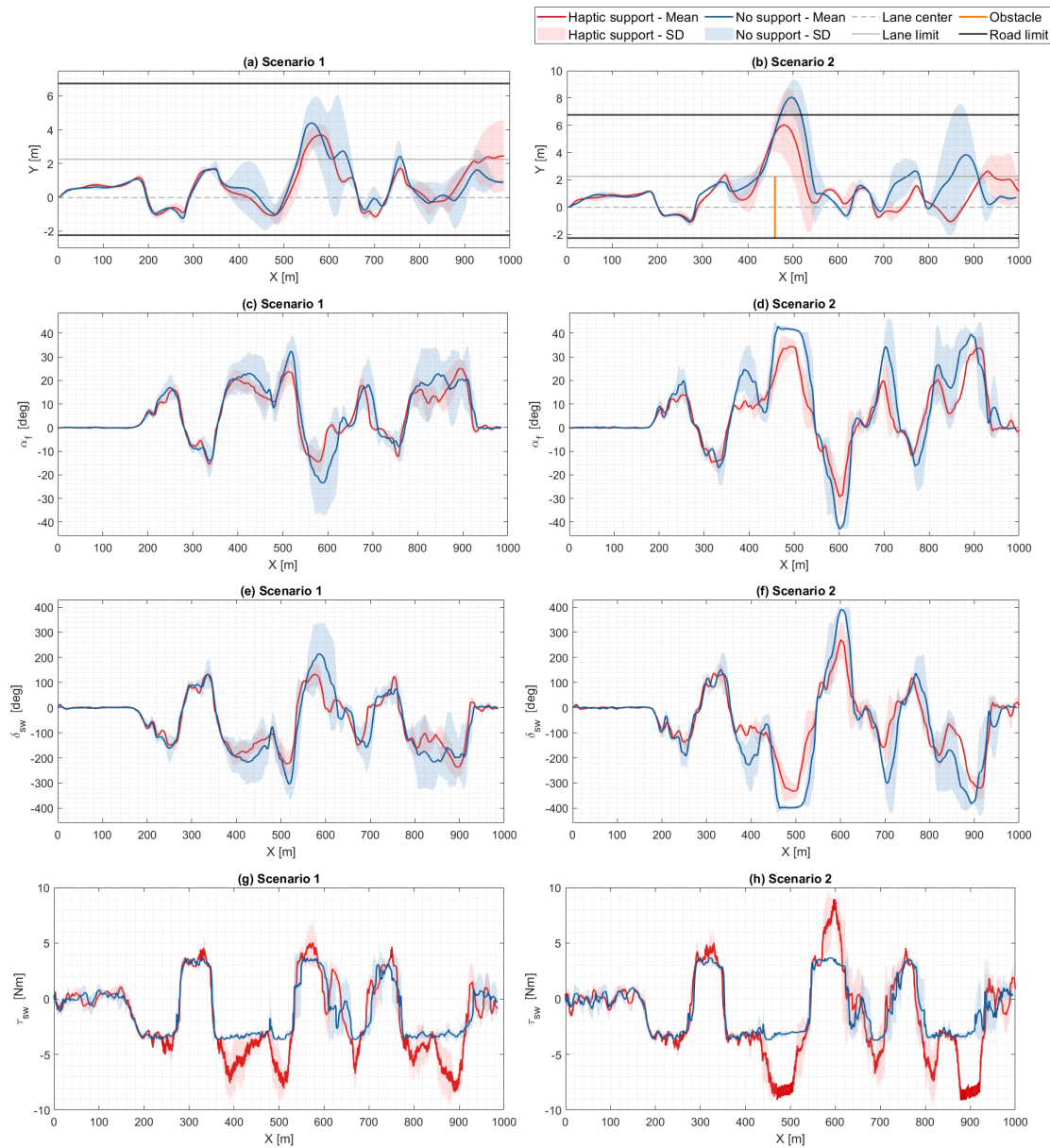


Figure E.12: Experimental results of driver 12: mean values (solid lines), and standard deviations (shaded areas) for the 2 support cases, plotted for both scenarios.

Metric	Scenario 1		Scenario 2	
	No support	Haptic support	No support	Haptic support
Mental demand	15	10	19	17
Physical demand	17	12	20	15
Performance	15	19	8	18
Frustration	8	4	18	8

Table E.12: NASA-TLX evaluation results for driver 12, for each driving mode, for both scenarios.

Driver 13

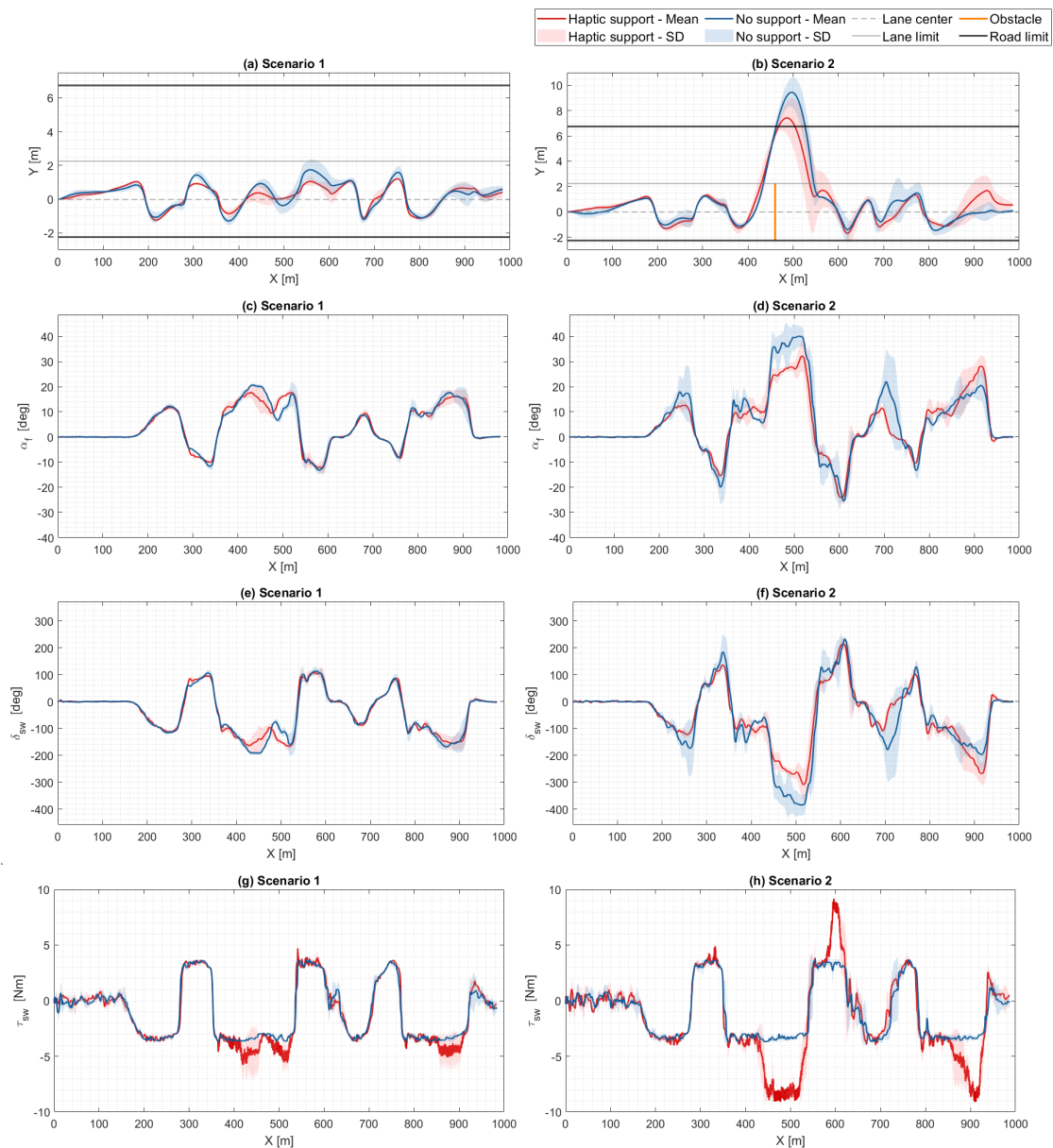


Figure E.13: Experimental results of driver 13: mean values (solid lines), and standard deviations (shaded areas) for the 2 support cases, plotted for both scenarios.

Metric	Scenario 1		Scenario 2	
	No support	Haptic support	No support	Haptic support
Mental demand	3	6	3	2
Physical demand	2	3	4	2
Performance	18	18	13	18
Frustration	6	8	8	5

Table E.13: NASA-TLX evaluation results for driver 13, for each driving mode, for both scenarios.

Driver 14

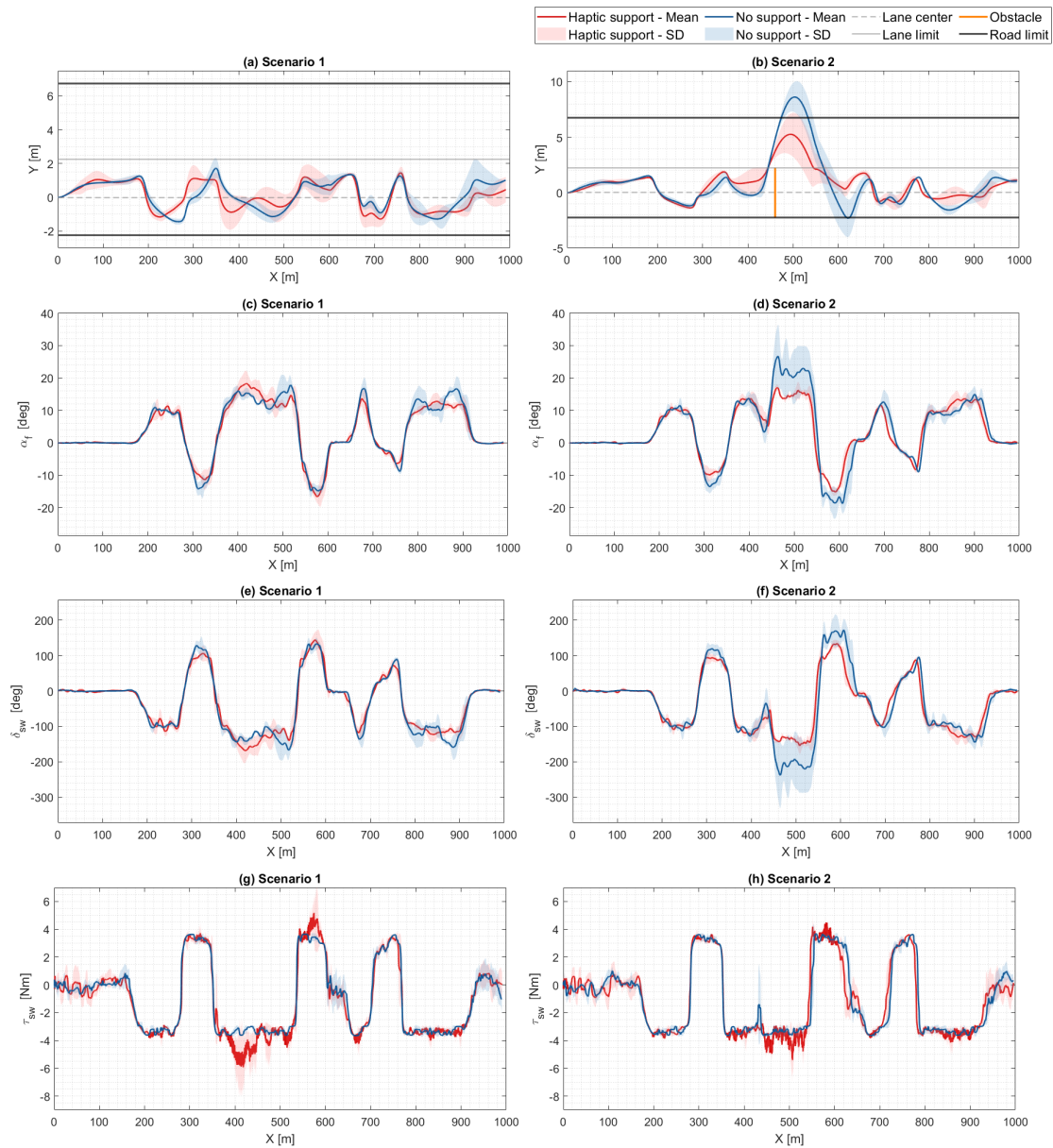


Figure E.14: Experimental results of driver 14: mean values (solid lines), and standard deviations (shaded areas) for the 2 support cases, plotted for both scenarios.

Metric	Scenario 1		Scenario 2	
	No support	Haptic support	No support	Haptic support
Mental demand	15	10	21	15
Physical demand	5	10	8	15
Performance	7	15	13	18
Frustration	16	8	20	14

Table E.14: NASA-TLX evaluation results for driver 14, for each driving mode, for both scenarios.

Driver 15

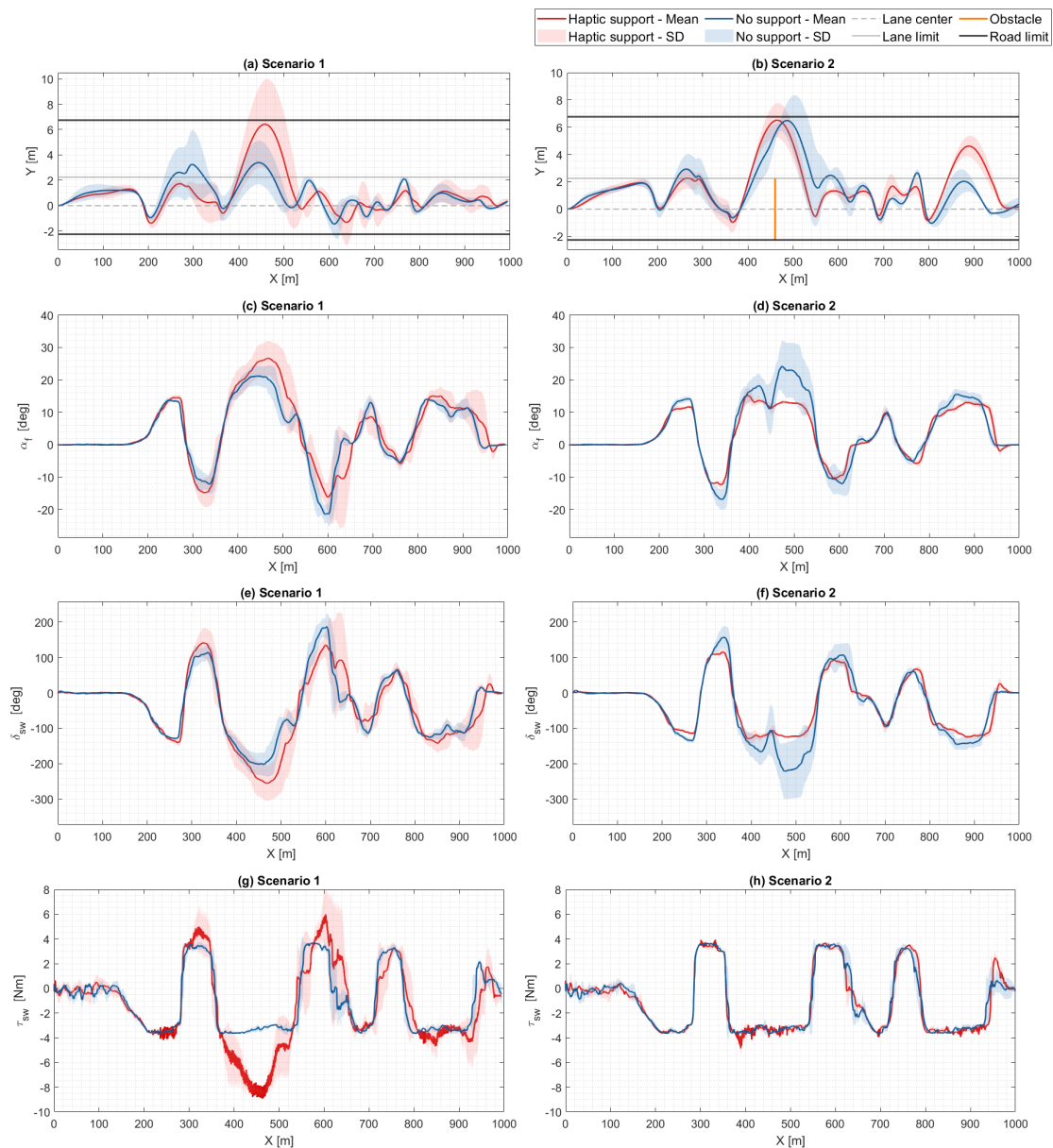


Figure E.15: Experimental results of driver 15: mean values (solid lines), and standard deviations (shaded areas) for the 2 support cases, plotted for both scenarios.

Metric	Scenario 1		Scenario 2	
	No support	Haptic support	No support	Haptic support
Mental demand	10	15	11	15
Physical demand	5	10	5	10
Performance	12	10	8	7
Frustration	5	15	10	15

Table E.15: NASA-TLX evaluation results for driver 15, for each driving mode, for both scenarios.

Driver 16

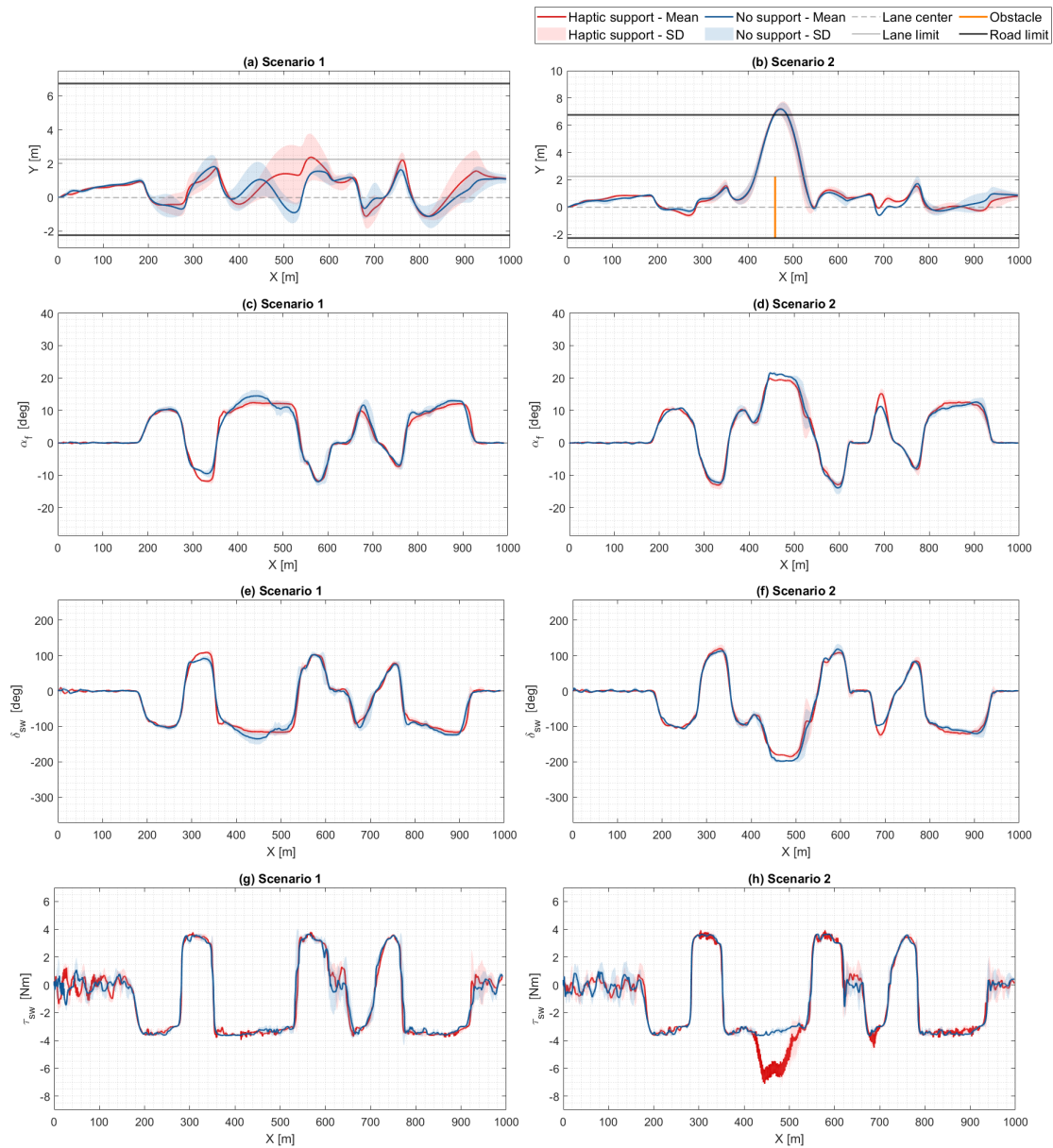


Figure E.16: Experimental results of driver 16: mean values (solid lines), and standard deviations (shaded areas) for the 2 support cases, plotted for both scenarios.

Metric	Scenario 1		Scenario 2	
	No support	Haptic support	No support	Haptic support
Mental demand	7	15	7	7
Physical demand	8	18	7	10
Performance	14	17	16	16
Frustration	15	8	4	4

Table E.16: NASA-TLX evaluation results for driver 16, for each driving mode, for both scenarios.

Driver 17

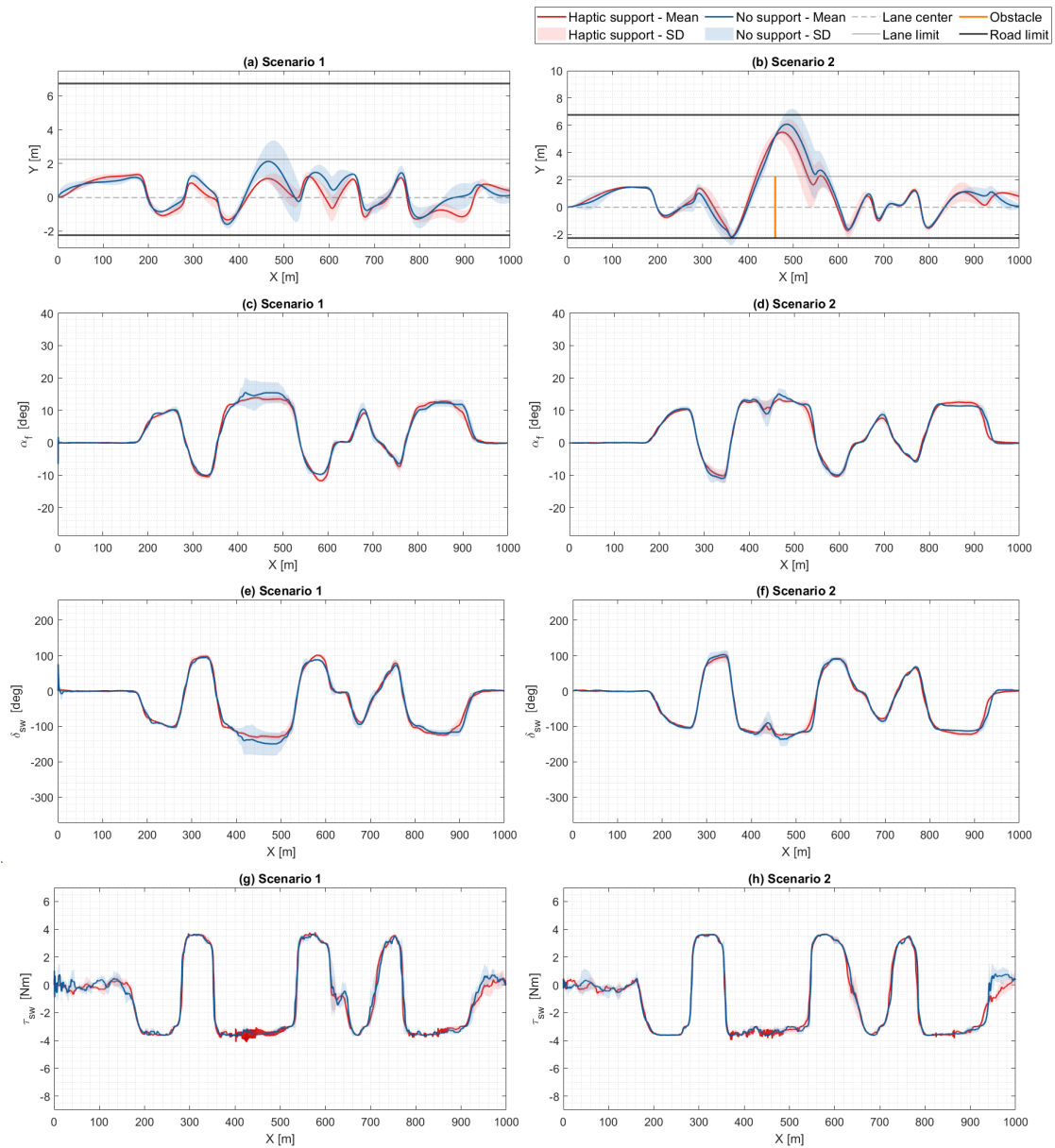


Figure E.17: Experimental results of driver 17: mean values (solid lines), and standard deviations (shaded areas) for the 2 support cases, plotted for both scenarios.

Metric	Scenario 1		Scenario 2	
	No support	Haptic support	No support	Haptic support
Mental demand	10	10	13	13
Physical demand	4	4	5	5
Performance	16	16	12	13
Frustration	3	3	5	7

Table E.17: NASA-TLX evaluation results for driver 17, for each driving mode, for both scenarios.

Driver 18

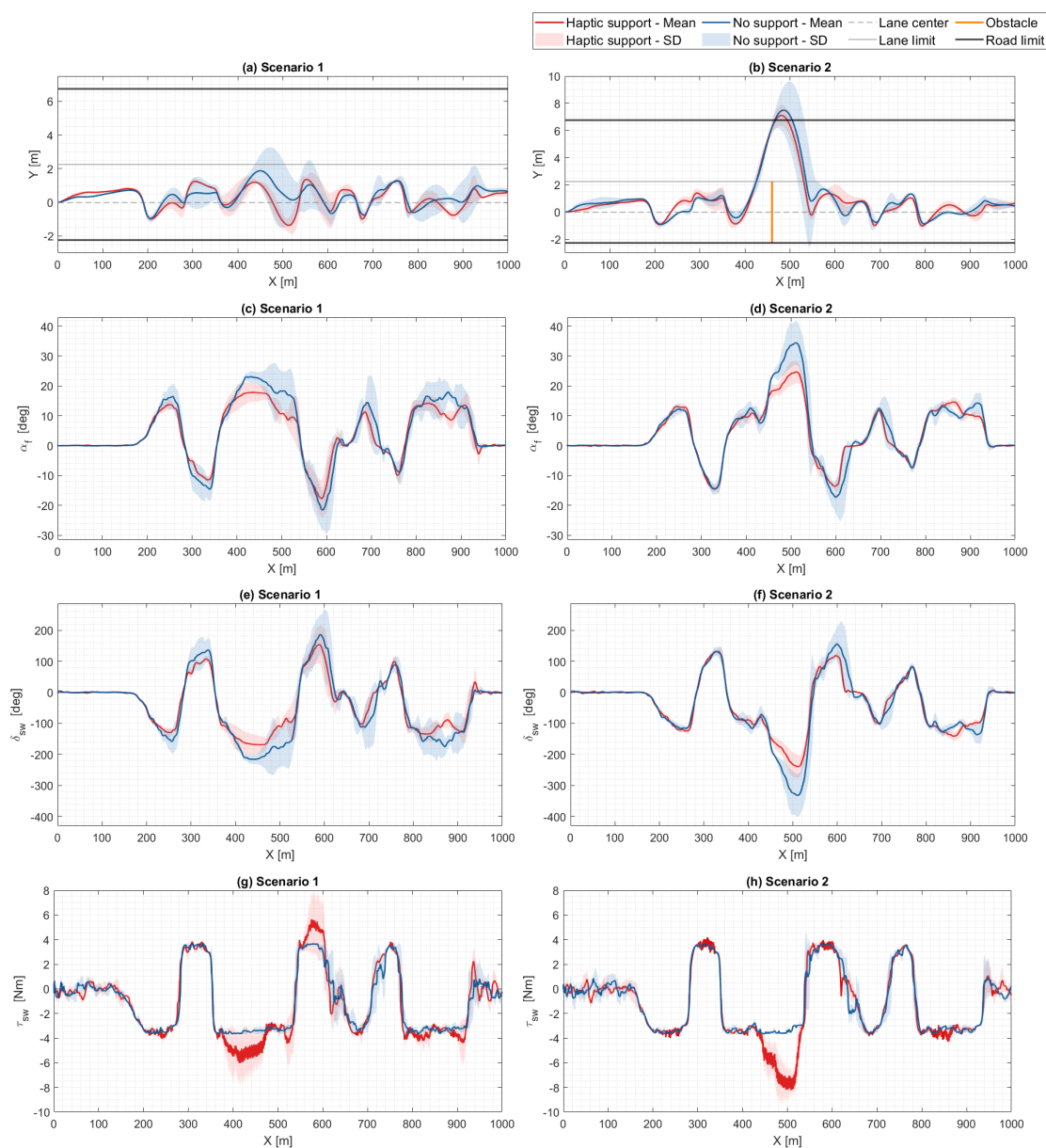


Figure E.18: Experimental results of driver 18: mean values (solid lines), and standard deviations (shaded areas) for the 2 support cases, plotted for both scenarios.

Metric	Scenario 1		Scenario 2	
	No support	Haptic support	No support	Haptic support
Mental demand	6	6	9	14
Physical demand	6	7	10	15
Performance	16	15	15	13
Frustration	3	7	6	10

Table E.18: NASA-TLX evaluation results for driver 18, for each driving mode, for both scenarios.

Driver 19

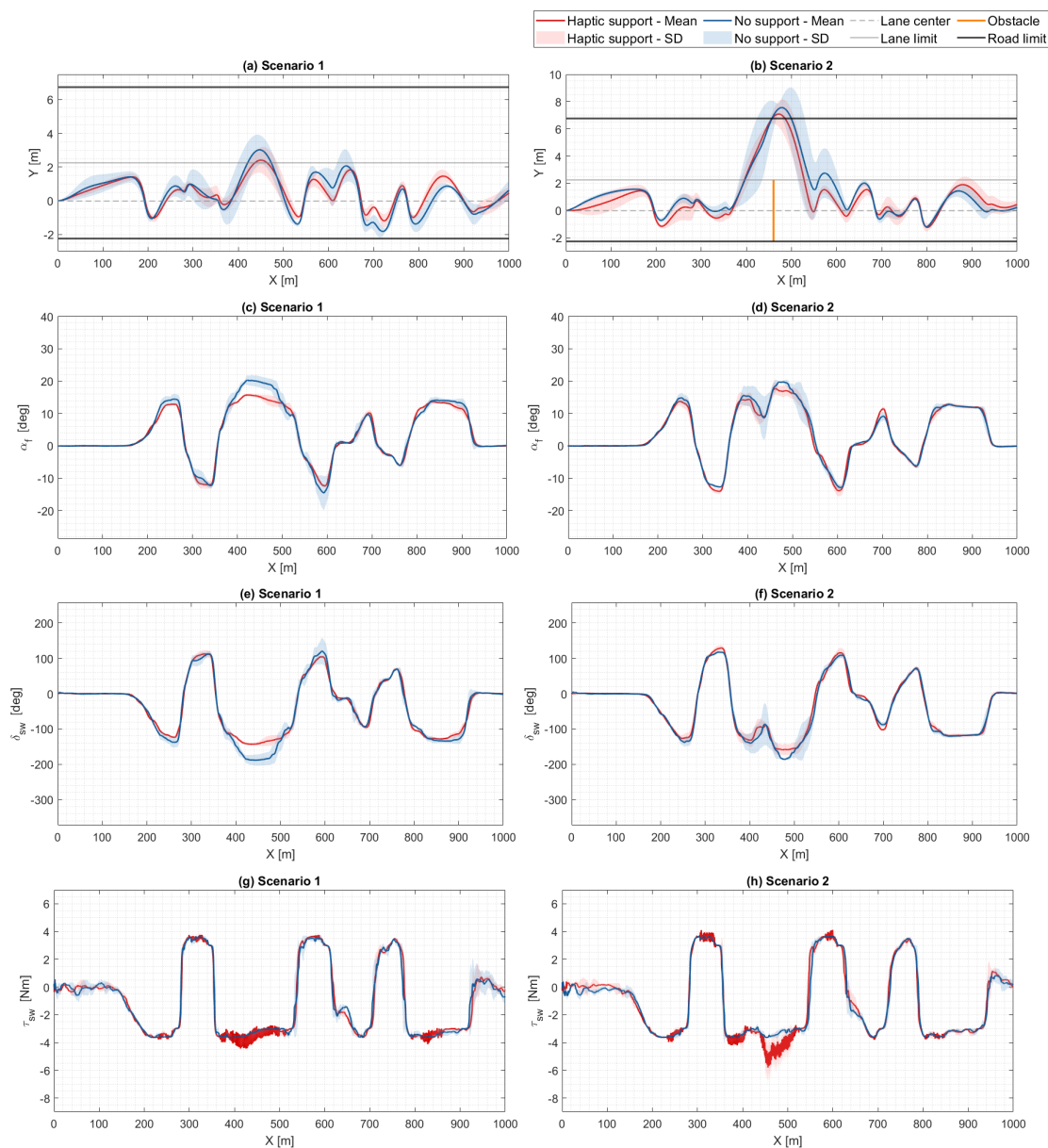


Figure E.19: Experimental results of driver 19: mean values (solid lines), and standard deviations (shaded areas) for the 2 support cases, plotted for both scenarios.

Metric	Scenario 1		Scenario 2	
	No support	Haptic support	No support	Haptic support
Mental demand	12	13	15	15
Physical demand	13	12	15	15
Performance	15	15	11	13
Frustration	11	11	13	11

Table E.19: NASA-TLX evaluation results for driver 19, for each driving mode, for both scenarios.

Driver 20

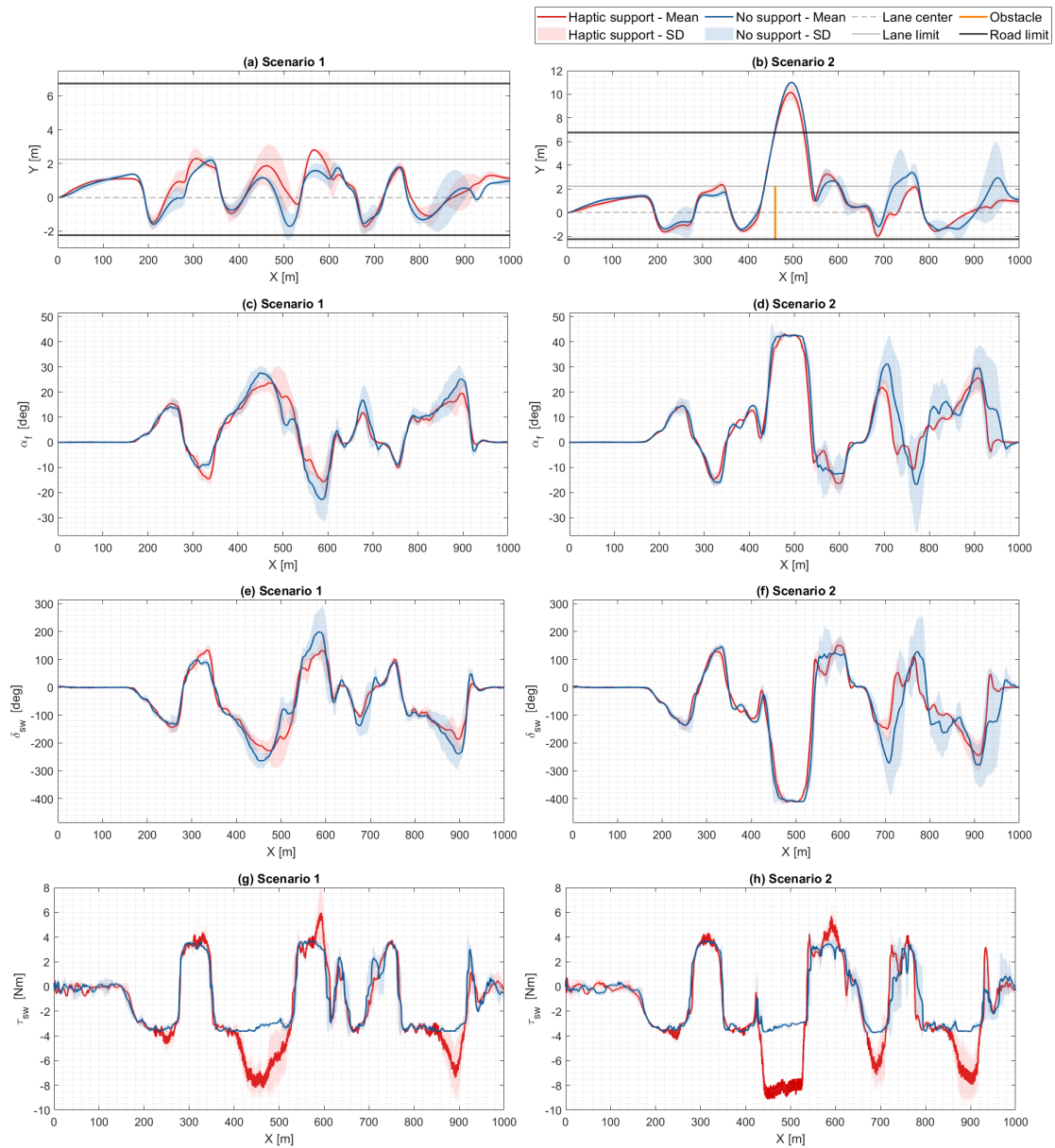


Figure E.20: Experimental results of driver 20: mean values (solid lines), and standard deviations (shaded areas) for the 2 support cases, plotted for both scenarios.

Metric	Scenario 1		Scenario 2	
	No support	Haptic support	No support	Haptic support
Mental demand	12	14	16	18
Physical demand	12	16	16	18
Performance	12	12	9	9
Frustration	10	12	13	14

Table E.20: NASA-TLX evaluation results for driver 20, for each driving mode, for both scenarios.

Driver 21

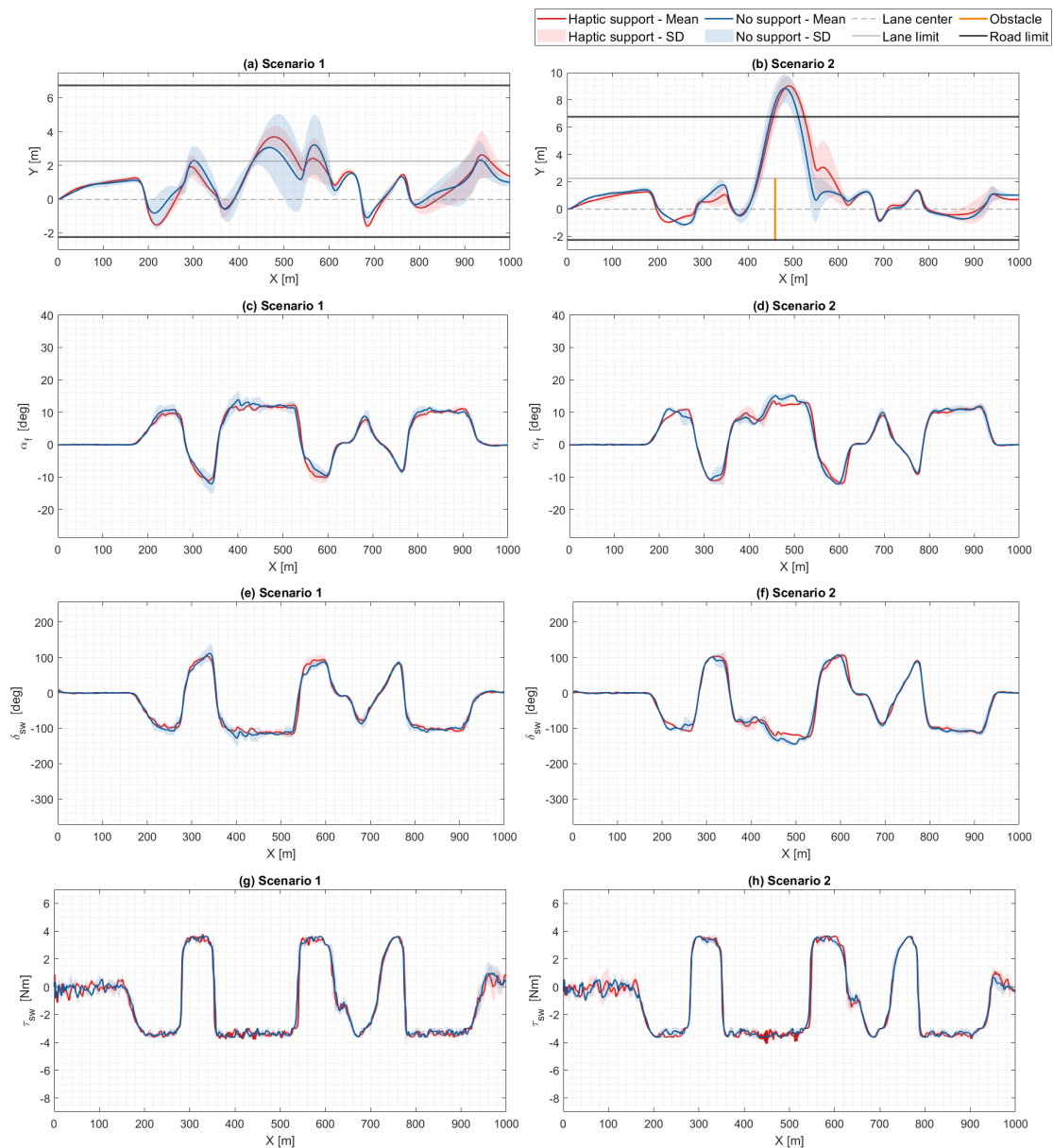


Figure E.21: Experimental results of driver 21: mean values (solid lines), and standard deviations (shaded areas) for the 2 support cases, plotted for both scenarios.

Metric	Scenario 1		Scenario 2	
	No support	Haptic support	No support	Haptic support
Mental demand	5	1	5	2
Physical demand	3	2	3	2
Performance	14	14	15	15
Frustration	7	1	8	2

Table E.21: NASA-TLX evaluation results for driver 21, for each driving mode, for both scenarios.

Driver 22

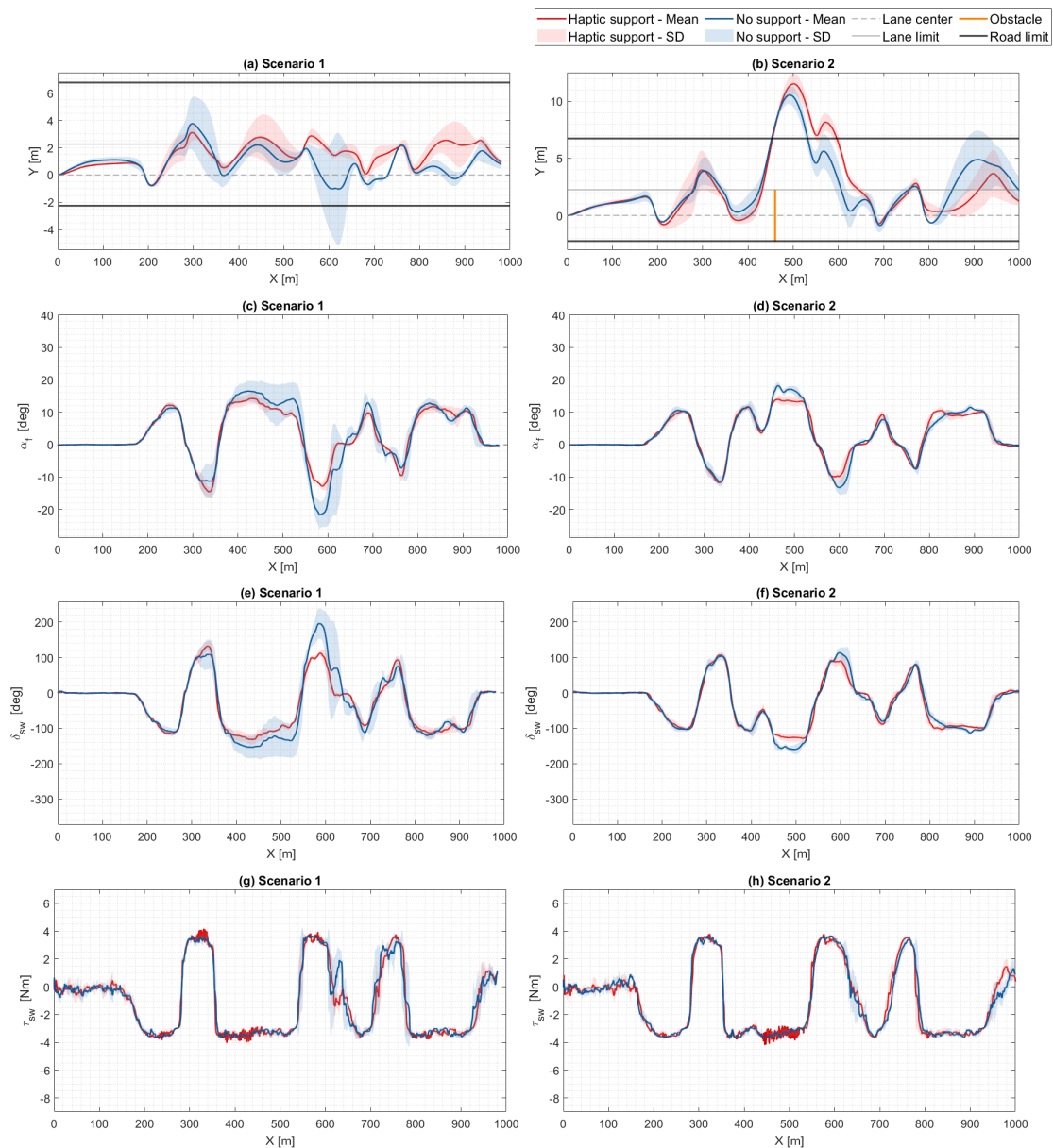


Figure E.22: Experimental results of driver 22: mean values (solid lines), and standard deviations (shaded areas) for the 2 support cases, plotted for both scenarios.

Metric	Scenario 1		Scenario 2	
	No support	Haptic support	No support	Haptic support
Mental demand	14	11	17	16
Physical demand	9	9	12	12
Performance	13	16	12	10
Frustration	12	10	12	11

Table E.22: NASA-TLX evaluation results for driver 22, for each driving mode, for both scenarios.

Driver 23

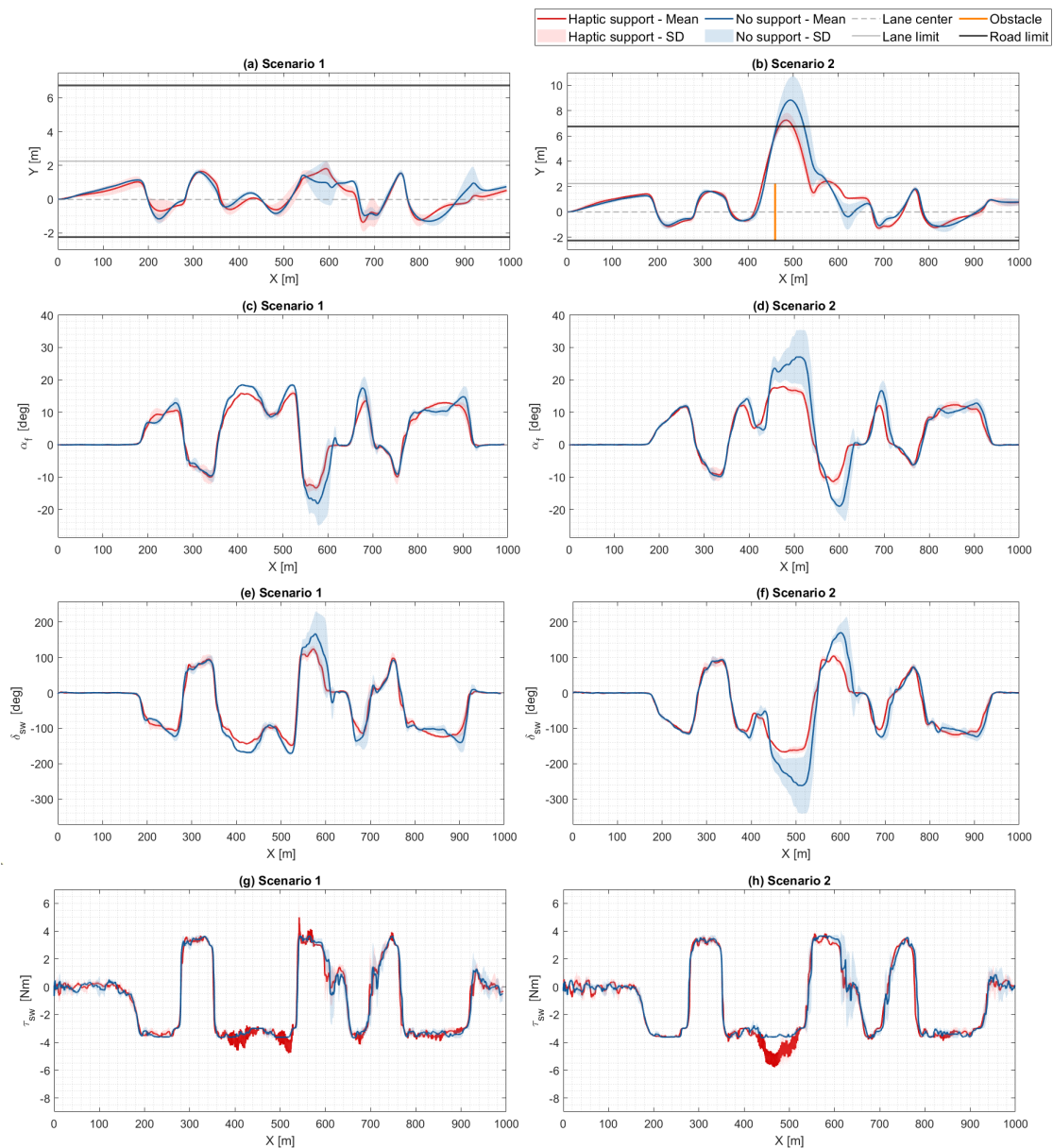


Figure E.23: Experimental results of driver 23: mean values (solid lines), and standard deviations (shaded areas) for the 2 support cases, plotted for both scenarios.

Metric	Scenario 1		Scenario 2	
	No support	Haptic support	No support	Haptic support
Mental demand	5	4	14	11
Physical demand	6	5	12	10
Performance	15	17	11	14
Frustration	5	4	12	9

Table E.23: NASA-TLX evaluation results for driver 23, for each driving mode, for both scenarios.

Driver 24

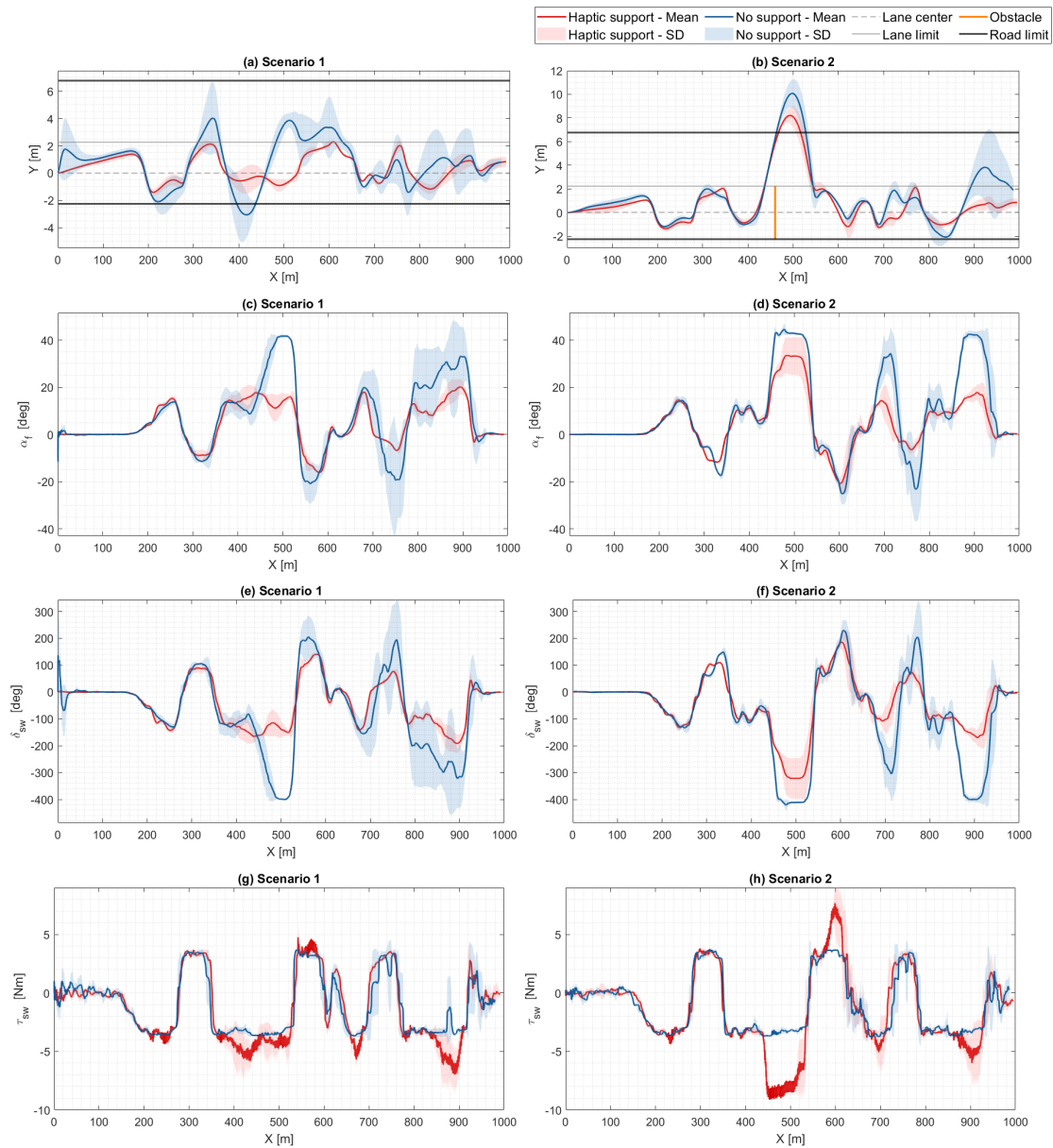


Figure E.24: Experimental results of driver 24: mean values (solid lines), and standard deviations (shaded areas) for the 2 support cases, plotted for both scenarios.

Metric	Scenario 1		Scenario 2	
	No support	Haptic support	No support	Haptic support
Mental demand	14	4	19	9
Physical demand	7	16	19	12
Performance	5	18	7	14
Frustration	16	2	14	7

Table E.24: NASA-TLX evaluation results for driver 24, for each driving mode, for both scenarios.

Driver 25

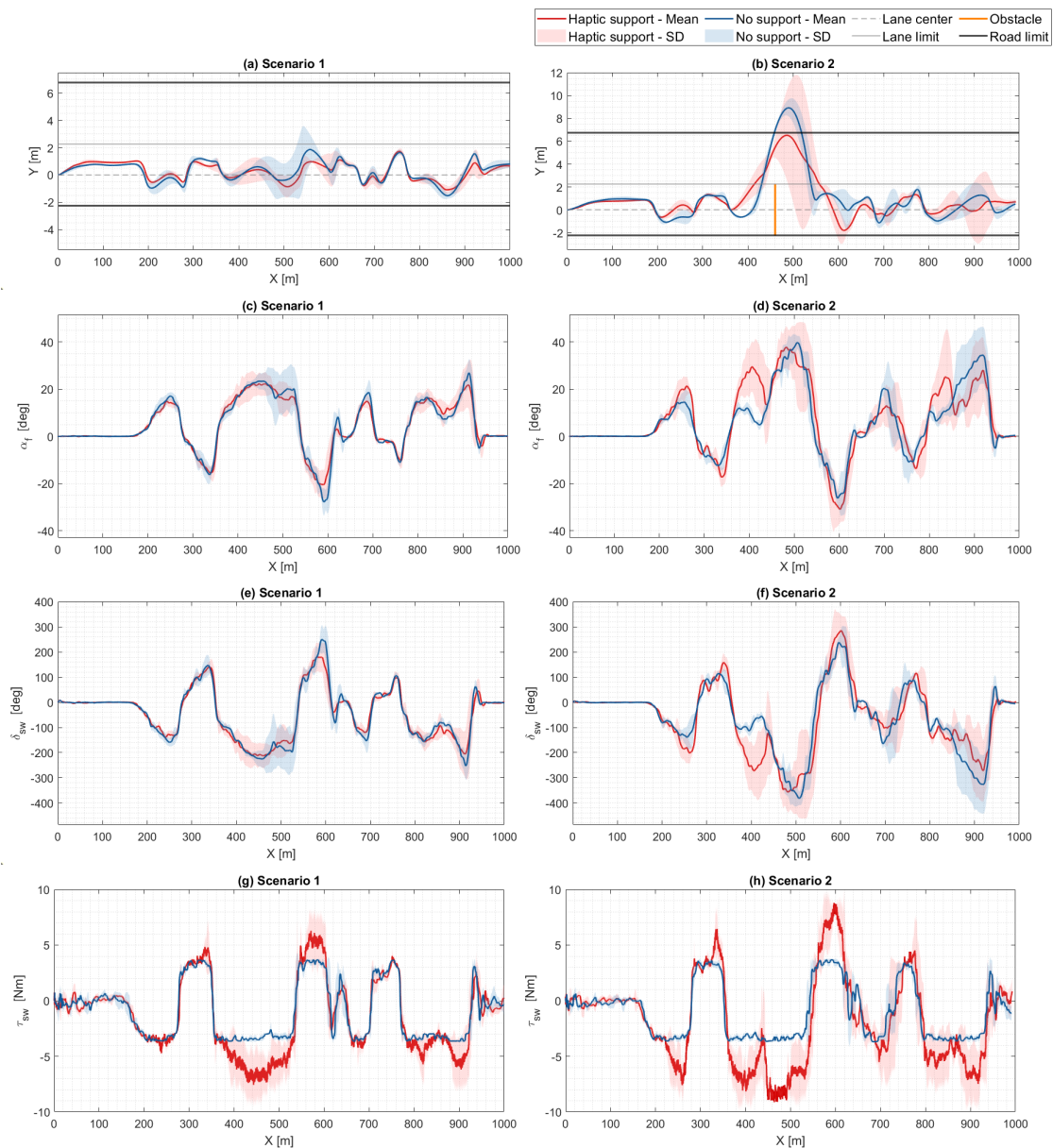


Figure E.25: Experimental results of driver 25: mean values (solid lines), and standard deviations (shaded areas) for the 2 support cases, plotted for both scenarios.

Metric	Scenario 1		Scenario 2	
	No support	Haptic support	No support	Haptic support
Mental demand	8	12	9	14
Physical demand	7	16	14	12
Performance	18	9	5	15
Frustration	8	17	10	14

Table E.25: NASA-TLX evaluation results for driver 25, for each driving mode, for both scenarios.

Driver 26

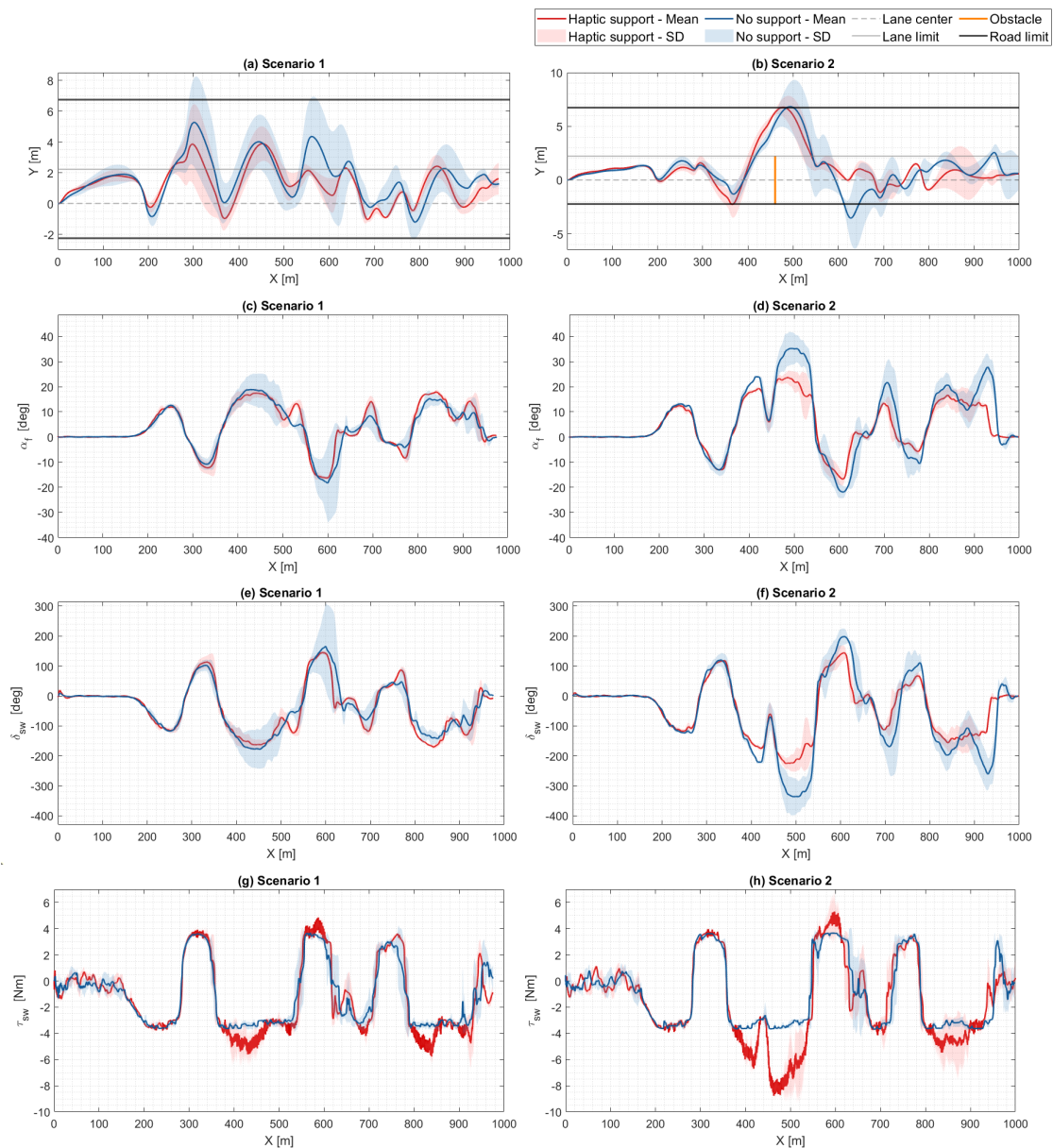


Figure E.26: Experimental results of driver 26: mean values (solid lines), and standard deviations (shaded areas) for the 2 support cases, plotted for both scenarios.

Metric	Scenario 1		Scenario 2	
	No support	Haptic support	No support	Haptic support
Mental demand	15	10	17	13
Physical demand	10	13	12	16
Performance	9	14	7	13
Frustration	15	11	16	13

Table E.26: NASA-TLX evaluation results for driver 26, for each driving mode, for both scenarios.

Driver 27

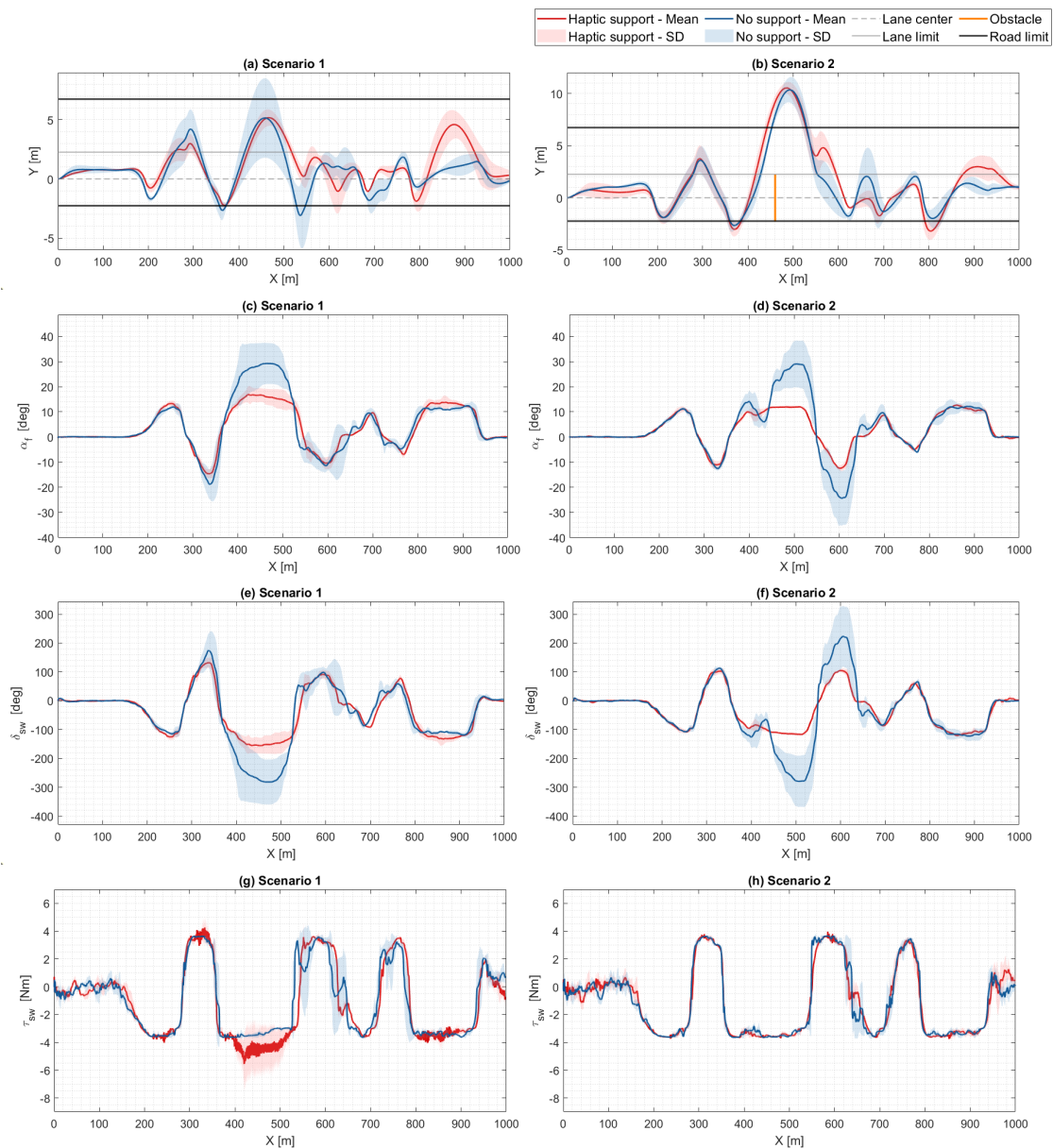


Figure E.27: Experimental results of driver 27: mean values (solid lines), and standard deviations (shaded areas) for the 2 support cases, plotted for both scenarios.

Metric	Scenario 1		Scenario 2	
	No support	Haptic support	No support	Haptic support
Mental demand	8	12	13	7
Physical demand	5	14	10	12
Performance	12	15	8	5
Frustration	4	7	10	10

Table E.27: NASA-TLX evaluation results for driver 27, for each driving mode, for both scenarios.

Driver 28

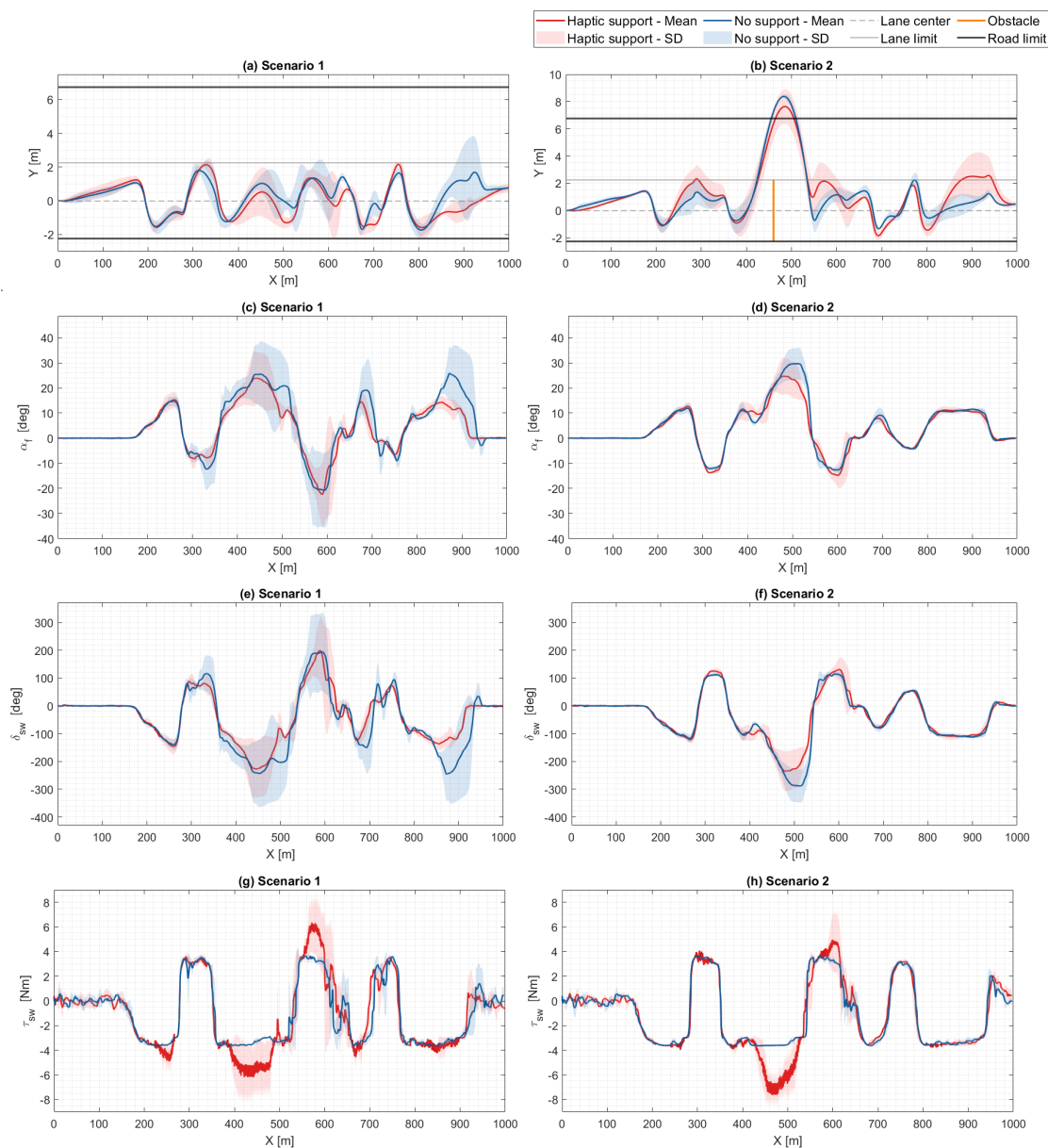


Figure E.28: Experimental results of driver 28: mean values (solid lines), and standard deviations (shaded areas) for the 2 support cases, plotted for both scenarios.

Metric	Scenario 1		Scenario 2	
	No support	Haptic support	No support	Haptic support
Mental demand	17	4	11	7
Physical demand	12	7	14	9
Performance	14	21	14	19
Frustration	11	5	10	5

Table E.28: NASA-TLX evaluation results for driver 28, for each driving mode, for both scenarios.

Driver 29

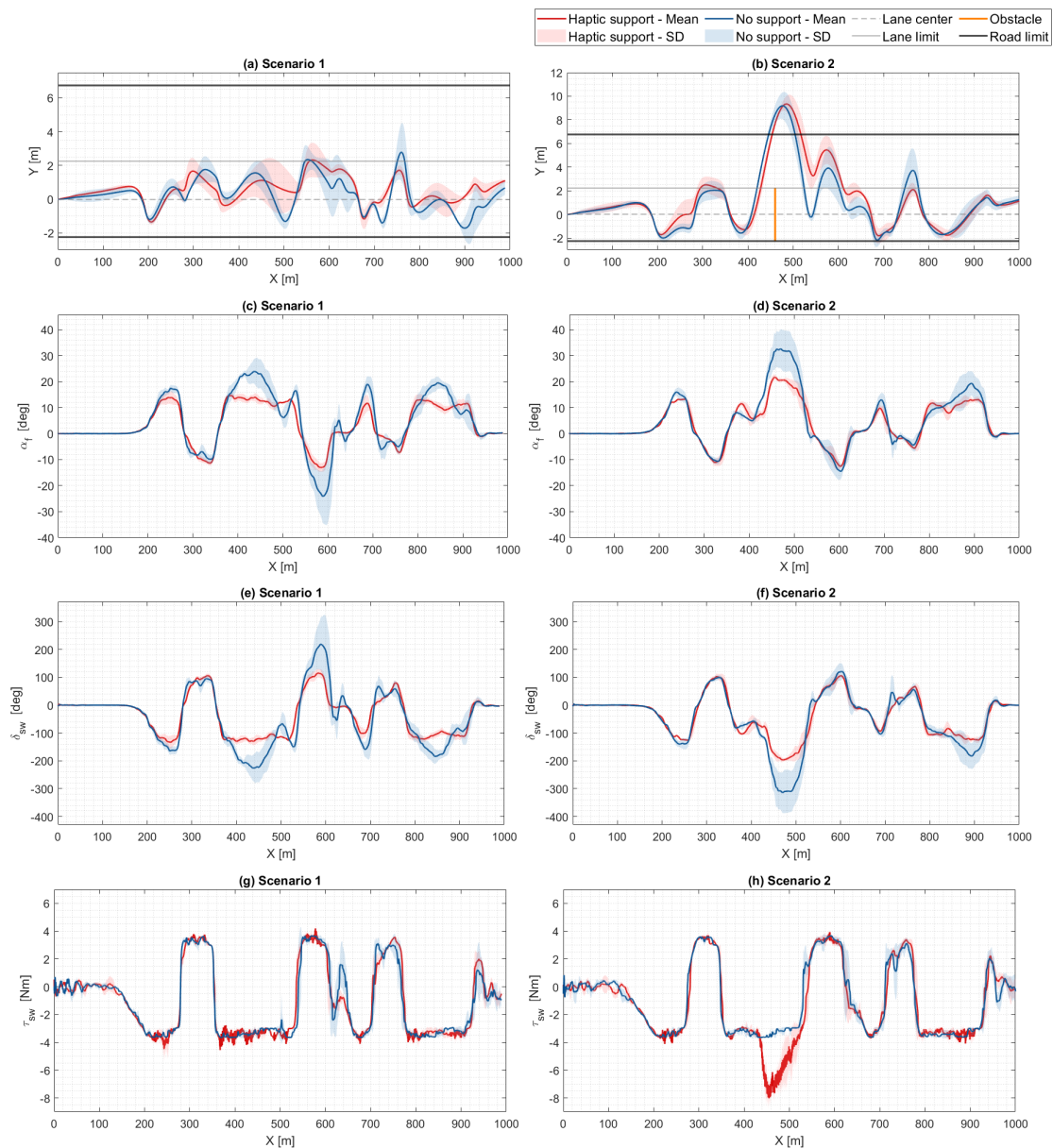


Figure E.29: Experimental results of driver 29: mean values (solid lines), and standard deviations (shaded areas) for the 2 support cases, plotted for both scenarios.

Metric	Scenario 1		Scenario 2	
	No support	Haptic support	No support	Haptic support
Mental demand	4	3	12	11
Physical demand	8	4	9	8
Performance	16	19	14	16
Frustration	5	5	8	7

Table E.29: NASA-TLX evaluation results for driver 29, for each driving mode, for both scenarios.

Driver 30

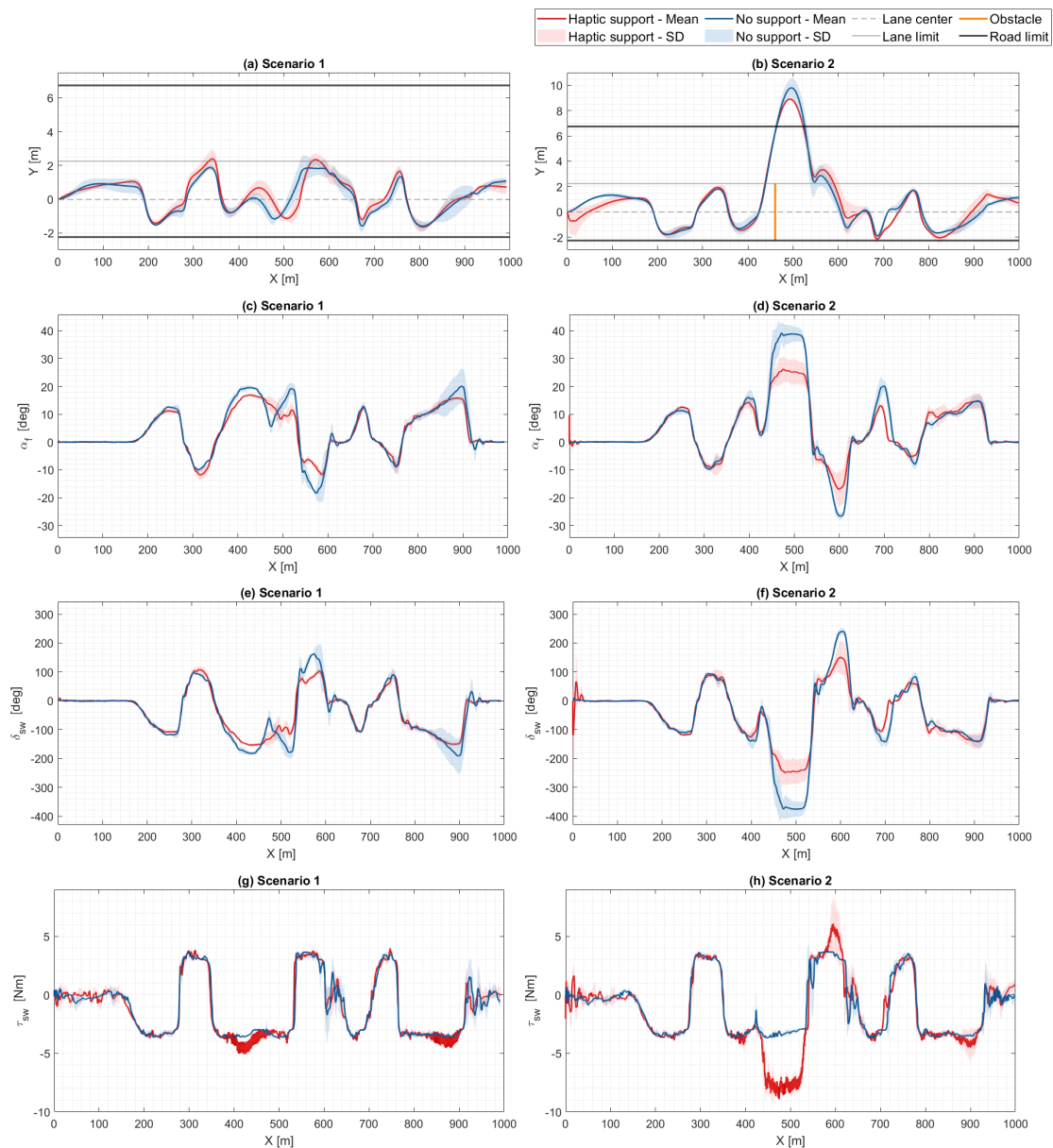


Figure E.30: Experimental results of driver 30: mean values (solid lines), and standard deviations (shaded areas) for the 2 support cases, plotted for both scenarios.

Metric	Scenario 1		Scenario 2	
	No support	Haptic support	No support	Haptic support
Mental demand	7	7	15	15
Physical demand	8	8	13	16
Performance	16	17	15	14
Frustration	7	6	10	12

Table E.30: NASA-TLX evaluation results for driver 30, for each driving mode, for both scenarios.

Driver 31

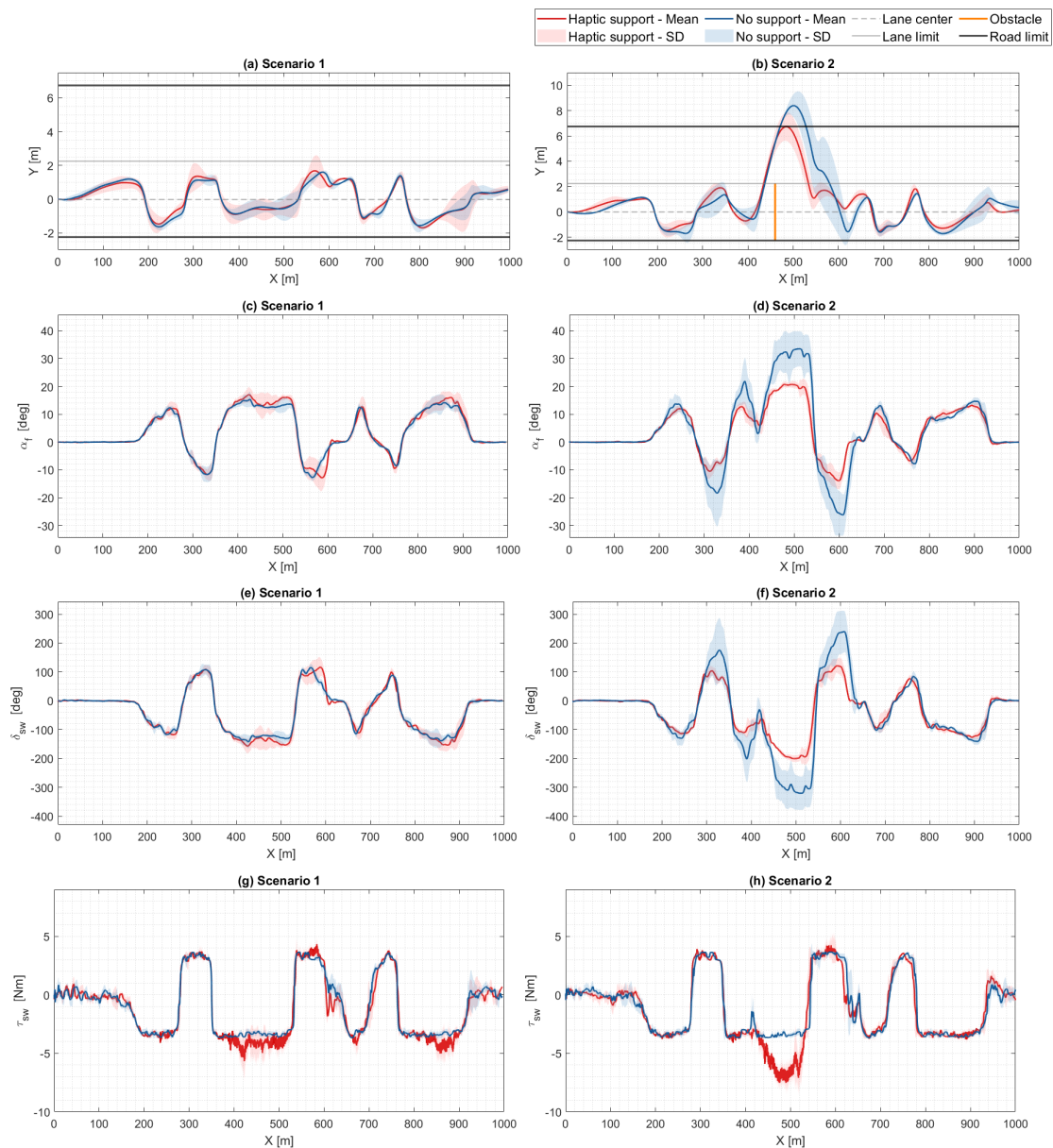


Figure E.31: Experimental results of driver 31: mean values (solid lines), and standard deviations (shaded areas) for the 2 support cases, plotted for both scenarios.

Metric	Scenario 1		Scenario 2	
	No support	Haptic support	No support	Haptic support
Mental demand	5	9	11	10
Physical demand	6	12	9	8
Performance	17	14	10	14
Frustration	3	3	9	8

Table E.31: NASA-TLX evaluation results for driver 31, for each driving mode, for both scenarios.

Driver 32

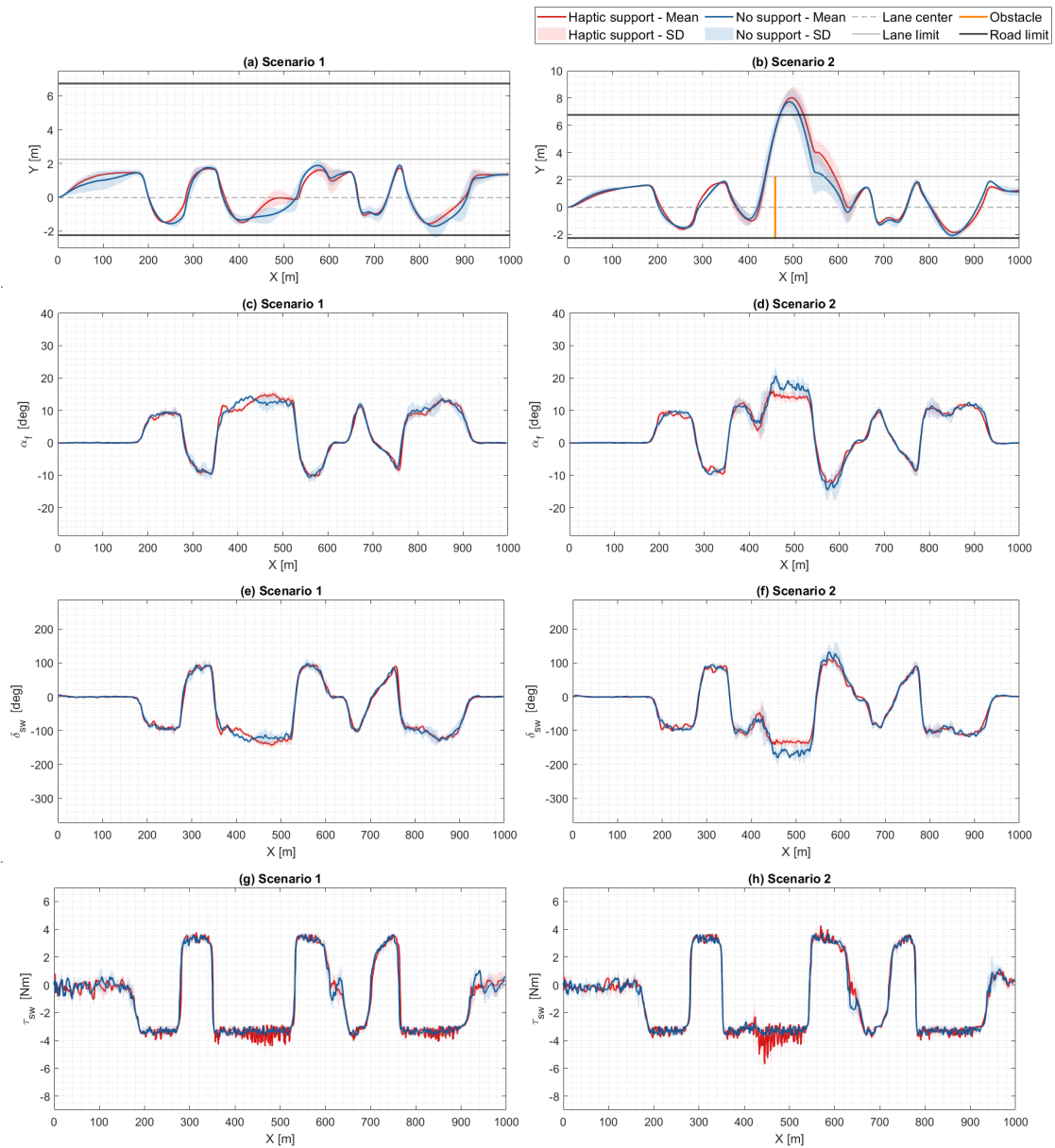
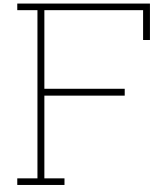


Figure E.32: Experimental results of driver 32: mean values (solid lines), and standard deviations (shaded areas) for the 2 support cases, plotted for both scenarios.

Metric	Scenario 1		Scenario 2	
	No support	Haptic support	No support	Haptic support
Mental demand	12	9	15	13
Physical demand	6	5	7	6
Performance	11	13	10	11
Frustration	3	4	5	4

Table E.32: NASA-TLX evaluation results for driver 32, for each driving mode, for both scenarios.



NASA-TLX Evaluation Form

Mental demand

How mentally demanding was the task?

Without haptic driver support:

1	2	3	4	5	6	7	8	9	10	11	12	13	14	15	16	17	18	19	20	21
---	---	---	---	---	---	---	---	---	----	----	----	----	----	----	----	----	----	----	----	----

Very low

Very high

With haptic driver support:

1	2	3	4	5	6	7	8	9	10	11	12	13	14	15	16	17	18	19	20	21
---	---	---	---	---	---	---	---	---	----	----	----	----	----	----	----	----	----	----	----	----

Very low

Very high

Physical demand

How physically demanding was the task?

Without haptic driver support:

1	2	3	4	5	6	7	8	9	10	11	12	13	14	15	16	17	18	19	20	21
---	---	---	---	---	---	---	---	---	----	----	----	----	----	----	----	----	----	----	----	----

Very low

Very high

With haptic driver support:

1	2	3	4	5	6	7	8	9	10	11	12	13	14	15	16	17	18	19	20	21
---	---	---	---	---	---	---	---	---	----	----	----	----	----	----	----	----	----	----	----	----

Very low

Very high

Performance

How successful were you in accomplishing your level of performance?

Without haptic driver support:

1	2	3	4	5	6	7	8	9	10	11	12	13	14	15	16	17	18	19	20	21
---	---	---	---	---	---	---	---	---	----	----	----	----	----	----	----	----	----	----	----	----

Failure

Perfect

With haptic driver support:

1	2	3	4	5	6	7	8	9	10	11	12	13	14	15	16	17	18	19	20	21
---	---	---	---	---	---	---	---	---	----	----	----	----	----	----	----	----	----	----	----	----

Failure

Perfect

Frustration

How insecure, discouraged, irritated, stressed, and annoyed were you?

Without haptic driver support:

1	2	3	4	5	6	7	8	9	10	11	12	13	14	15	16	17	18	19	20	21
---	---	---	---	---	---	---	---	---	----	----	----	----	----	----	----	----	----	----	----	----

Very low

Very high

With haptic driver support:

1	2	3	4	5	6	7	8	9	10	11	12	13	14	15	16	17	18	19	20	21
---	---	---	---	---	---	---	---	---	----	----	----	----	----	----	----	----	----	----	----	----

Very low

Very high



Conference Paper

The content of this Appendix has been submitted and accepted to the 39th FISITA World Congress, as part of a conference on Integrated Safety, Connected & Automated Driving in Barcelona, Spain. The paper will be presented on the 13th of September 2023.

PREDICTIVE HAPTIC DRIVER SUPPORT NEAR VEHICLE'S HANDLING LIMITS

Kazimierz Dokurno^{1,2,3}, Andrea Michelle Rios Lazcano², Xabier Carrera Akutain², and Barys Shyrokau³

¹University of Twente

Drienerlolaan 5, 7522 NB Enschede, Netherlands (E-mail: k.dokurno@student.utwente.nl)

²Toyota Motor Europe NV/SA

Hoge Wei 33B, 1930 Zaventem, Belgium (E-mail: {andrea.lazcano, xabier.carrera.akutain}@toyota-europe.com)

³Delft University of Technology

Mekelweg 2, 2628 CD Delft, The Netherlands (E-mail: b.shyrokau@tudelft.nl)

ABSTRACT: This research presents a novel driver assistance system that anticipates and mitigates understeer by delivering haptic support to the driver via the steering wheel. The proposed system calculates a safe steering envelope using a Model Predictive Control (MPC) framework, considering the saturation limits of the vehicle's front tires. If the predicted driver steering angle violates the safe envelope, haptic feedback is provided through the steering wheel in the form of an increased opposing torque with vibrations. Thus, the system aims to notify drivers of potential understeer and guide them in reducing the steering angle if they exceed the safe steering limits. To evaluate the effectiveness of the proposed support system, a total of 32 drivers participated in a driving simulator experiment at Toyota Motor Europe. The scenario involved an obstacle avoidance maneuver in the middle of a turn at high velocity. Two levels of automation were investigated: 1) haptic support where the additional haptic torque is provided at the steering wheel, and 2) no support which is equivalent to manual steering. The results demonstrate that haptic support has a positive impact on regular drivers, supporting them to mitigate understeer and significantly reducing lane deviation. No significant difference in performance was noted for expert drivers. Novice drivers report significantly reduced mental workload and lower frustration when the haptic support is active. Subjective evaluation indicates strong acceptance of the proposed assistance system.

KEY WORDS: Haptic shared control, model predictive control, human-machine interaction, handling limits, safety envelope.

1. Introduction

Recent developments in sensing, actuation, and computer processing technologies allow the introduction of more enhanced Advanced Driver Assistance Systems (ADAS). This enables the support of the driver in a wider range of conditions and improves driving safety [1]. Despite these advances, statistics still show high rates of accidents caused by unintended lane or road departures, especially during cornering maneuvers [2]. This can be related to excessive vehicle *understeer* when the vehicle speed is too high to negotiate the turn, resulting in an unexpected deviation from the desired path [3][4]. Current state-of-the-art vehicle stability control (VSC) systems can mitigate understeer to some degree through direct yaw control (DYC). Although this approach is effective in aligning the vehicle's heading angle with the turn direction, it relies on differential braking which can saturate the front tires (especially close to the handling limits). This reduces the cornering force and causes the vehicle to follow a wider path than desired.

Different understeer prevention techniques have been proposed that simultaneously aim to limit understeer and improve road holding. Gordon et al. [5] formulated the trade-off between path tracking and yaw rate correction as an optimal control problem. By efficiently using differential braking, the assistance system outperformed classic DYC in minimizing lateral path deviation during cornering. This solution was further improved through the addition of active front steering by Gao et al. [6] and the extension to independent front steering by Fors et al. [7]. However, all of these approaches re-

quire prior knowledge of the desired trajectory. If the predicted path deviates substantially from the driver's intention, it can result in driver frustration, loss of trust, and lack of user acceptance [8].

Takahashi et al. [9] proposed a trajectory-agnostic method to understeer mitigation inspired by the driver longitudinal control model developed by Yamakado and Abe [10]. In the study, differential braking is applied proportionally to the lateral jerk, reducing understeer through a combination of deceleration and weight transfer to the front axle. Although this approach does not rely on knowledge of the desired trajectory, it could lead to dangerous situations involving following traffic due to excessive braking.

While the above-mentioned solutions (partially) overrule the driver in emergency situations, another type of systems relies on the concept of shared steering control [11]. These systems promote collaboration such that the assistance system and the driver act together to perform the maneuver successfully. Katzourakis [12] proposed haptic shared control (HSC) as a method for understeer mitigation. The system informs the driver of the handling limits by emphasizing the drop of the self-aligning moment on the steering wheel. This is achieved by inferring the front axle slip angle, which is used to generate haptic torque in case the slip angle is close to the peak lateral slip. The experimental results showed a positive impact of the proposed system on vehicle performance with a reduction in slip angles indicating a better utilization of the front tires. Van Doornik [13] proposed an alternative to Katzourakis' model-based method. Instead of relying on a tire model, direct measurements of the tire

lateral force and the self-aligning moment are used by load-sensing bearings [14]. The ratio between lateral force and self-aligning moment is used to generate haptic feedback which decreases the perceived steering wheel stiffness. Although the drop in self-aligning moment can be considered as an early indicator of tire saturation, the self-aligning moment itself is very sensitive to the vertical tire load, tire-road friction and even the type of tire compounds used [15]. Thus, detecting understeer from the self-aligning moment drop is not robust for dynamic and unknown operating conditions.

Hildebrandt et al. [16] developed a haptic driver understeer assistance which increases the perceived steering torque when understeer is detected by an on-board VSC. The system showed a positive impact on drivers, who used smaller steering inputs near handling limits, resulting in smaller lateral deviation from the lane. However, the system is reactive rather than proactive due to understeer detection by VSC, which relies on the comparison of yaw rate and lateral acceleration with a reference behaviour. This indicates that significant understeer has to happen in order to be detected, informing the driver only after the situation has already become critical.

Hence, there is a lack of systems which include the driver in the control loop and simultaneously predict the approaching handling limits.

This study addresses this gap with an intuitive haptic driver support system with predictive capabilities for understeer mitigation. Haptic torque is used to alert the driver about incoming handling limits and offers guidance for handling the situation in a safer manner. The proposed system adheres to the following principles:

1. the occurrence of understeer is predicted in advance,
2. the driver is part of the control loop at all times,
3. no knowledge of the desired path is required,
4. the system intervenes only when necessary.

Using model predictive control (MPC), this study proposes a controller to predict the future vehicle states and steering input based on a bicycle model with a brush tire model. A safe steering envelope is computed based on the predicted states for the prediction horizon by a low-level controller. In case the predicted steering input violates the safe steering envelope, the low-level controller generates a haptic torque directly on the steering wheel. This alerts the driver about the incoming saturation of the front tires and offers guidance towards a safer steering input.

The remainder of this paper is organized as follows. Section 2 presents the model used to quantify the vehicle dynamics and develop the safe steering envelope, which is subsequently used in Section 3 for the design of the haptic driver support system. The performed driving simulator experiment is presented in Section 4 and the study results are shown in Section 5. Conclusions are drawn in Section 6 along with recommendations for future work.

2. Vehicle Model

The predictive haptic driver support relies on two models. The vehicle model is used to predict the lateral and rotational velocities of the car, while the tire model allows to calculate the forces at the tire-road contact patch.

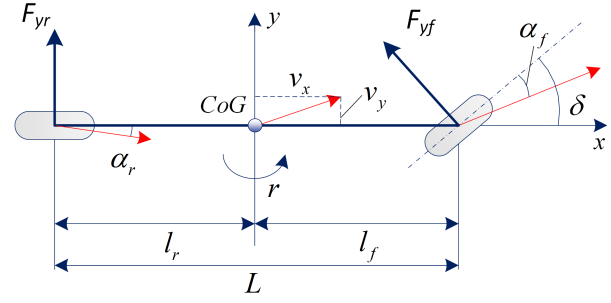


Figure 1. Bicycle model

2.1. Bicycle Model

The vehicle model used is a single-track model with two degrees of freedom [17]. The bicycle model, illustrated in Figure 1, considers the tires on each axle lumped together and assumes a constant longitudinal velocity v_x , no load transfers and no vertical motion of the vehicle. The equations of motion can be written in terms of the front and rear tire forces, F_{yf} and F_{yr} , as

$$\dot{v}_y = \frac{F_{yf} + F_{yr}}{m} - rv_x, \quad (1)$$

$$\dot{r} = \frac{l_f F_{yf} - l_r F_{yr}}{I_{zz}}, \quad (2)$$

where v_y is the lateral velocity, r is the yaw rate, l_f and l_r are the distances from the center of gravity (CoG) to the front and rear axle, m is the vehicle mass and I_{zz} is the moment of inertia. From kinematics, the equations for the tire slip angles at the front (α_f) and at the rear (α_r) can be found as

$$\alpha_f = \frac{v_y + l_f r}{v_x} - \delta, \quad (3)$$

$$\alpha_r = \frac{v_y - l_r r}{v_x}, \quad (4)$$

where δ is the road-wheel steer angle.

2.2. Tire Brush Model

In this study, a nonlinear brush model proposed by Fiala [18] has been chosen due to its accurate description of tire behavior up to the tire saturation limits and light complexity ensuring real-time application. An adapted version of the model formulated by Pacejka [15] is used. The model assumes a parabolic pressure distribution at the contact patch, a rigid tire carcass and a constant friction coefficient μ . Given these assumptions, the relation between the lateral tire force $F_{y[f,r]}$ and $\alpha_{[f,r]}$ is described by

$$F_y = \begin{cases} C_\alpha \tan \alpha - \frac{C_\alpha^2}{3\mu F_z} |\tan \alpha| \tan \alpha \\ \quad + \frac{C_\alpha^3}{27\mu^2 F_z^2} \tan^3 \alpha, & \text{if } |\alpha| \leq \alpha_{lim} \\ \mu F_z \text{sgn} \alpha, & \text{else} \end{cases} \quad (5)$$

where C_α is the tire cornering stiffness, F_z is the normal load and α_{lim} is the slip angle at which the tire has reached the limits of friction, equal to

$$\alpha_{lim} = \tan^{-1} \left(\frac{3\mu F_z}{C_\alpha} \right). \quad (6)$$

2.3. Safe Steering Envelope

Based on the concept of *envelope control* [19], the support system only acts to help the driver maintain the vehicle in a region of operation delimited by safe boundaries, while remaining inactive away from these limits.

Substituting (6) into (3) and isolating δ yields an expression for the upper and lower boundary of the road-wheel angle δ_{lim} at which F_{yf} reaches its peak value, respectively:

$$\delta_{lim}^+ = \frac{v_y + l_f r}{v_x} + \tan^{-1} \left(\frac{3\mu F_z}{C_\alpha} \right), \quad (7)$$

$$\delta_{lim}^- = \frac{v_y + l_f r}{v_x} - \tan^{-1} \left(\frac{3\mu F_z}{C_\alpha} \right). \quad (8)$$

As long as δ remains within the bounds given in (7) and (8), the front tire slip angle will remain under its saturation value.

3. Haptic Support System Design

The goal of the controller is to keep the vehicle within the handling limits, by restricting the road-wheel angle to the boundaries defined in (7) and (8). In order to achieve this objective while keeping the driver in the control loop, the following control architecture is proposed. A high-level MPC controller is designed for predicting the vehicle states and the road-wheel angle over a certain time horizon. These predictions serve as input to the low-level HSC controller which calculates the safe steering envelope for every predicted timestep and subsequently provides haptic feedback on the steering wheel in case the envelope is violated. The overall structure of the predictive haptic driver support system is shown in Figure 2.

3.1. High-level Control

An optimization problem is solved over a receding time horizon, while taking into account modelled vehicle dynamics, constraints, and desired objectives. In this study, the state vector x is defined as $x = [v_y, r, \delta]$ and the control input u is the steering velocity $u = \dot{\delta}$. The goal of the controller is to predict the driver input as closely as possible, without *a priori* knowledge of the path. For short time intervals, the steering velocity can be assumed constant such that the future road-wheel angle is computed by integrating the steering velocity over time. Furthermore, the input $\dot{\delta}$ should not be too large and the resulting δ should not deviate significantly from the initial road-wheel angle at the start of the prediction. These requirements are reflected in the chosen least-squares cost function. The optimization problem that the MPC solves to predict the future vehicle states is formulated as follows:

$$\begin{aligned} \min_{\dot{\delta}} \quad & \sum_{k=1}^{N_p} \left(\|\dot{\delta}_k\|_{Q_1}^2 + \|\dot{\delta}_k - \dot{\delta}_0\|_{Q_2}^2 + \|\delta_k - \delta_0\|_{Q_3}^2 \right) \\ \text{s.t.} \quad & x[k+1] = Ax[k] + Bu[k] + d[k] \\ & -\frac{\pi}{2} \leq \delta \leq \frac{\pi}{2} \end{aligned} \quad (9)$$

In the cost function, δ_0 and $\dot{\delta}_0$ are the initial road-wheel angle and velocity, respectively, and Q_1 , Q_2 and Q_3 are the tuning weights. Furthermore, A , B and d are respectively the system matrix, the input matrix and the disturbance input associated with the current state from the discrete state-space vehicle model. The discrete state-space is obtained by discretizing the continuous bicycle model defined in (1) and (2), combined with the slip and tire model defined

in (3), (4), (5) and (6). The constraint on δ reflects the actuation limits of the steering system.

3.2. Low-level Control

From the obtained predictions, the low-level controller calculates the safe steering envelope boundaries for each timestep of the prediction horizon using (7) and (8). If the predicted road-wheel angle exceeds the calculated limits at any point, an error term is generated for that particular timestep as follows:

$$e_k = \begin{cases} \delta_{lim,k}^- - \delta_k, & \text{if } \delta_k < \delta_{lim,k}^- \\ 0, & \text{if } \delta_{lim,k}^- \leq \delta_k \leq \delta_{lim,k}^+ \\ \delta_{lim,k}^+ - \delta_k, & \text{if } \delta_{lim,k}^+ < \delta_k \end{cases} \quad (10)$$

The error of each particular timestep k is multiplied by a decreasing weighting term $(N_p - k + 1)$ in order to assign more importance to imminent errors compared to errors further ahead in the horizon. The weighted sum is scaled by a tuning factor K in order to generate a haptic torque τ_{hap} which is noticeable but can also be overruled by the driver:

$$\tau_{hap} = K \sum_{k=1}^{N_p} (N_p - k + 1) e_k, \quad (11)$$

In addition to the increase in steering torque, torque vibrations τ_{vib} of fixed amplitude A_{vib} and frequency f_{vib} are also added to the steering wheel. These vibrations were perceived as a positive influence on user acceptance during the pilot study. The total support torque τ_s delivered by the system to the steering wheel is equal to $\tau_{hap} + \tau_{vib}$.

3.3. Implementation

The resulting optimization problem in (9) is nonlinear and requires the use of efficient solvers in order to guarantee real-time implementation. For this study, the problem is solved using FORCES PRO NLP solver [20][21], using the real-time variant of the sequential quadratic programming method. The controller has been implemented in MATLAB Simulink, with a sample time of 0.01s. It was noted that without information about the incoming path, for normal driving conditions, predictions based on the current vehicle state and driver input are only accurate for around 0.5s. Beyond this time, steering velocity cannot be assumed to be approximately constant anymore and predictions deviate significantly from the actual states. Therefore, a prediction horizon of 0.5s was chosen as it results in good prediction accuracy while allowing enough margin for understeer to be detected ahead of time. MPC tuning weights were adjusted to improve the accuracy of the state prediction. The selection of the haptic torque tuning factor K was done during the pilot study with an expert driver to achieve a desired level of control authority. All relevant controller parameters are summarized in Table 1.

Figure 3 illustrates the controller operation during one of the experimental trials described in the next section. The two uppermost plots show the predicted states, \hat{r} and \hat{v}_y , coming from the MPC at $t = 38.17s$ for the length of the prediction horizon, until $t = 38.67s$. The predicted steering input $\hat{\delta}$ exceeds the calculated safe steering boundary around the 38.6s mark, as shown in the third plot. The support torque τ_s is provided as soon as the limit violation is predicted, as can be seen in the last plot. For reference, the recorded vehicle states and driver input are also shown.

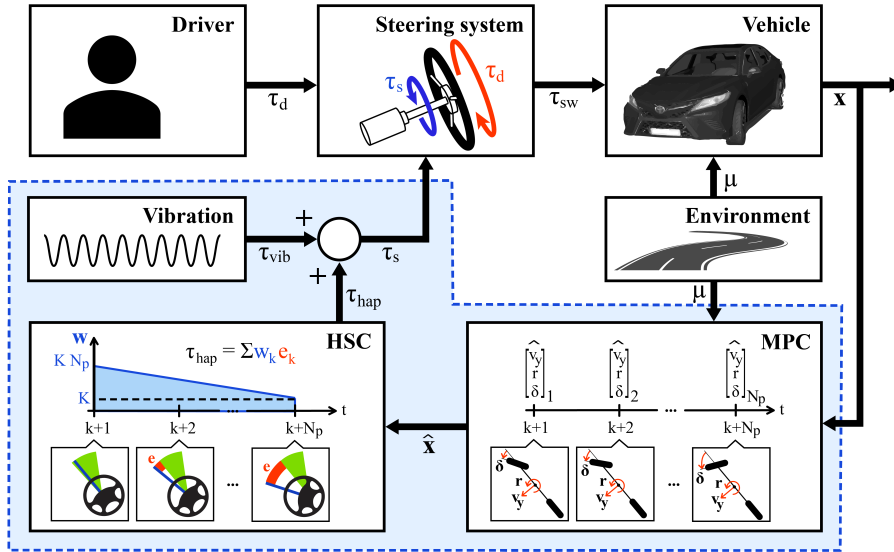


Figure 2. Controller diagram: The MPC predicts the future vehicle states, which are then used to compute the safe steering envelope (in green) for each timestep of the prediction horizon. An error e (in red) is produced if the predicted steering angle leaves the envelope. The generated haptic torque τ_{hap} is equal to the weighted sum of the errors where the weighting function w is linearly decreasing. The total support torque τ_s is equal to the sum of τ_{hap} and τ_{vib} .

Parameter	Description	Value
T_c	controller sample time in s	0.01
N_p	number of timesteps in prediction horizon	50
Q_1	weight on steering velocity	10
Q_2	weight on steering velocity deviation	2000
Q_3	weight on steering angle deviation	0.1
K	haptic torque tuning factor	0.05
A_{vib}	haptic vibration amplitude in Nm	0.5
f_{vib}	haptic vibration frequency in Hz	21

Table 1. Controller parameters

4. Experiment Design

In order to validate the proposed system, a driver-in-the-loop study was performed at Toyota Motor Europe on a high-fidelity driving simulator, which uses a static mock-up of a Toyota production vehicle in front of a 210° projection screen. The graphics were rendered with rFpro software based on an IPG CarMaker scenario. The simulator uses a vehicle dynamics model with a proprietary steer-by-wire model and a Toyota production vehicle parametrisation. The control loading system is used to measure the driver's steering input and provide realistic steering feedback during driving [22], alongside the additional torque provided by the haptic support system. The complete setup can be seen in Figure 4.

Two variations of the haptic support system have been investigated:

- *No support*: this case represents manual steering equivalent to a conventional vehicle with electric power assisted steering. There is no additional haptic torque added to the steering wheel. This variation is used as baseline.
- *Haptic support*: in this case, there is additional haptic torque together with vibrations added to the steering wheel when the controller predicts the violation of the safe steering envelope.

4.1. Driving Scenario

The aim of the conducted experiments was to validate the proposed system under naturalistic driving conditions during which the vehicle approaches the limits of handling. A 1km long circuit was designed with straight sections as well as curves with a constant 50m cornering radius. The tire-road friction coefficient μ was set to 0.8. The vehicle velocity was set to 70km/h to recreate a situation in which the vehicle enters a corner with excessive speed and is close to the limits of handling. Similar to the study of Othman et al. [23] on overtaking maneuvers in curves, an obstacle was set to obstruct the right lane on one of the corners. As a consequence, participants are forced to perform an avoidance maneuver in the middle of a turn. This situation is known to cause a large lateral acceleration peak which makes it even more difficult to negotiate the turn. The complete circuit can be seen in Figure 5.

4.2. Participants

In total, 32 participants conducted the experiment, all with a valid driving license. Among them, there were expert test drivers with professional experience in handling limit driving. Prior to conducting the experiment, each participant completed 6 practice runs on the same circuit, but without the obstacle: 3 runs without steering support and 3 runs with the haptic support enabled. This allowed them to become familiar with the driving simulator and the additional haptic torque on the steering wheel. The participants were instructed to remain in the right lane while driving, without using the gas or brake pedal. The practice runs without haptic support have been used to classify between regular and novice drivers. Those who managed to stay within the lane's boundaries were classified as regular drivers (N=15), while those who left the lane were classified as novice drivers (N=12). Expert drivers (N=5) were selected based on their professional qualifications.

From self-reported data, the mean age of an expert driver was 39.4 years (SD = 4.22), with an average driving license possession of

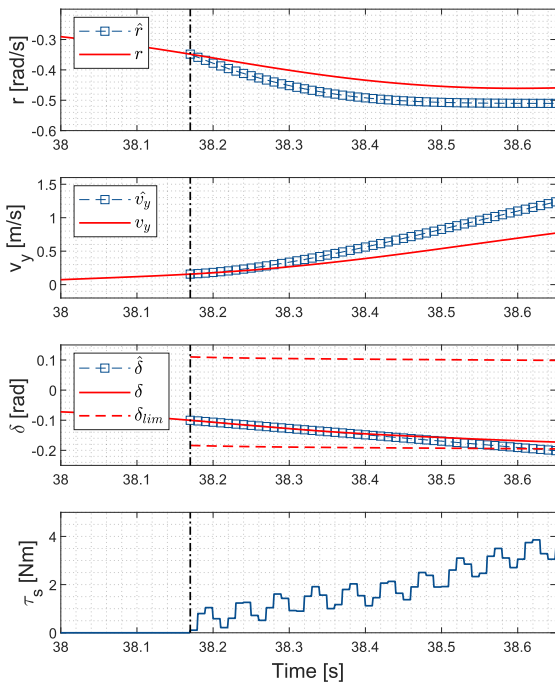


Figure 3. State prediction at $t = 38.17s$ during a driver-in-the-loop experimental trial



Figure 4. Driving simulator at Toyota Motor Europe, Belgium

20.8 years (SD = 5.07). The average age of a regular driver was 28.53 years (SD = 7.12) with an average driving license possession of 10.4 years (SD = 7.11). Finally, the average age of a novice driver was 25.33 years (SD = 2.39) with an average driving license possession of 5.51 years (SD = 2.98).

4.3. Experimental Procedure

The experimental trials were performed immediately after the practice session. Each participant was instructed to keep the right lane as much as possible, with the gas and brake pedals deactivated. An obstacle was obstructing the right lane at the 460m mark, right in the middle of a corner. Participants were asked to avoid any obstacle by moving to the left lane and then returning to the right lane as fast as they could. Each test subject performed 6 runs on the circuit: 3 runs with the haptic support and 3 runs without any support. The runs were in random order (Randomised Latin Square

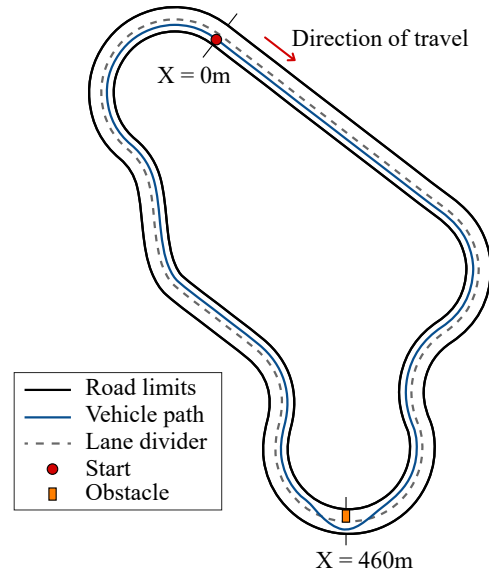


Figure 5. Experimental circuit

Method) to mitigate the learning effect. The collected data includes information such as vehicle states, tire forces and slip angles, the position of the vehicle on the circuit, as well as the steering angle and torque. At the end of the experiment, participants were asked to complete the NASA task load index (TLX) evaluation form to assess the following subjective metrics: *mental demand*, *physical demand*, *performance* and *frustration*. Participants were asked to evaluate each metric on a scale from 1 to 21.

5. Results

The collected data from the runs with and without support of all 32 participants was averaged separately, first per participant and then across all participants of the same category. Statistical significance of the results is assessed using a two-tailed paired t -test, at 5% significance level.

5.1. Objective Evaluation

Figure 6 presents the experimental results as a function of the distance for each of the three driver categories. The first row of plots (plots 6a to 6c) shows the vehicle lateral deviation from the center of the lane. As can be seen, the influence of haptic support on the vehicle path varies for different driver categories. In the case of expert drivers, the haptic support has no noteworthy effect with both trajectories largely overlapping. Novice drivers reduced their peak lateral deviation when driving with the haptic support. A significant change in trajectory is observed in the case of regular drivers. Table 2 presents a comparison of the means of the maximum lateral deviations calculated for each driver category. Regular drivers significantly reduced their peak lateral deviation by 11.28% when driving with haptic support compared to baseline.

The analysis of the averaged root-mean-square (RMS) value of the steering wheel angle in the vicinity of the obstacle, from $X=400m$ to $X=550m$, is shown in Table 3. The haptic steering support significantly reduced the steering angle for regular and novice drivers, by 16.91% and 25.74% respectively. The difference in steering angle during the experiment can also be observed in Figure 6 (plots 6d to 6f).

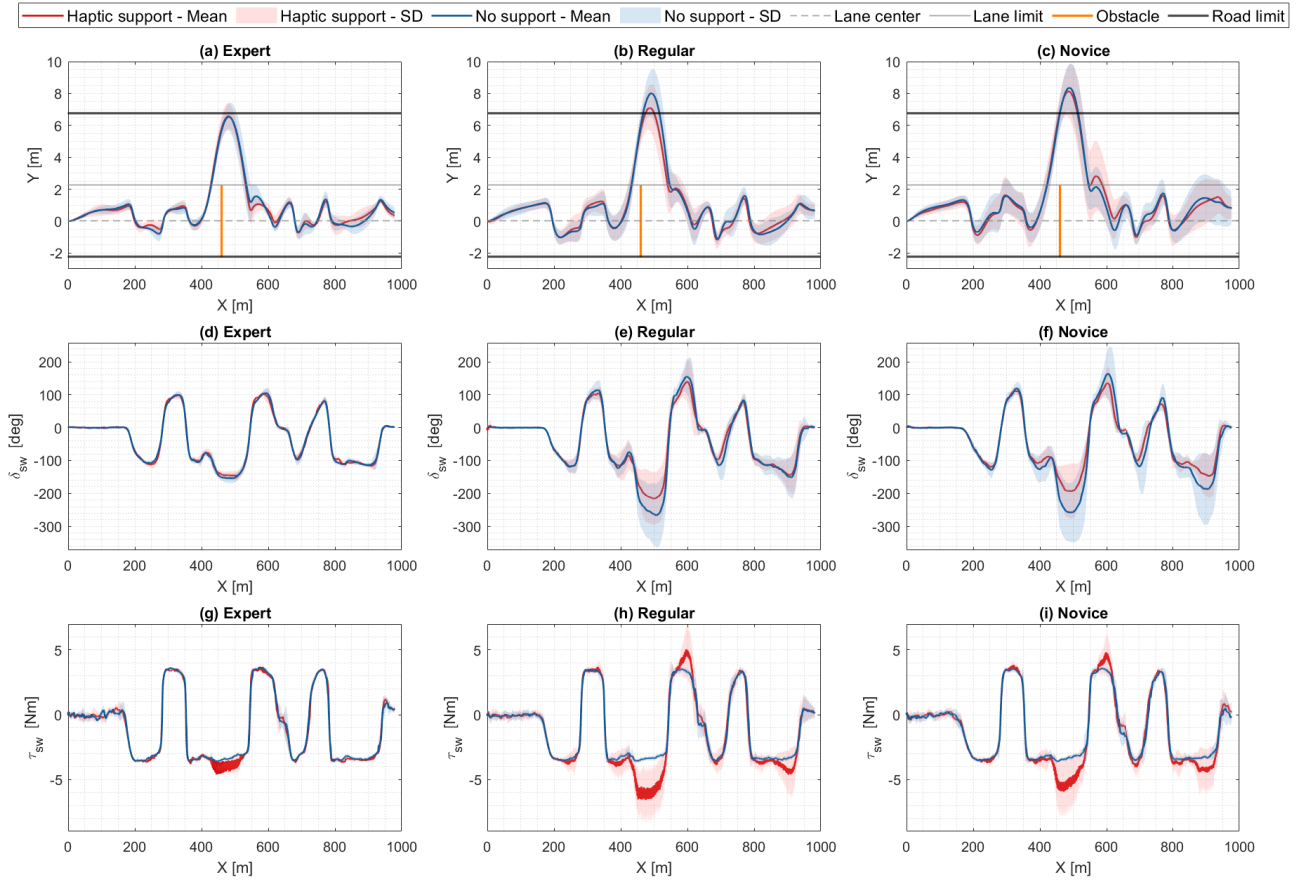


Figure 6. Experimental results: mean values (solid lines), and standard deviations (shaded areas) for the 2 support cases, plotted for each driver group

Drivers	No support	Haptic support	p-value
Expert	6.63m (0.87)	6.60m (0.91)	0.9595
Regular	8.14m (1.51)	7.22m (1.52)	0.0113
Novice	8.55m (1.52)	8.30m (1.68)	0.4568

Table 2. Averaged maximum lateral deviation for each driving mode, for each driver category (standard deviations in parentheses)

Drivers	No support	Haptic support	p-value
Expert	125.15° (7.65)	121.28° (8.67)	0.3846
Regular	200.31° (61.33)	166.45° (56.69)	0.0025
Novice	195.24° (68.32)	144.99° (46.84)	0.0077

Table 3. Averaged RMS values of steering wheel angle from X=400m to X=550m (around the obstacle) for each driving mode, for each driver category (standard deviations in parentheses)

Table 4 presents the RMS values of the total torque on the steering wheel on the interval from X=400m to X=550m. The difference in total steering torque between baseline and proposed system is significant for all categories of drivers, with an increase in torque of 10.23%, 38.83%, and 27.27% for expert, regular, and novice drivers, respectively. This indicates that the haptic support activated on average for all participants, regardless of their driving skills. This is illustrated in Figure 6 (plots 6g to 6i), which shows

an increase in the measured torque on the steering wheel between X=400m and X=550 for all drivers.

Drivers	No support	Haptic support	p-value
Expert	3.24N (0.03)	3.60N (0.30)	0.0390
Regular	3.20N (0.07)	4.98N (1.30)	<0.001
Novice	3.20N (0.08)	4.39N (1.28)	0.0095

Table 4. Averaged RMS values of steering wheel torque from X=400m to X=550m (around the obstacle) for each driving mode, for each driver category (standard deviations in parentheses)

Lastly, the RMS lateral force values for the front axle can be found in Table 5, on the interval from X=400m to X=550m. A significant difference can be noted for regular and novice drivers, who utilised respectively 1.00% and 1.03% additional lateral force during the obstacle avoidance maneuver when driving with haptic support.

5.2. Subjective Evaluation

The averaged results of the NASA-TLX evaluation form are summarized separately for expert, regular and novice driver categories, in Tables 6, 7 and 8, respectively. A significant decrease in mental demand is reported by novice drivers. Regular drivers report a significant increase in self-assessed performance when driving with haptic support. Also, a significant decrease in perceived frustration

Drivers	No support	Haptic support	p-value
Expert	6896.5N (79.14)	6963.3N (101.44)	0.0965
Regular	6737.1N (204.39)	6804.9N (174.14)	0.0424
Novice	6758.2N (228.62)	6828.8N (204.15)	0.0106

Table 5. Averaged RMS values of lateral force at the front axle from X=400m to X=550m (around the obstacle) for each driving mode, for each driver category (standard deviations in parentheses)

can be observed for novice drivers when aided by haptic support compared to no support.

Metric	No support	Haptic support	p-value
Mental demand	6.80 (5.36)	6.60 (5.13)	0.3739
Physical demand	5.20 (5.02)	6.00 (4.47)	0.3739
Performance	15.40 (2.97)	16.00 (2.65)	0.2080
Frustration	8.6 (6.80)	9.8 (8.70)	0.3883

Table 6. NASA-TLX evaluation results for expert drivers, for each driving mode (standard deviations in parentheses)

Metric	No support	Haptic support	p-value
Mental demand	12.00 (4.50)	11.60 (4.24)	0.6044
Physical demand	9.60 (3.81)	10.07 (4.48)	0.5892
Performance	12.47 (3.56)	14.67 (3.58)	0.0176
Frustration	9.33 (4.81)	9.13 (4.75)	0.8003

Table 7. NASA-TLX evaluation results for regular drivers, for each driving mode (standard deviations in parentheses)

After the experiment, participants were also asked about their interest in having the haptic support system in their own personal vehicle, should such technology become available on the market. The results revealed that 3 out of 5 expert drivers are interested in having such a system installed. In the case of regular drivers, a vast majority of 13 out of 15 participants expressed their desire for its implementation. Similarly, among novice drivers, 10 out of 12 participants showed interest in having haptic support installed in their vehicles.

5.3. Discussion

The results show that haptic driver support does impact the drivers, however, the degree to which a driver is influenced greatly depends on their driving skills. Regular drivers seem to particularly benefit from the haptic support, which allows them to deviate significantly less from the road. This is also reflected by the increase in self-assessed performance for regular drivers in the NASA-TLX form. This improvement in performance can be linked to the decrease in steering wheel angle during obstacle avoidance, which allows more lateral force to be generated at the front axle. It should be noted that regular drivers exhibit similarities with expert drivers in terms of steering wheel angle, front axle lateral force and lateral deviation when driving with the haptic support system.

Novice drivers also show a significant reduction in their steering input, along with a significant increase in lateral force on the front

Metric	No support	Haptic support	p-value
Mental demand	14.50 (4.03)	11.58 (5.00)	0.0431
Physical demand	12.08 (5.79)	10.67 (4.77)	0.3474
Performance	10.58 (3.94)	11.33 (5.16)	0.6975
Frustration	11.58 (4.56)	8.33 (4.33)	0.0310

Table 8. NASA-TLX evaluation results for novice drivers, for each driving mode (standard deviations in parentheses)

axle. However, no significant decrease in lane deviation is noticed. More research is needed in this area, however, factors like reaction time and how early a driver starts the evasive maneuver could be of importance. Nevertheless, novice drivers scored significantly lower on the reported frustration metric and mental demand. Hence, the proposed system also has a positive influence on less experienced drivers and can help reduce the perceived workload during an emergency maneuver.

Lastly, no significant differences can be found for expert drivers in terms of objective or subjective metrics other than the total measured torque on the steering wheel. While driving with both controller variations, expert drivers outperformed all the other drivers in terms of minimizing lane deviation. On average, they generated the largest lateral force at the front axle while using the smallest steering input to perform the evasive maneuver. Furthermore, they scored the lowest on both mental and physical demand metrics. Therefore, haptic support systems have no significant influence on expert drivers, who can reliably assess the situation by themselves. In fact, haptic support could be linked with a slight increase in frustration reported by expert drivers, however the difference is not statistically significant. More research should be done on identifying relevant differences between expert and regular/novice drivers in emergency scenarios that could be linked with safer maneuvers.

6. Conclusion and Future Work

In this study, a predictive haptic driver support system was proposed with the aim of mitigating vehicle understeer. The system operates by intuitively alerting the driver about incoming front tire saturation limits in advance. In order to validate the system, a driving simulator study was performed involving an obstacle avoidance maneuver in the middle of a turn. Results demonstrate that haptic support has a positive impact on regular drivers' behavior, characterized by a reduced RMS steering angle value compared to manual steering. This results in higher lateral force at the front axle which translates to a smaller lateral deviation from the lane. The proposed system also positively influenced novice drivers in reducing their steering input during the maneuver, and significantly increased the lateral force at the front tires. However, no significant decrease in lane deviation has been observed for novice drivers. Subjective evaluation indicates a significant increase in self-assessed performance for regular drivers who drove with haptic support. Similarly, novice drivers report significantly reduced mental demand and frustration when haptic support is active. Expert drivers are the least affected by the haptic support system and show no significant difference in performance or reported subjective metrics.

Future research focuses on adapting the proposed haptic driver support to scenarios with varying vehicle speeds. The system could be extended to provide support in adjusting the speed and the steering input at the same time with integrated vehicle control. The combination of the haptic driver support with differential braking offers an interesting direction for further investigation.

References

- [1] M. Kyriakidis, C. van de Weijer, B. van Arem, and R. Happee. “The deployment of Advanced Driver Assistance Systems in Europe”. In: *Proceedings of 22nd ITS World Congress, Bordeaux, France*. 2015.
- [2] R. Elvik. “International transferability of accident modification functions for horizontal curves”. In: *Accident Analysis & Prevention* 59 (2013), pp. 487–496.
- [3] M. Klomp, M. Lidberg, and T. Gordon. “On optimal recovery from terminal understeer”. In: *Proceedings of the Institution of Mechanical Engineers, Part D: Journal of Automobile Engineering* 228.4 (2014), pp. 412–425.
- [4] S. Othman, R. Thomson, and G. Lannér. “Identifying critical road geometry parameters affecting crash rate and crash type”. In: *Annals of advances in automotive medicine/annual scientific conference*. Vol. 53. 2009, pp. 155–165.
- [5] T. Gordon, M. Klomp, and M. Lidberg. “Strategies for Minimizing Maximum Off-tracking resulting from Over-speed in Curves”. In: *Proceedings of 11th International Symposium on Advanced Vehicle Control, Seoul, South Korea*. 2012.
- [6] Y. Gao and T. Gordon. “Optimal control of vehicle dynamics for the prevention of road departure on curved roads”. In: *IEEE Transactions on Vehicular Technology* 68.10 (2019), pp. 9370–9384.
- [7] V. Fors, B. Olofsson, and L. Nielsen. “Yaw-moment control at-the-limit of friction using individual front-wheel steering and four-wheel braking”. In: *IFAC-PapersOnLine* 52.5 (2019), pp. 458–464.
- [8] A. Lazcano, T. Niu, X. Akutain, D. Cole, and B. Shyrokau. “MPC-based haptic shared steering system: A driver modeling approach for symbiotic driving”. In: *IEEE/ASME Transactions on Mechatronics* 26.3 (2021), pp. 1201–1211.
- [9] J. Takahashi, M. Yamakado, S. Saito, and A. Yokoyama. “A hybrid stability-control system: combining direct-yaw-moment control and G-Vectoring Control”. In: *Vehicle system dynamics* 50.6 (2012), pp. 847–859.
- [10] M. Yamakado and M. Abe. “An experimentally confirmed driver longitudinal acceleration control model combined with vehicle lateral motion”. In: *Vehicle System Dynamics* 46.S1 (2008), pp. 129–149.
- [11] D. Abbink, T. Carlson, M. Mulder, J. De Winter, F. Amiravan, T. Gibo, and E. Boer. “A topology of shared control systems—finding common ground in diversity”. In: *IEEE Transactions on Human-Machine Systems* 48.5 (2018), pp. 509–525.
- [12] D. Katzourakis. “Driver steering support interfaces near the vehicle’s handling limits”. PhD dissertation, Faculty of Mechanical, Maritime and Materials Engineering, Delft University of Technology, 2012.
- [13] J. Van Doornik. “Haptic feedback on the steering wheel near the vehicle’s handling limits using wheel load sensing”. MSc thesis, Faculty of Mechanical, Maritime and Materials Engineering, Delft University of Technology, 2014.
- [14] Stijn Kerst, Barys Shyrokau, and Edward Holweg. “A model-based approach for the estimation of bearing forces and moments using outer ring deformation”. In: *IEEE Transactions on Industrial Electronics* 67.1 (2019), pp. 461–470.
- [15] H. B. Pacejka. *Tire and Vehicle Dynamics, 3rd ed.* Oxford, U.K.: Butterworth-Heinemann, 2012.
- [16] C. Hildebrandt, M. Schmidt, M. Sedlmayr, O. Pion, G. Büyükyıldız, and F. Küçükay. “Intuitive steering assistance in critical understeer situations”. In: *Traffic injury prevention* 16.5 (2015), pp. 484–490.
- [17] R. Rajamani. *Vehicle dynamics and control*. Springer Science & Business Media, 2011.
- [18] E. Fiala. “Lateral forces on rolling pneumatic tires”. In: *Zeitschrift VDI* 96.29 (1954), pp. 973–979.
- [19] C. E. Beal and J.C. Gerdes. “Model predictive control for vehicle stabilization at the limits of handling”. In: *IEEE Transactions on Control Systems Technology* 21.4 (2012), pp. 1258–1269.
- [20] A. Domahidi and J. Jerez. *FORCES Professional*. Embotech AG, url=https://embotech.com/FORCES-Pro. 2014–2019.
- [21] A. Zanelli, A. Domahidi, J. Jerez, and M. Morari. “FORCES NLP: an efficient implementation of interior-point methods for multistage nonlinear nonconvex programs”. In: *International Journal of Control* (2017), pp. 1–17.
- [22] Mircea Damian, Barys Shyrokau, Xabier Carrera Akutain, and Riender Happee. “Experimental validation of torque-based control for realistic handwheel haptics in driving simulators”. In: *IEEE Transactions on Vehicular Technology* 71.1 (2021), pp. 196–209.
- [23] S. Othman, R. Thomson, and G. Lannér. “Are driving and overtaking on right curves more dangerous than on left curves?” In: *Annals of Advances in Automotive Medicine/Annual Scientific Conference*. Vol. 54. 2010, pp. 253–264.

References

- [1] D. A. Abbink, M. Mulder, and E. R. Boer. “Haptic shared control: smoothly shifting control authority?” In: *Cognition, Technology and Work* 14.1 (2012), pp. 19–28.
- [2] D. A. Abbink et al. “A topology of shared control systems—finding common ground in diversity”. In: *IEEE Transactions on Human-Machine Systems* 48.5 (2018), pp. 509–525.
- [3] M. Abe. *Vehicle handling dynamics: Theory and application*. 2nd ed. Elsevier, 2015.
- [4] A. Balachandran et al. “Predictive haptic feedback for obstacle avoidance based on model predictive control”. In: *IEEE Transactions on Automation Science and Engineering* 13.1 (2015), pp. 26–31.
- [5] C. E. Beal and J.C. Gerdes. “Model predictive control for vehicle stabilization at the limits of handling”. In: *IEEE Transactions on Control Systems Technology* 21.4 (2012), pp. 1258–1269.
- [6] K. Bengler et al. “Three decades of driver assistance systems: Review and future perspectives”. In: *IEEE Intelligent Transportation Systems Magazine* 6.4 (2014), pp. 6–22.
- [7] *CarMaker - IPG Automotive*. (n.d.) <https://ipg-automotive.com/en/products-solutions/software/carmaker/>. Accessed: November 12, 2022.
- [8] European Commission. *Annual statistical report on road safety in the EU, 2022*. European Road Safety Observatory. Brussels, European Commission, Directorate General for Transport. 2023.
- [9] European Commission. *Facts and figures single vehicle crashes*. European Road Safety Observatory. Brussels, European Commission, Directorate General for Transport. 2023.
- [10] M. Diehl, H. J. Ferreau, and N. Haverbeke. “Efficient numerical methods for nonlinear MPC and moving horizon estimation”. In: *Lecture notes in control and information sciences: Vol. 384. Nonlinear model predictive control*. 2009, pp. 391–417.
- [11] A. Domahidi and J. Jerez. *FORCES Professional*. Embotech AG, <https://embotech.com/FORCES-Pro>. 2014–2019.
- [12] R. Elvik. “International transferability of accident modification functions for horizontal curves”. In: *Accident Analysis & Prevention* 59 (2013), pp. 487–496.
- [13] S. M. Erlien. “Shared vehicle control using safe driving envelopes for obstacle avoidance and stability”. PhD dissertation, Stanford University, 2015.
- [14] S. M. Erlien, S. Fujita, and J. C. Gerdes. “Shared steering control using safe envelopes for obstacle avoidance and vehicle stability”. In: *IEEE Transactions on Intelligent Transportation Systems* 17.2 (2016), pp. 441–451.
- [15] E. Fiala. “Lateral forces on rolling pneumatic tires”. In: *Zeitschrift VDI* 96.29 (1954), pp. 973–979.
- [16] *FORCES Pro User Manual (2023)*. <https://forces.embotech.com/Documentation/introduction/index.html>, Accessed: June 21, 2023.
- [17] V. Fors, B. Olofsson, and L. Nielsen. “Yaw-moment control at-the-limit of friction using individual front-wheel steering and four-wheel braking”. In: *IFAC-PapersOnLine* 52.5 (2019), pp. 458–464.

- [18] Y. Gao and T. Gordon. "Optimal control of vehicle dynamics for the prevention of road departure on curved roads". In: *IEEE Transactions on Vehicular Technology* 68.10 (2019), pp. 9370–9384.
- [19] T. Gordon, M. Klomp, and M. Lidberg. "Strategies for Minimizing Maximum Off-tracking resulting from Over-speed in Curves". In: *Proceedings of 11th International Symposium on Advanced Vehicle Control, Seoul, South Korea*. 2012.
- [20] M. Harrer and P. Pfeffer. *Steering handbook*. 1st ed. Springer International Publishing, 2017.
- [21] M. Hasenjäger and H. Wersing. "Personalization in advanced driver assistance systems and autonomous vehicles: A review". In: *2017 IEEE 20th International Conference on Intelligent Transportation Systems (ITSC), Yokohama, Japan*. 2017, pp. 1–7.
- [22] C. Hildebrandt et al. "Intuitive steering assistance in critical understeer situations". In: *Traffic Injury Prevention* 16.5 (2015), pp. 484–490.
- [23] G. R. J. Hockey. "Compensatory control in the regulation of human performance under stress and high workload: A cognitive-energetical framework". In: *Biological Psychology* 45.1-3 (1997), pp. 73–93.
- [24] D. Hrovat et al. "The development of model predictive control in automotive industry: A survey". In: *2012 IEEE International Conference on Control Applications*. 2012, pp. 295–302.
- [25] Y. Hsu, S.M. Laws, and J.C. Gerdes. "Estimation of tire slip angle and friction limits using steering torque". In: *IEEE Transactions on Control Systems Technology* 18.4 (2010), pp. 896–907.
- [26] D. Katzourakis. "Driver steering support interfaces near the vehicle's handling limits". PhD dissertation, Faculty of Mechanical, Maritime and Materials Engineering, Delft University of Technology, 2012.
- [27] M. Klomp, M. Lidberg, and T. J. Gordon. "On optimal recovery from terminal understeer". In: *Proceedings of the Institution of Mechanical Engineers, Part D: Journal of Automobile Engineering*. Vol. 228. 4. 2014, pp. 412–425.
- [28] M. Kyriakidis et al. "The deployment of Advanced Driver Assistance Systems in Europe". In: *Proceedings of 22nd ITS World Congress, Bordeaux, France*. 2015.
- [29] A. Lazcano et al. "MPC-based haptic shared steering system: A driver modeling approach for symbiotic driving". In: *IEEE/ASME Transactions on Mechatronics* 26.3 (2021), pp. 1201–1211.
- [30] Jay H Lee. "Model predictive control: Review of the three decades of development". In: *International Journal of Control, Automation and Systems* 9 (2011), pp. 415–424.
- [31] C. C. Macadam. "Understanding and modeling the human driver". In: *Vehicle System Dynamics* 40.1-3 (2003), pp. 101–134.
- [32] M. Marcano et al. "A review of shared control for automated vehicles: Theory and applications". In: *IEEE Transactions on Human-Machine Systems* 50.6 (2020), pp. 475–491.
- [33] D. T. McRuer and H. R. Jex. "A review of quasi-linear pilot models". In: *IEEE Transactions on Human Factors in Electronics* 3 (1967), pp. 231–249.
- [34] S. Othman, R. Thomson, and G. Lannér. "Identifying critical road geometry parameters affecting crash rate and crash type". In: *Annals of Advances in Automotive Medicine/Annual Scientific Conference*. Vol. 53. 2009, pp. 155–165.

- [35] H. Pacejka. *Tire and vehicle dynamics*. 3rd ed. Elsevier, 2012.
- [36] R. Parasuraman and V. Riley. “Humans and automation: Use, misuse, disuse, abuse”. In: *Human Factors* 39.2 (1997), pp. 230–253.
- [37] S. M. Petermeijer et al. “The effect of haptic support systems on driver performance: A literature survey”. In: *IEEE Transactions on Haptics* 8.4 (2015), pp. 467–479.
- [38] M. Plöchl and J. Edelmann. “Driver models in automobile dynamics application”. In: *Vehicle System Dynamics* 45.7-8 (2007), pp. 699–741.
- [39] R. Rajamani. *Vehicle dynamics and control*. Springer Science & Business Media, 2011.
- [40] N. Rashevsky. “Automobile driving as psychophysical discrimination”. In: *The Bulletin of Mathematical Biophysics* 24.3 (1962), pp. 319–325.
- [41] J. Rasmussen. “Skills, rules, and knowledge; signals, signs, and symbols, and other distinctions in human performance models”. In: *IEEE Transactions on Systems, Man, and Cybernetics*. Vol. SMC-13. 1983, pp. 257–266.
- [42] J. Reason. *Human error*. Cambridge University Press, 1990.
- [43] T. B. Sheridan and W. L. Verplank. “Human and computer control of undersea teleoperators”. Massachusetts Institute of Technology Cambridge: Man-Machine Systems Lab, 1978.
- [44] J. Svendenius. “Tire Modeling and Friction Estimation”. PhD dissertation, Department of Automatic Control, Lund Institute of Technology, Lund University, 2007.
- [45] J. Takahashi et al. “A hybrid stability-control system: combining direct-yaw-moment control and G-Vectoring Control”. In: *Vehicle System Dynamics* 50.6 (2012), pp. 847–859.
- [46] H. S. Tan et al. “Characterizing Driving Skill Based on Entropy Analysis of Steering Frequency Response”. In: *ASME 2010 Dynamic Systems and Control Conference*. Vol. 2. 2010, pp. 887–894.
- [47] A. Tustin. “The nature of the operator’s response in manual control, and its implications for controller design”. In: *Journal of the Institution of Electrical Engineers - Part IIA: Automatic Regulators and Servo Mechanisms* 94.2 (1947), pp. 190–206.
- [48] J. Van Doornik. “Haptic feedback on the steering wheel near the vehicle’s handling limits using wheel load sensing”. MSc thesis, Faculty of Mechanical, Maritime and Materials Engineering, Delft University of Technology, 2014.
- [49] A. T. Van Zanten. “Evolution of electronic control systems for improving the vehicle dynamic behavior”. In: *Proceedings of the 6th International Symposium on Advanced Vehicle Control*. Vol. 2. 2. 2002, p. 9.
- [50] K. J. Vicente and J. Rasmussen. “Ecological interface design: Theoretical foundations”. In: *IEEE Transactions on Systems, Man, and Cybernetics*. Vol. 22. 4. 1992, pp. 589–606.
- [51] C. D. Wickens et al. *Engineering psychology and human performance*. 4th ed. Routledge, 2013. Chap. Automation and human performance, pp. 332–354.
- [52] Wang Yaping et al. “Co-simulation based on ADAMS and simulink for direct yaw moment control system of 4WD-EV”. In: *Intelligent Robotics and Applications: 12th International Conference, ICIRA 2019, Shenyang, China, August 8–11, 2019, Proceedings, Part VI* 12. 2019, pp. 595–606.
- [53] A. Zanelli et al. “FORCES NLP: an efficient implementation of interior-point methods for multistage nonlinear nonconvex programs”. In: *International Journal of Control* (2017), pp. 1–17.

-
- [54] L. Zhang et al. “Human-centered torque vectoring control for distributed drive electric vehicle considering driving characteristics”. In: *IEEE Transactions on Vehicular Technology* 70.8 (2021), pp. 7386–7399.